

## AN ABSTRACT OF THE THESIS OF

Kim C. Bredensteiner for the degree of Master of Science in  
Botany and Plant Pathology presented on August 24, 1998

Title: An Investigation of Vegetation - Hydrology Interactions in Watershed 1 at the H.J. Andrews Experimental Forest

Abstract Approved: Redacted for privacy

Ronald P. Neilson

For management purposes, it would be useful to be able to predict streamflow response to forest practices in small, unmonitored basins. The primary objective of this study is to investigate the influence of early successional vegetation on summer streamflow levels. The long-term data records from watershed 1 at the H.J. Andrews Experimental Forest provide a case study of vegetation dynamics and streamflow changes during the first three decades following clear-cut harvest. This study documents the vegetation dynamics in watershed 1, based on long-term vegetation plot data and aerial photos. Hypotheses about the mechanisms by which vegetation influences streamflow levels are presented and explored using a spatially explicit watershed model, MAPSS-W (Daly, 1994).

In order to test these hypotheses of vegetation - hydrology interaction, spatially distributed climate, soils and vegetation datasets were developed for MAPSS-W. MAPSS-W was calibrated and evaluated for use in watersheds 1 & 2 at the H.J. Andrews Experimental Forest. Following calibration and evaluation of MAPSS-W, experimental simulations were run to explore the hypotheses of vegetation - hydrology interaction.

These analyses of long-term vegetation data and results from watershed simulations indicate that changes in summer streamflow levels in watershed 1 are related to shifts in the dominant vegetation in the watershed. Rapid growth of herbaceous vegetation appears to influence summer streamflow during the first 5-10 years following harvest. Summer streamflow deficits appear to be related to the dominance of deciduous broadleaf vegetation in the watershed during the second decade following harvest. Conifers appear to begin to play a significant hydrologic role during the third decade following harvest.

An Investigation of Vegetation - Hydrology Interactions  
in Watershed 1 at the H.J. Andrews Experimental Forest

by

Kim C. Bredensteiner

A Thesis Submitted

to

Oregon State University

In partial fulfillment of  
the requirements for the  
degree of

Master of Science

Presented August 24, 1998  
Commencement June 1999

Master of Science thesis of Kim C. Bredensteiner presented on August 24, 1998

Approved:

Redacted for privacy

---

Major Professor, representing Botany and Plant Pathology

Redacted for privacy

---

Chairman of Department of Botany and Plant Pathology

Redacted for privacy

---

Dean of Graduate School

I understand that my thesis will become part of the permanent collection of Oregon State University libraries. My signature below authorizes release of my thesis to any reader upon request.

Redacted for privacy

---

Kim C. Bredensteiner, Author

## Acknowledgments

As a watershed modeler, I must first acknowledge my source of reality. The climate, vegetation, and streamflow datasets used in this study were provided by the Forest Science Data Bank, a partnership between the Department of Forest Science, Oregon State University, and the U.S. Forest Service Pacific Northwest Research Station, Corvallis, Oregon. Significant funding for these data was provided by the National Science Foundation Long-Term Ecological Research program (NSF Grant numbers BSR-90-11663 and DEB-96-32921). In particular I would like thank Ted Dyrness, Al Levno, and Steve Acker for their insights about the vegetation and soils of these small watersheds.

I am grateful to the organizations that financially supported my work. These include the USDA Forest Service (PNW93-0474), the H.J. Andrews Experimental Forest LTER (DEB-96-32921), and the Department of Botany and Plant Pathology at Oregon State University.

Many thanks go to my thesis committee for their advice, guidance and encouragement. Thanks to Dr. Ron Neilson for providing the tools and allowing me the independence to pursue my interests. Thanks to Dr. Julia Jones for helping to keep me focused. Thanks to Dr. Bill Winner for asking key, pertinent questions.

I also acknowledge my appreciation of the members of the global climate change research group, with particular thanks to: Dr. Chris Daly for mentoring me through the modeling maze; Dr. Dominique Bachelet for daily guidance, insights, and tidbits; and Dr. Ray Drapek for sharing technical tricks. Finally, my deepest gratitude goes to my family and friends for their continual support and encouragement through phone calls, visits, shared badminton games, beach trips, ridge walks, dance lessons, bike rides, sushi parties, and life stories.

## Table of Contents

	<u>page</u>
1. Chapter 1: General Introduction	1
2. Chapter 2: Development and Comparison of Spatial Data Sets for Watersheds 1 & 2 at the H.J. Andrews Experimental Forest	4
2.1. Introduction & Objectives	4
2.2. Methods	5
2.2.1. Site Description: H.J. Andrews Experimental Forest Watersheds 1 & 2	7
2.2.1.1. Climate	7
2.2.1.2. Topography/Soils/Geology	8
2.2.1.3. Vegetation	9
2.2.1.4. Hydrology	10
2.2.2. Spatially Distributed Data Development	11
2.2.2.1. Topography	14
2.2.2.2. Climate	14
2.2.2.2.1. Precipitation	15
2.2.2.2.2. Temperature	18
2.2.2.2.3. Vapor Pressure	19
2.2.2.2.4. Wind Speed	20
2.2.2.2.5. Daily Climate Adjustments	21
2.2.2.3. Soils	21
2.2.2.4. Vegetation	22
2.3. Results	23
2.3.1. Spatially Distributed Data Layers	23
2.3.2. Data Comparisons	28
2.3.2.1. Topographic Resolution	28
2.3.2.2. Climate	29
2.3.2.2.1. Precipitation Interpolation	29
2.3.2.2.2. Temperature Lapse Rates	29
2.3.2.2.3. Vapor Pressure	31
2.3.2.2.4. Wind Speed	31
2.3.2.3. Soil Survey Map Units	33
2.4. Discussion	34
2.4.1. Spatial Considerations	34
2.4.2. Data Extrapolation	34
2.5. Conclusions	35

## Table of Contents (Continued)

	<u>page</u>
3. Chapter 3: Calibration and Evaluation of MAPSS-W for application at the H.J. Andrews Experimental Forest	37
3.1. Introduction	37
3.2. Background	37
3.2.1. Streamflow Measurements	37
3.2.2. MAPSS-W	38
3.3. Materials and Methods	42
3.3.1. HJA WS 1 & 2 Measured Streamflow	42
3.3.2. HJA - MAPSS-W Parameterization	42
3.3.2.1. Snow Dynamics	46
3.3.2.2. Soil Hydrology	47
3.3.2.3. Seasonality	47
3.3.2.4. Leaf Area	48
3.3.2.5. Transpiration	49
3.3.3. Sensitivity Analysis	50
3.3.4. Resolution & Parameterization Comparisons	50
3.3.5. Data Comparisons	51
3.4. Results	51
3.4.1. Calibration - Single Parameter Sensitivity Analysis	52
3.4.1.1. Snow Dynamics	52
3.4.1.2. Soil Hydrology	52
3.4.2. Evaluation - Variation Between Simulated Water Years	62
3.4.3. Resolution & Parameterization Comparison	63
3.4.4. Climate Comparisons	80
3.4.4.1. Precipitation	80
3.4.4.2. Temperature	80
3.4.4.3. Vapor Pressure	85
3.4.4.4. Wind Speed	85
3.4.5. Soils Comparisons	86
3.5. Discussion	89
3.5.1. Streamflow Simulations	89
3.5.2. Model Generalization	90
3.5.3. Model Assumptions	91
3.5.3.1. Soils	91
3.5.3.2. Vegetation	92
3.6. Conclusions	93

## Table of Contents (Continued)

	<u>page</u>
4. Chapter 4: An Investigation of Early Successional Vegetation Influences on Summer Streamflow Following Clear-Cut Harvest in the Western Cascades	94
4.1. Introduction	94
4.2. Background	95
4.2.1. Influences of Forest Management on Streamflow	95
4.2.2. Vegetation Water Use Habits	97
4.2.3. Plant - Atmosphere Interactions	101
4.3. Materials and Methods	103
4.3.1. HJA WS 1 Summer Streamflow Analysis	103
4.3.2. WS 1 Vegetation Dynamics	104
4.3.3. WS 1 Hydrologic Hypotheses	108
4.3.3.1. Increased Summer Streamflow During Harvest	111
4.3.3.2. Initial Return to Pre-harvest Streamflow Levels	111
4.3.3.3. Summer Streamflow Deficit	112
4.3.3.4. Second Return to Pre-harvest Streamflow Levels	113
4.3.3.5. Future Summer Streamflow Patterns	113
4.3.4. Definition of Hydrologic Plant Functional Groups	114
4.3.5. Vegetation Pattern Analysis	116
4.3.5.1. Aerial Photo Interpretation	116
4.3.5.2. Vegetation Plot Data	118
4.3.5.2.1. Spatial Analysis	119
4.3.5.2.2. Repeated Measures Analysis	119
4.3.6. MAPSS-W Simulations	121
4.3.6.1. MAPSS-W Vegetation Layers	121
4.3.6.2. Vegetation - Hydrology Hypothesis Testing	123
4.3.6.3. Evaluation of MAPSS-W Simulations	125
4.4. Results	125
4.4.1. Vegetation Analysis	125
4.4.1.1. Aerial Photo Cover Maps	125
4.4.1.2. Vegetation Plot Data	128
4.4.1.2.1. Spatial Analysis	130
4.4.1.2.2. Repeated Measures Analysis	130
4.4.1.3. Vegetation Data Comparison	133
4.4.2. MAPSS-W Simulations	133
4.4.2.1. Summer Streamflow Results	133

## Table of Contents (Continued)

	<u>page</u>
4.4.2.3. Deciduous vs. Evergreen Broadleaf Comparison	134
4.5. Discussion	136
4.5.1. Repeated Measures Analysis - Influence of Environmental Factors on Percent Cover	136
4.5.2. Implications of Vegetation-Hydrology Interactions	137
4.5.2.1. Role of Herbaceous Vegetation	137
4.5.2.2. Role of Deciduous Broadleaf Shrubs and Trees	137
4.5.2.2.1. Riparian	137
4.5.2.2.2. Hillslope	138
4.5.2.3. Role of Evergreen Broadleaf Shrubs and Trees	139
4.5.2.4. Role of Conifers	139
4.5.3. Additional Influences on Summer Streamflow	140
4.6. Conclusions	140
5. Chapter 5: Conclusions	143
5.1. Accomplishments	143
5.2. Lessons	143
Bibliography	145
Appendices	151
Appendix A: Vegetation Data Summary	152
Appendix B: Photo Interpretation Assessment Results	167

## List of Figures

Figure		page
2-1	Location of WS 1 & 2 and Meteorological Stations (CS2met, Vanmet, & Primet) in the H.J. Andrews Experimental Forest	8
2-2	Monthly Total Precipitation Measured at CS2met for 12 Water Years of Interest	12
2-3	Monthly total Streamflow Measured at WS 2 Gage for 12 Water Years of Interest	12
2-4	Monthly Streamflow/Precipitation Ratio	13
2-5	Topographic Grids and Watershed Boundaries	16
2-6	Soils Series Maps for the 1964 Soil Survey and the Small Watershed Survey	24
2-7	Small Watershed Soil Survey Maps Showing Soil Series, Soil Phase, Landform, & Slope	25
2-8	Seasonal Pattern of Temperature Datasets	30
2-9	Seasonal Pattern in Vapor Pressure Datasets	30
2-10	Seasonal Pattern in Wind Speed Datasets	30
2-11	Soil Series Comparison	32
3-1	WS 1 & 2 Measured Monthly Streamflow Patterns	39
3-2	Schematic of Processes Represented in MAPSS-W	40
3-3	Snow Parameters Comparison - Annual & Monthly Results	45
3-4	Snow Parameters Comparison - Sensitivity Analysis Results	53
3-5	Vertical Saturated Hydraulic Conductivity - Annual Results	55
3-6	Lateral Saturated Hydraulic Conductivity - Annual Results	55
3-7	Vertical Saturated Hydraulic Conductivity -Monthly Results	56
3-8	Lateral Saturated Hydraulic Conductivity - Monthly Results	57
3-9	Surface-Baseflow Coefficient - Annual Results	58
3-10	Lateral Flux Coefficient - Annual Results	58
3-11	Porosity - Annual Results	58
3-12	Surface-Baseflow Coefficient - Monthly Results	59
3-13	Lateral Flux Coefficient - Monthly Results	60
3-14	Porosity - Monthly Results	61
3-15	Daily & Monthly Streamflow Comparisons for WS 1 & 2	64

## List of Figures (cont.)

<b>Figure</b>		<b>page</b>
3-16	Resolution & Parameterization Comparisons - Annual Results	77
3-17	Resolution & Parameterization - WS 1 Monthly Results	78
3-18	Resolution & Parameterization - WS 2 Monthly Results	79
3-19	Climate Dataset Comparisons - Annual Results	81
3-20	Temperature Dataset Comparisons - Monthly Results	82
3-21	Vapor Pressure Dataset Comparisons - Monthly Results	83
3-22	Wind Speed Dataset Comparisons - Monthly Results	84
3-23	Soils Dataset Comparisons - Annual Results	87
3-24	Soils Dataset Comparisons - Monthly Results	88
4-1	Stomatal Response to Soil Moisture Deficit	100
4-2	Stomatal Response to Vapor Pressure Deficit	100
4-3	WS 1 Streamflow Response	105
4-4	Hypothesized Changes in WS 1 Vegetation Function Following Clear-Cut Harvest	110
4-5	Location of Vegetation Transects in WS 1	120
4-6	Aerial Photo Interpretation by Vegetation Functional Group as % of Watershed Area	126
4-7	Vegetation Plot Data Trajectories by Functional Group	129
4-8	Repeated Measures ANOVA - Environmental Influences on Vegetation Cover	131
4-9	Summer Streamflow Simulation Results	135

## List of Tables

<b>Table</b>		<b>page</b>
2-1	Meteorological Station Summary	15
2-2	Summary of Climate Data Distribution Methods	17
2-3	H.J. Andrews Soil Attributes Used for MAPSS-W Soils Datasets	26
2.4	MAPSS-W 30m Resolution Data Layers	27
2-5	WS 1 & 2 Topographic Resolution Statistics	28
3-1	Key MAPSS-W Parameters	44
3-2	Hydrologic Functional Groups - Vegetation Parameters	50
4-1	Streamflow, Vegetation, & Local Climate Changes Following Harvest in WS 1	109
4-2	Plant Functional Groups - Species List	115
4-3	HJA Aerial Photos Used for WS 1 & 2 Vegetation Analysis	116
4-4	Maximum Leaf Area Index Values	123
4-5	Key Transpiration Parameters in MAPSS-W	124
4-6	Repeated Measures ANOVA Results - Environmental Influences on Vegetation Cover	132

## List of Appendix A Figures

<u>Figure</u>	<u>page</u>
Vegetation Plot Data	153
1962	
1967	
1972	
1979	
1990	
Aerial Photos	158
1959	
1967	
1972	
1979	
1990	
Aerial Photo Cover Maps	163
1959	
1972	
1979	
1990	

# **An Investigation of Vegetation - Hydrology Interactions in Watershed 1 at the H.J. Andrews Experimental Forest**

## **1. Chapter 1: General Introduction**

The basic premise of many experimental watershed programs is that human activities influence the quantity and quality of water resources. Water has become a primary forest resource management issue and watersheds have become the primary unit of management, land use and policy planning (Swank & Johnson, 1994). In the Pacific Northwest, much of the water consumed by households, industry and agriculture originates in small mountain streams during the wet, winter season. Mountain streams are also used for recreation and are the spawning and rearing habitat of native and anadromous fish species, and amphibians (Fredriksen & Harr, 1979). The quantity, quality and timing of streamflow influences the habitat of stream and riparian flora and fauna.

Changes in the quality, quantity, and timing of streamflow can be used as an indicator of the long-term success or failure of land management (Swank & Johnson, 1994). Evidence from long term experimental watershed research at the H.J. Andrews Experimental Forest in Oregon shows a period of decreased summer streamflow during the second decade of vegetation regeneration following clear-cut harvest. In the Pacific Northwest, diminished streamflows during the summer dry season, June to September, may adversely affect stream inhabitants, decrease downstream water supplies, and effect water chemistry (Hicks et al., 1991; Rothacher, 1970). These concerns about the ecological impact of forest practices on water resources and species habitat lead to questions about the environmental influences on summer streamflow levels.

For management purposes, it would be useful to be able to predict streamflow responses to forest practices in small, unmonitored basins. Climate, soils and vegetation all influence streamflow response. Two important controls on the hydrological response of a watershed are the spatial patterns and species composition of the vegetation. The primary objective of this study is to investigate the influences of vegetation on summer streamflow levels during the first three decades

of revegetation following timber harvest in a small watershed in the western Cascades of Oregon. This study describes the vegetation patterns and dynamics in terms of hydrologically distinct behavior and explores hypotheses of vegetation - hydrology interaction. These hypotheses are based on measurable vegetation and environmental characteristics such as leaf area, canopy structure, soil moisture, and stomatal conductance.

The long-term vegetation and streamflow data records from WS 1 suggest that the dominant vegetation groups (herbs, deciduous broadleaf, evergreen broadleaf and conifers) play distinct hydrological roles during early succession following clear-cut logging in the Pacific Northwest. Watershed 1 in the H. J. Andrews Experimental Forest was used as a case study to describe the changes in vegetation and canopy structure that occurred during the first 30 years of secondary succession following harvest. Hydrologically relevant vegetation functional groups were defined based on physiological characteristics of woody vegetation. These functional groups were used to analyze long-term vegetation plot data and aerial photos. The results from the vegetation analysis were used in conjunction with climate and soil datasets to provide input variables for a spatially explicit watershed model, MAPSS-W (Daly, 1994). MAPSS-W was used to explore the mechanistic hypotheses of vegetation influence on summer streamflow.

This thesis contains three chapters. The first, chapter 2, provides background information about watersheds 1 & 2 (WS 1 & 2) at the H.J. Andrews Experimental Forest. This chapter also describes the data and data development methods used to create spatially distributed datasets for use with MAPSS-W. Additionally, this chapter presents comparisons between alternative climate and soils datasets, which were created to explore questions of watershed function.

Chapter 3 provides a brief description of MAPSS-W, and presents the calibration and evaluation of the model for WS 1 & 2 at the Andrews. Single parameter sensitivity analyses are presented as a part of the calibration process. Climate and soils dataset comparison simulations are presented along with streamflow comparisons in the evaluation of MAPSS-W.

Chapter 4 describes the temporal and spatial vegetation patterns which occurred in WS 1. These descriptions were developed from analysis of aerial photos and long-

term vegetation plot data. Hypotheses of vegetation - hydrology interactions are presented and tested using the watershed model MAPSS-W.

## **2. Chapter 2: Development and Comparison of Spatial Datasets for Watersheds 1 & 2 at the H.J. Andrews Experimental Forest**

### **2.1 Introduction & Objectives**

One of the goals of land management is to limit the impact of landuse on the quantity, quality and timing of streamflow (Swank & Johnson, 1994). Streamflow analysis is one of the primary methods for detecting and monitoring changes in watershed processes. While basins may be analyzed as single units, spatially distributed models have been developed in an effort to better understand and predict the influences of spatially heterogeneous environmental factors (Duan, 1996). Spatially distributed models break the landscape up into homogeneous landscape units, based on topographic characteristics. Within these units the environmental characteristics are assumed to be uniform, and variation in the environmental characteristics occurs between these landscape units. The hydrologic response of each unit is computed in spatial sequence with the neighboring unit (Duan, 1996). TOPMODEL (Beven & Kirby, 1979), PRMS (Leavesley et al., 1983), SHE (Abbott et al., 1986), THALES (Grayson et al., 1992), DHSVM (Wigmosta et al., 1994) and MAPSS-W (Daly, 1994) are some of the spatially distributed models that have been developed for watershed analysis.

The spatial data layers in these models are inherently map based and may be represented in raster (gridded), vector, or triangular irregular network (TIN) formats (Duan, 1996). Raster formats represent the landscape as units of uniform size and shape. Vector and TIN formats generally represent the landscape as units of irregular size and shape. The underlying data layer for all spatially distributed models represents the topography of the landscape. Additional spatially distributed data layers generally include climate variables, particularly precipitation, and may included spatially distributed layers of soil and vegetation characteristics. These data layers are then used in calculations of water movement through the hydrologic cycle.

In this study, MAPSS-W (Daly, 1994) was used to explore the vegetation-hydrology interactions that have influenced streamflow during 30 years of post-harvest revegetation in watershed 1 at the H.J. Andrews Experimental Forest. MAPSS-W is a raster based

model that calculates water balance and distributes water between grid cells on a daily basis. The spatially distributed data layers used by MAPSS-W include the underlying topographic layer, four climate variables (precipitation, air temperature, vapor pressure, and wind speed), three soils variables (soil depth, texture and rock fragment), and three vegetation layers (trees, shrubs, and herbs). The first objective of this chapter is to describe the spatially distributed datasets developed as input layers for MAPSS-W. The second objective is to evaluate the relative accuracy of these datasets.

## **2.2 Methods**

Gridded topographic, climate, soils and vegetation datasets were developed for the H.J. Andrews Experimental Forest watersheds 1 & 2 (WS 1 & 2). These datasets were prepared for use in the MAPSS-W watershed model (Daly, 1994). MAPSS-W (Mapped Atmosphere-Plant-Soil System - Watershed) is a version of the MAPSS (Mapped Atmosphere-Plant-Soil System) biogeography model (Neilson, 1995), which incorporates belowground water transfer algorithms from the DHSVM (Distributed Hydrology-Soil-Vegetation Model) watershed model (Wigmosta et al., 1994).

MAPSS-W requires gridded input data layers, representing the spatial distribution of topography, climate, soils and vegetation. A 30 x 30m digital elevation model (DEM) was used as the basis for the topographic data layers and distributed climate datasets. The 30m DEM is the finest resolution elevation grid available for the Andrews small watersheds and distinctly represents the stream channels and hillslope topography in both watersheds. Soil and vegetation maps were converted to 30m grid format to match the topographic and climate datasets.

Distributed climate datasets were developed from point measurements for 12 water years chosen from the streamflow record from WS 1. These years were chosen to represent five periods of streamflow change in the WS 1 summer water record. These periods in the streamflow record were identified by Hicks et al. (1991), and are hypothesized to coincide with changes in vegetation cover. These hypothesized vegetation-streamflow interactions are the focus of this study. A set of four years were chosen to represent the pre-harvest period and pairs of water years which coincide with

four sets of aerial photos represent the post-harvest period. Four pre-harvest years were chosen to encompass inter-annual variability in climate conditions. These 12 water years (1958-61, 1967, 1968, 1972, 1973, 1979, 1980, 1990, 1991) will be referred to as the water years of interest. The significance of these time periods are discussed more extensively in Chapter 4.

Two soils datasets were created in order to compare the functional differences between the two soil surveys available for WS 1 & 2. A uniform vegetation dataset was created for calibration purposes. Five additional vegetation datasets were created for each of the five periods of interest in the WS 1 streamflow record. Additionally, datasets were created at 200 m resolution in order to make a comparison of the MAPSS-W Andrews parameterization against the previous Reynolds Creek parameterization (Daly, 1994).

The topographic, climate, soils, vegetation and streamflow data used in this study were available through the Forest Service Data Bank (FSDB), a data archive that is run collaboratively by the Department of Forest Science at Oregon State University and the U.S. Forest Service Pacific Northwest Research Station. The DEM and maps of roads, stream network, the 1964 soil survey, and stream gage and climate station locations were available in ArcInfo and ArcGrid format (ESRI, 1996). These maps were used in the process of dataset preparation. Measurements from three Andrews climate stations, Primet, CS2met, and Vanmet were used to create the distributed climate data layers. The field copies of the small watershed survey map and notes were made available by Ted Dymess.

Datasets were developed using ArcInfo and ArcGrid 7.0.4 (ESRI, 1996) and GRASS 4.1 (USA-CERL, 1993) geographic information systems. ArcInfo and ArcGrid 7.0.4 (ESRI, 1996) were used for data development tasks including; digitizing, watershed delineation, vector to raster data conversions, climate distribution and spatial analysis. GRASS 4.1 (USA-CERL, 1993) was used primarily for data transfer into IPW format (Frew, 1990) and visualization of model simulation results. MAPSS-W input datasets were stored in Imaging Processing Workbench (IPW) format (Frew, 1990).

### **2.2.1 Site Description: Andrews Watersheds 1 & 2**

WS 1, 2 & 3 at the H.J. Andrews Experimental Forest provide the longest running record of hydrology and vegetation succession data in the Pacific Northwest. These watersheds are located 45 miles east of Eugene, Oregon, in the western Cascades. Figure 2-1 illustrates the location of WS 1 & 2 in the Lookout Creek basin.

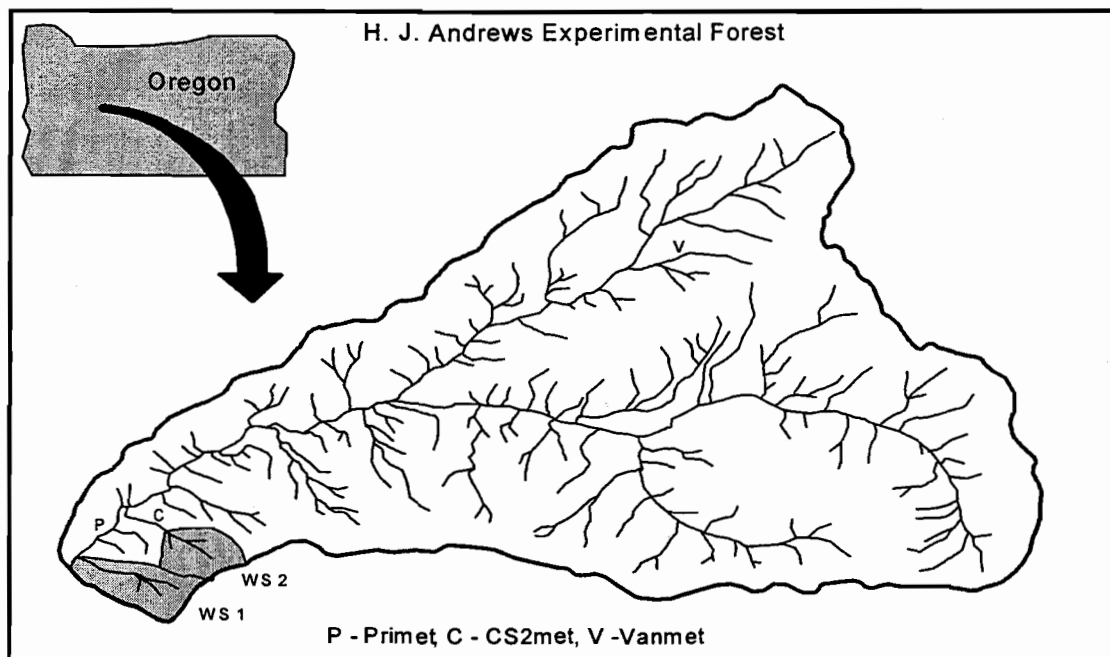
Lookout Creek drainage was designated as the H.J. Andrews Experimental Forest in 1948. In 1952, WS 1, 2, & 3 were chosen for the intensive study of road-building and logging effects on water quality and quantity (Rothacher et al., 1967). In 1952, CS2met, a meteorological data station, was installed in WS 2. Concurrently stream gages were installed in each of the three small watersheds (Rothacher et al., 1967). The calibration period, for streamflow measurements in the paired watersheds, began in the fall of 1952 and continued through the summer of 1962. Harvest began in WS 1 in 1962 and continued through 1966. WS 1 was 100% clear-cut using a skyline yarding system followed by a broadcast burn in October 1966. WS 2 was not treated and has been maintained as the control watershed for comparison with WS 1 & 3 (Rothacher et al., 1967). Understory vegetation plots were laid out and measured in 1962 (pre-harvest), and measurements were resumed after the completion of harvest in the summer of 1966 (Dyrness, 1973). Vegetation and streamflow measurements are ongoing.

#### **2.2.1.1 Climate**

The climate of the region is mild, with cool, wet winters and warm, dry summers. The seasonal trend of precipitation is inversely related to temperature and potential evapotranspiration (McKee & Bierlemeier, 1987). Annual precipitation averages 2300 mm, but only 6% falls between June and August. July and August are sometimes entirely storm free. Most precipitation in this area is associated with warm, moist air masses which move in from the Pacific Ocean during the late fall, winter and spring. Rainfall intensities are low, rarely exceeding 10 mm/hr (Rothacher et al., 1967). Temperatures range from average minimums of -5.5 °C in January and 11.9 °C in August, to average maximums of 5.5 °C in January and 23.3 °C in July (Rothacher et al., 1967).

Measurements of relative humidity at the CS2meteorological station show that mean monthly relative humidity is about 90% during the winter and between 60 and 70% during summer. Very little of the annual precipitation falls as snow, because the watersheds are located in the transient snow zone of the western Cascades. Snow that does fall in this zone, (400 - 1100m a.m.s.l.) usually melts in 3-4 days during subsequent rain (Harr, 1977).

**Figure 2-1: Location of WS 1 & 2 and Meteorological Stations (CS2met, Vanmet, & Primet) at the H.J. Andrews Experimental Forest.**



### 2.2.1.2 Topography/Geology/Soils

WS 1 & 2 are typical of the mature, dissected topography of the western Cascades. Elevations ranges from 442 - 1082m a.m.s.l. and slopes average greater than 50% (Rothacher et al., 1967). Oriented in a north-northwest direction, the watersheds feed two of the lowest tributaries to Lookout Creek which drains the entire experimental forest and feeds into the Blue River.

The soil parent materials are derived primarily from soft tuffs and breccias, although basalts and andesites are also present (Rothacher et al., 1967). Soils overlay extensive colluvial deposits and are characterized by poor profile development, loamy textures, high porosity and high water storage capacities. In some areas solid bedrock may be as much as 16m beneath the soil surface (Rothacher et al., 1967; Dyrness, 1969; Harr, 1977). There have been extensive mass movements of soil and rock material in the watersheds, leading to areas of unconsolidated material (Rothacher et al., 1967). A detailed soil survey of the three experimental watersheds resulted in the delineation of eight soil series based on 85 complete soil profile descriptions (Dyrness, 1969). The soils have high saturated hydraulic conductivity rates due to the highly aggregated and porous nature of the surface horizons (Dyrness, 1969; Harr, 1977). The average retention storage capacity for the surface 1.2m is approximately 200 to 350 mm (Dyrness, 1969). Storage capacity decreases with increases in percent rock fragment (Dyrness, 1969).

### 2.2.1.3 Vegetation

The pre-harvest vegetation in WS 1 and current vegetation in WS 2 is typical of the western hemlock (*Tsuga heterophylla* (Raf.) Sarg.) zone (Franklin & Dyrness, 1973). The forest canopy is dominated by a mixture of old-growth (300-500 yr. old) and mature (125 yr. old) Douglas-fir (*Pseudotsuga menziesii* (Mirbel) Franco) (Dyrness, 1973). The old-growth overstory canopy is patchy and the average height of the trees is 35m (+/- 17m) (Hawk et al., 1978). Western hemlock dominates the sub-canopy. Understory broadleaf tree species include: bigleaf maple (*Acer macrophyllum* Pursh.), red alder (*Alnus rubra* Bong.), Pacific dogwood (*Cornus nuttallii* Aud. ex T. & G.), madrone (*Arbutus menziesii* Pursh.), and golden chinquapin (*Castanopsis chrysophylla* (Dougl. A. DC.). Understory broadleaf shrub species include: vine maple (*Acer circinatum* Pursh.), California hazel (*Corylus cornuta* var. *californica* Marsh.), oceanspray (*Holodiscus discolor* (Pursh.) Maxim.), manzanita (*Arctostaphylos columbiana* Piper), Oregon grape (*Berberis nervosa* Pursh.), salal (*Gaultheria shallon* Pursh.), and Pacific rhododendron (*Rhododendron macrophyllum* G.) (Halpern, 1987).

The pre-harvest understory (< 6m tall) vegetation in WS 1 was classified into six plant communities related to a soil moisture gradient (Rothacher et al., 1967). Post-harvest vegetation dynamics in WS 1 follow the traditional trajectory of vegetation succession (Franklin & Dyrness, 1988). A peak in herbaceous vegetation cover was followed by dominance by evergreen and deciduous broadleaf shrubs, which was followed by conifer canopy closure. However, this successional pattern has not been uniform throughout the watershed. The vegetation patterns in WS 1 are discussed in more detail in Chapter 4. Previous analysis of the vegetation plot data has focused on understory community composition, structure, species distribution and dynamics. These analyses are presented in Dyrness (1973), Halpern (1987), Halpern (1988), and Halpern (1989).

#### **2.2.1.4 Hydrology**

Precipitation in the Pacific Northwest has a distinct, seasonal pattern. Precipitation falls primarily during the fall, winter and spring; and winter precipitation levels are highly variable. This variability is illustrated in Figure 2-2, a plot of the total monthly precipitation for the 12 water years of interest. Streamflow patterns in WS 1 & 2 are characteristic of watersheds where rain is the principal form of precipitation (Rothacher et al., 1967). The seasonal influence of snow is minimal in these basins. While some snow occurs, it generally melts long before the dry summer season begins (Rothacher, et al., 1967). This seasonal pattern contrasts sharply with watersheds that have well-developed snowpacks, in which spring snowmelt contributes significantly to streamflow (Rothacher, et al., 1967). In WS 1 & 2, the highest flows occur after long duration, low intensity storms have thoroughly wet the soil mantle; and the lowest flows occur during the summer, following extended periods (60 to 100 days) of minimal precipitation Rothacher, et al. 1967). The average total annual streamflow is high compared to other forest systems. Average total annual streamflow is 1270mm/year, which represents 55% of the average precipitation. Streamflow is seasonally distributed with high flows during the winter months averaging 250mm, and extremely low flows in late summer, with flows in

August frequently less than 10mm. This seasonal pattern is illustrated in Figure 2-3, which is a plot of the monthly total streamflows for the 12 water years of interest.

The runoff to precipitation ratio is low during the fall as the soils recharge after the summer dry season, and increases during the winter once the soils are fully hydrated. The runoff to precipitation ratio peaks in mid-summer. In July & August streamflow may be 30 - 90 times greater than incoming precipitation. Figures 2-4 a & b illustrate this runoff to precipitation ratio trend. This highlights the importance of baseflow drainage in these watersheds during the summer dry season.

Overland flow rarely occurs on undisturbed forest soils in the western Cascades, but streams respond quickly to precipitation (Harr, 1977). This quick streamflow response can be explained by the steep topography, high surface soil permeability, and high hydraulic conductivity values. The absence of overland flow is also related to high vegetation interception rates, detention storage within the deep litter layer, and the low rainfall intensities that are common to the western Cascades. Macropores contribute to the highly porous, well-aggregated surface soil structure and aid in infiltration and percolation of the precipitation that reaches the soil surface (Harr, 1977). Pore size decreases and rock fragment increases with depth. These changes in soil structural characteristics decreases hydraulic conductivity with depth (Harr, 1977).

Soil profile measurements describe maximum soil depths between .7m and 2.5m (Dyrness, 1969). It is believed that these surface soils overlay unconsolidated material and fractured bedrock that may be 16m deep (Rothacher, et al., 1967). These deeper soils appear to contribute substantially to summer streamflow and may contribute to the pool of plant available water for some deeply rooted species.

### **2.2.2 Spatially Distributed Data Development**

Gridded datasets were created for WS 1 & 2 at 30m resolution. This grid resolution was chosen because it was the finest resolution digital elevation model (DEM) available for the Andrews small watersheds. All gridded climate, topographic, soils and vegetation datasets were projected in UTM zone 10 coordinates, using the Clark 1866 spheroid and datum NAD27. All distributed datasets were transferred to IPW format (Frew, 1990) for use in MAPSS-W. In addition, 200m datasets were created for scale

Figure 2-2: Monthly Total Precipitation Measured at CS2met for 12 Water Years of Interest

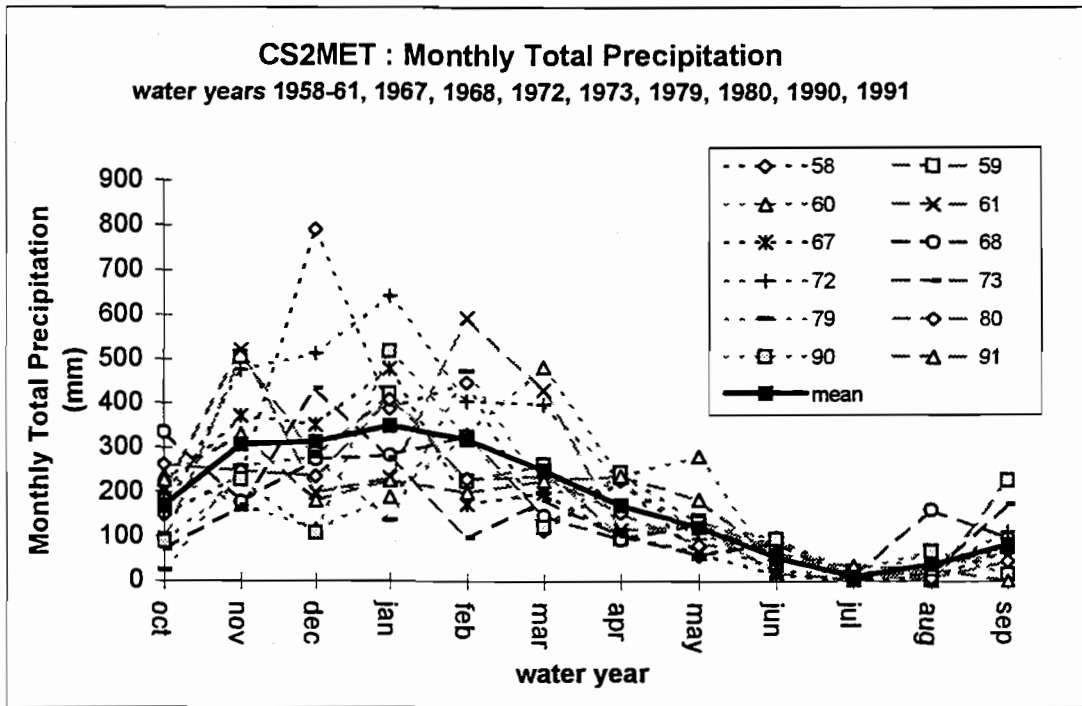


Figure 2-3: Monthly Total Streamflow Measured at WS2 12 Water Years of Interest

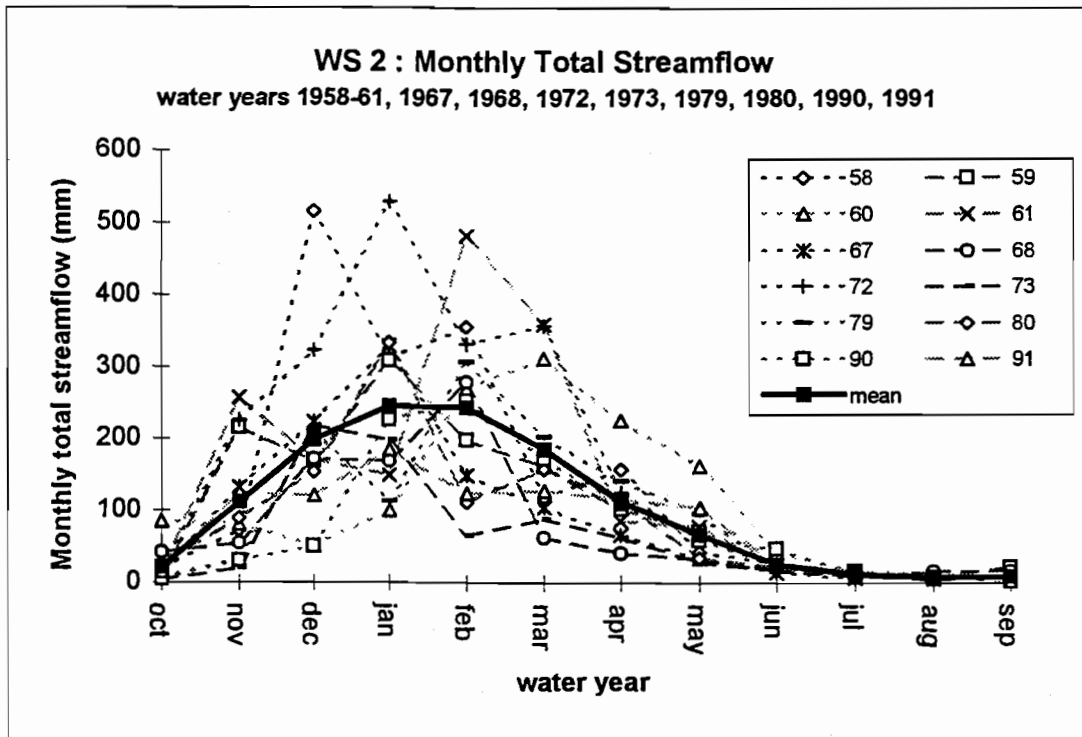
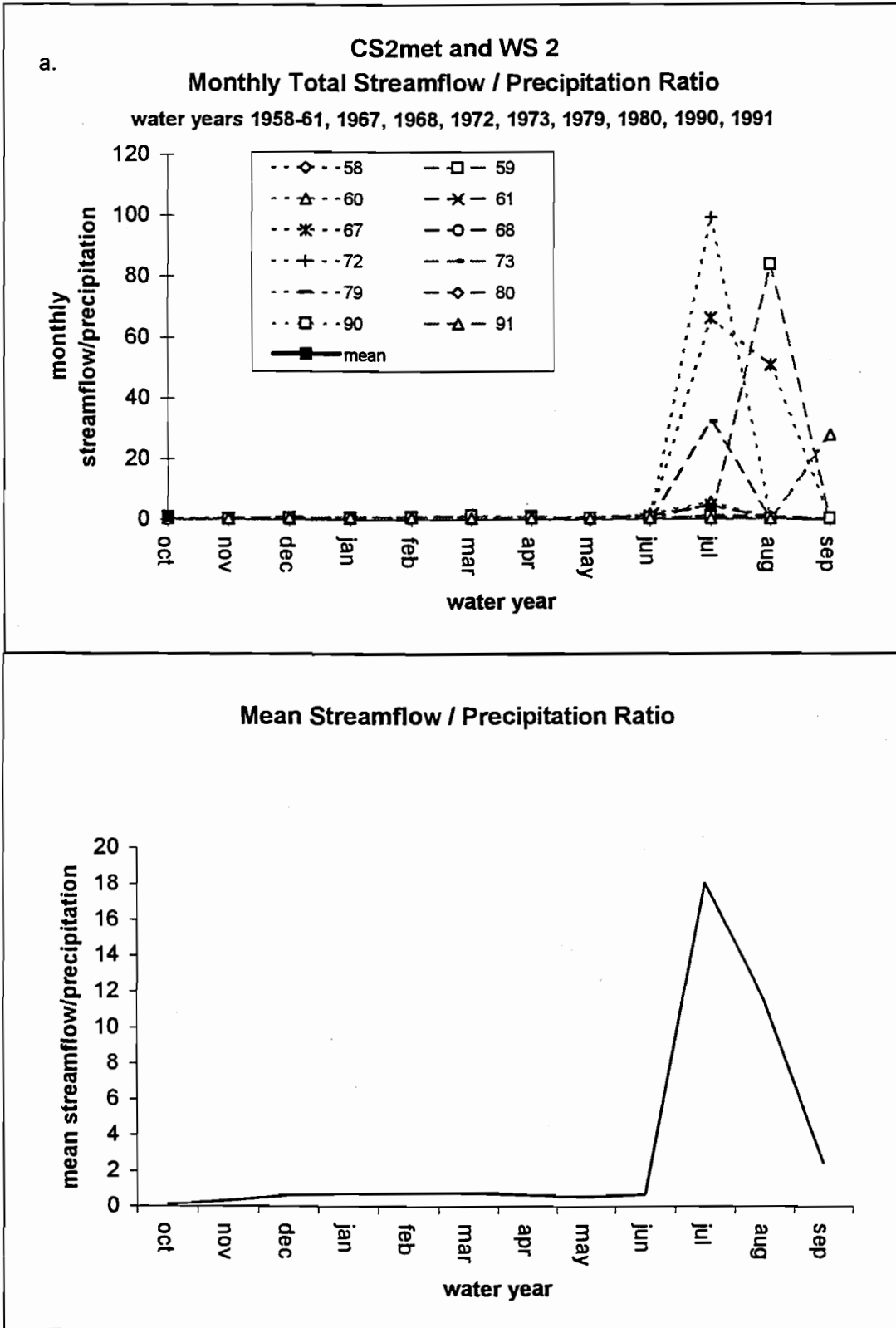


Figure 2-4a & b: Monthly Streamflow/Precipitation Ratio for 12 Water Years of Interest



and parameterization comparisons with the previous Reynolds Creek application of MAPSS-W (Daly, 1994).

### **2.2.2.1 Topography**

The 30m DEM serves as the basic topographic layer for MAPSS-W. This DEM was produced by USFS Region 6 for the Andrews Experimental Forest and was obtained, for this study, from the Andrews GIS archive (FSDB). In addition to the DEM grid, MAPSS-W requires a mask grid delineating the watershed boundaries and a slope grid which specifies the change in elevation between a grid cell and the eight grid cells surrounding it (Wigmosta, 1994 & Daly, 1994). This slope file determines the routing of water between grid cells.

The DEM was used to create masks of the watershed boundaries using the surface hydrologic analysis routines in ArcGrid 7.0.4 (ESRI, 1996). The slope file was created in ASCII format using slope2asc (unpublished). The 200m DEM was created from the 30m DEM using a cubic transformation in ArcGrid 7.0.4 (ESRI, 1996). The cubic transformation was chosen in order to create smooth transitions between grid cells (ESRI, 1996). The difference in watershed boundaries and topographic resolution between the 30m and 200m grids are illustrated in Figure 2-5.

### **2.2.2.2 Climate**

CS2met, the meteorological station in WS 2, is the primary data source for daily measurements that were used to create distributed climate datasets for the MAPSS-W simulations discussed in this study. CS2met was installed in 1957 in an old-growth opening. Wind speed is not recorded at CS2met, so it was necessary to use wind speed data from other meteorological stations. Wind speed data was used from Primet, the primary meteorological station for the experimental forest, and Vanmet, an upper elevation meteorological station. A summary of the elevation, aspect, and measurement

dates for relevant climate variables is provided in Table 2-1. Figure 2-1 illustrates the locations of these meteorological stations.

**Table 2-1: Meteorological Station Summary**

<b>Meteorological Station</b>	<b>Elevation(amsl)</b>	<b>Aspect</b>	<b>Beginning of Measurements</b>
CS2met	485m	NW	precipitation - 1957; temperature & relative humidity - 1958
Primet	430m	flat ground	wind speed - 1973
Vanmet	1273m	south	wind speed - 1987

Climate datasets were developed for each of the 12 water years of interest. All distributed climate datasets were developed in ArcGrid 7.0.4 (ESRI, 1996) from point measurements and were based primarily on changes in elevation. Table 2-2 summarizes the data sources and methods of distribution for these datasets.

#### 2.2.2.2.1 Precipitation

For each water year of interest, monthly total precipitation was calculated from measurements of daily precipitation at CS2met. These monthly total precipitation values were distributed across WS 1 & 2 based on a pre-existing 100m spatial distribution of precipitation for the Andrews (Daly, unpublished). This 100m distribution was created using the Precipitation-elevation Regressions on Independent Slopes Model (PRISM) (Daly et al., 1994) and is based on averaged monthly data for 1980-89 from 14 climate stations located in and around the Lookout Creek basin. PRISM uses point data and a digital elevation model to generate gridded estimates of precipitation over the landscape. These estimates accounts for the influences of elevation and aspect on precipitation distribution (Daly et al., 1994).

Figure 2-5: Topographic Grids & Watershed Boundaries. Watershed outlines at 30m and 200m grid resolutions, 30m and 200m DEM resolutions.

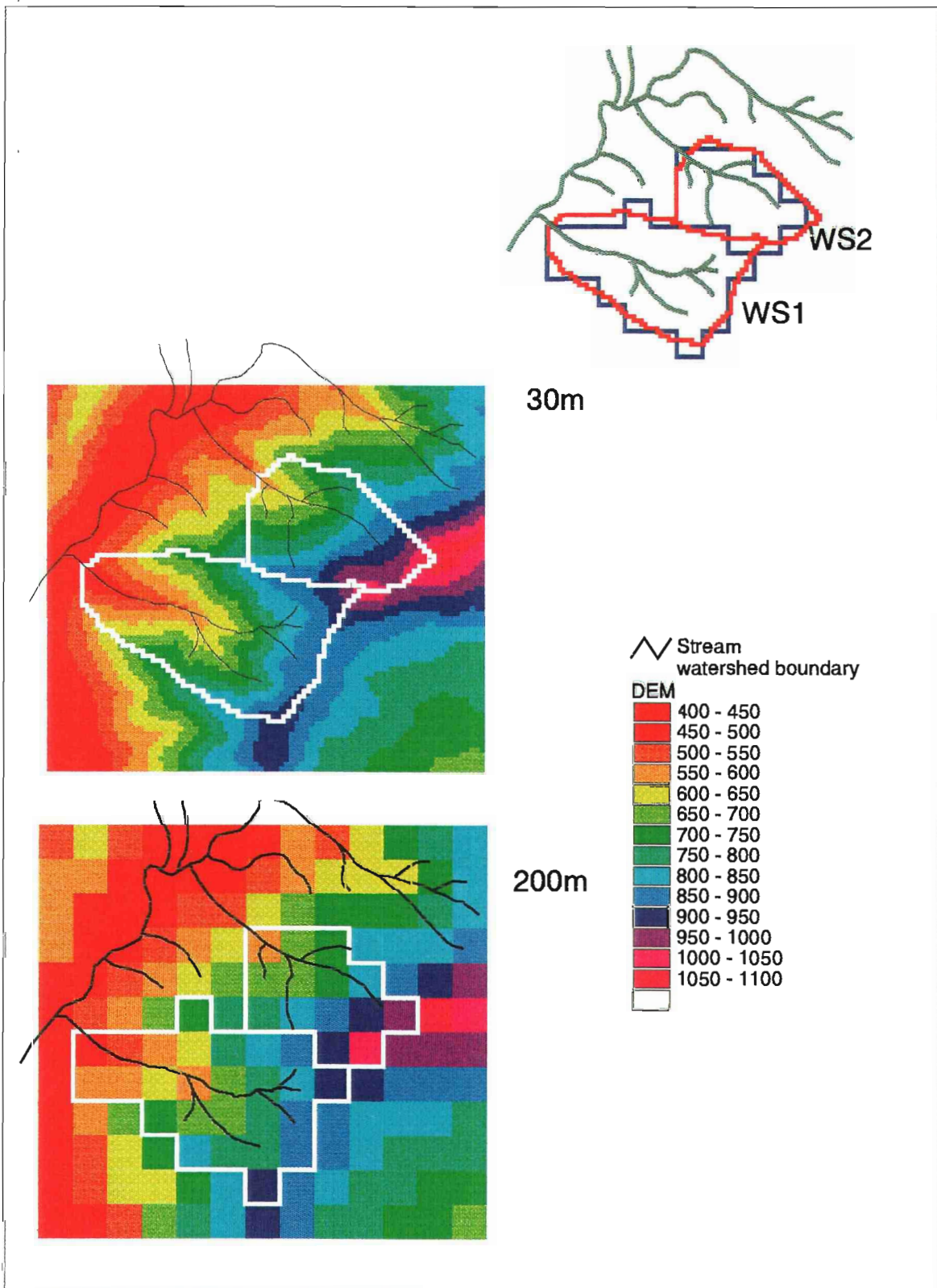


**Table 2-2: Summary of Climate Data Distribution Methods**

Variable	Data Source	Method	Daily variation
Total Precipitation	Daily total ppt from CS2met for WY* of interest	<ol style="list-style-type: none"> <li>1) Resampling of monthly, 100m PRISM (Daly et al, 1994) distributions (Daly, unpublished)</li> <li>2) Normalization of monthly grids for CS2met station</li> <li>3) Monthly totals calculated from daily totals</li> <li>4) Distributions of monthly totals for each water year over normalized grids</li> </ol>	Proportion of monthly total
Mean Temperature	Daily max/min temp from CS2met for WY* of interest	<ol style="list-style-type: none"> <li>1) Daily mean calculated from daily max/min</li> <li>2) Monthly means calculated from daily means</li> <li>3) Distribution of monthly means based on three elevation lapse rates:  Standard Adiabatic (-6oC/km)  HJA Monthly Lapse Rate  HJA Monthly Lapse Rate with Inversion</li> </ol>	Departure from monthly mean
Mean Vapor Pressure	Daily max/min RH from CS2met for WY* of interest Daily max/min temp from CS2met for WY of interest	<ol style="list-style-type: none"> <li>1) Daily mean RH calculated from daily max/min</li> <li>2) Monthly means calculated from daily means</li> <li>3) Flat RH grids created for each month</li> <li>4) Monthly mean VPR grids created in IPW using rhvp on 2 band mean tmp, RH grids</li> <li>5) Monthly min VPR grids created in IPW using rhvp on 2 band min tmp, mean RH grids</li> </ol>	Proportion of monthly mean (Daily VPR calculated from daily mean tmp and RH)
Mean Wind Speed	Daily mean wind speed from Vanmet, 1988-1996 Daily mean wind speed from Primet, 1974-1996	<ol style="list-style-type: none"> <li>1) All measurement heights converted to 12m effective height</li> <li>2) Average wind year created for each station</li> <li>3) Monthly means calculated from daily means</li> <li>4) Flat grids created based on each station</li> <li>5) Distributed grids created using simple linear regression with elevation</li> </ol>	Proportion of monthly mean

\* water years of interest: 1958-61, 1967, 1968, 1972, 1973, 1979, 1980, 1990, 1991

In order to distribute the CS2met data for the water years of interest, the 100m monthly grids were interpolated to 30m resolution in ArcGrid 7.0.4 (ESRI, 1996) using two resampling methods: nearest neighbor interpolation and cubic spline (ESRI, 1996). While the nearest neighbor interpolation maintains the pattern of the 100m grid, the cubic spline smooths the precipitation pattern over the 30m grid.

Once the 100m monthly grids were resampled to 30m monthly grids, each grid was divided by the precipitation value of the CS2met grid cell for that month. This created two sets of normalized precipitation grids, one set (January - December) for each resampling method. In these normalized precipitation grids, the value for each grid cell was based on that cell's fractional relationship to the cell containing the CS2met meteorological station. These normalized precipitation grids were then used to create monthly precipitation grids for each month in each water year. The normalized precipitation grid for each month was multiplied by the total monthly precipitation for that month as measured at the CS2met station. The 200m grids were created using the above procedures, but only for the cubic spline resampling method.

#### 2.2.2.2.2 Temperature

The spatial distributions of mean monthly temperature data from CS2met for the water years of interest were based on elevation lapse rates. Three sets of temperature distributions were created. The first was an application of the dry adiabatic lapse rate ( $-6^{\circ}\text{C}/\text{km}$  increase in elevation) for all months. The other two sets of lapse rates were developed by Lynn Rosentrater's (1996) analysis of the Andrews temperature data record. The first set are simple monthly lapse rates; the second set are paired monthly lapse rates above and below an inversion height of 650-700m a.m.s.l. This inversion level falls in the middle of the WS 1 & 2 elevation range.

For each water year of interest, daily maximum and minimum temperatures measured at CS2met were averaged to obtain an estimate of the daily mean temperature. The daily mean temperature estimate was averaged on a monthly basis to obtain monthly mean temperatures which were distributed using the three elevation lapse rates and a normalized elevation grid. The normalized elevation grid was created

by subtracting the elevation of the grid cell containing the CS2met station from every grid cell. For each dataset, this normalized elevation grid was multiplied by the monthly temperature lapse rates, and the mean monthly temperature for each month was added to the appropriate lapse rate grid. An additional temperature dataset was created for the 200 m resolution using these procedures with the adiabatic lapse rate.

#### 2.2.2.2.3 Vapor Pressure

For each water year of interest, monthly temperature and monthly relative humidity estimates were combined to create monthly vapor pressure grids. The CS2met daily maximum and minimum relative humidity measurements were averaged to obtain an estimate of mean daily relative humidity. Mean daily relative humidity estimates were averaged monthly and the monthly average was used to create a uniform relative humidity grid, in which each grid cell had the same value as the CS2met grid cell. These monthly relative humidity grids were processed in conjunction with monthly temperature grids using the IPW utility rh2vp (Frew, 1990). Saturated vapor pressure was calculated for each grid cell based on the temperature of the grid cell, and this saturated vapor pressure grid was multiplied by the relative humidity grid. Because relative humidity was not adjusted for elevation or aspect, the spatial distribution of vapor pressure was based solely on the spatial distribution of the temperature grids.

An additional vapor pressure dataset was developed using the processes described above and the monthly mean of the daily minimum temperature measurements from CS2met. The monthly mean of the daily minimum temperature was distributed as described in the temperature section, but using monthly lapse rates for minimum temperatures (Rosentrater, 1997). This dataset was created because of a need to increase simulated evaporation and transpiration during the winter in the MAPSS-W simulations for the Andrews watersheds. A 200m dataset was created using the above procedures based on the mean monthly temperature.

#### 2.2.2.2.4 Wind Speed

Wind speed is not measured at CS2met, thus it was necessary to use data from alternative meteorological stations for this variable. In comparison with the three other climate variables required by MAPSS-W, wind speed data are sparse at the Andrews. Wind speed measurements began in 1973, but have significant gaps. Due to the gaps in the data record, a single average wind speed year was developed for each of the two meteorological stations with records longer than 5 years, Primet (low elevation) and Vanmet (high elevation). Wind speed has been measured at three different heights at Primet (5m, 12m, and 10m) and at 6m at Vanmet (FSDB). Since measurement height differences can have a significant effect on wind speed magnitude, all wind speeds were adjusted to 12m effective height using the standard logarithmic profile (Oke, 1978). For these calculations, roughness length (2.6m +/- 1.3m) and zero plane displacement (27.3m +/- 13.3m) were calculated using the Jarvis et al. equations for coniferous forests (1976). A pre-harvest canopy height for WS 1 & 2 was estimated to be 35m +/- 17m (Hawk et al., 1978).

For each meteorological station, the height-adjusted daily measurements were averaged through the years of record to create an average wind speed year. Mean monthly wind speeds were calculated from the mean daily wind speed averages for each meteorological station, and used to create gridded wind speed datasets. Wind speed was distributed uniformly over both watersheds for each month, creating grids with the same value for all grid cells. An additional wind speed dataset was created using a simple linear interpolation between the Primet and Vanmet measurements based on elevation. The difference in wind speed between the two stations was calculated for each month and divided by the difference in elevation (840m) between the two stations. These monthly lapse rates were applied to a normalized elevation grid, based on the Primet elevation (similar to the CS2met normalized grid described above). Primet monthly wind speeds were added to the monthly lapse rate grids. Wind speed was the only distributed climate variable that was not based on actual water year climate data. The average wind speed grids were used for all of the water years of interest.

#### 2.2.2.2.5 Daily Climate Adjustments

MAPSS-W simulates herbaceous vegetation growth and site water balance on a daily basis, however, the gridded climate datasets represent monthly climate data. This is one way to keep the size of input datasets manageable (Daly, 1994). The variation in daily climate is represented by calculations of each day's proportion of the total monthly precipitation, proportions of the monthly mean vapor pressure and monthly mean wind speed, and the difference from the monthly mean temperature. These calculations were the same for the entire watershed area. This assumes that the bulk of the spatial variability is represented in the monthly fluctuations and that daily fluctuations are fairly constant across the watershed. This is generally acceptable for small regions (Daly, 1994).

For each water year of interest, the daily proportions and differences were calculated and stored in ASCII format. Daily precipitation proportions were calculated as a percentage of the monthly total precipitation based on the daily data from CS2met. Daily temperature differences were calculated as the difference between the daily temperature and the mean monthly temperature at CS2met. Daily vapor pressure proportions were calculated as a percentage of the monthly mean vapor pressure. Daily vapor pressure values were calculated from the multiplication of mean daily relative humidity and daily saturated vapor pressure values, which were calculated from daily temperatures. Daily wind speeds were calculated as a percentage of the monthly mean wind speed for the averaged wind speed years created for Vanmet and Primet.

#### **2.2.2.3 Soils**

In order to calculate effective soil depth and hydraulic conductivity, MAPSS-W requires information about soil depth, soil texture and rock fragment. MAPSS-W can use generic sandy loam soil parameters or gridded soil datasets. Two soil surveys exist for the Andrews small watersheds. Soils datasets were developed from both surveys to test MAPSS-W sensitivity to variations in soil variables. Figure 2-6 shows the soil series in WS 1, 2 & 3 for each survey. The 1964 soil survey is the soils dataset used by most

researchers at the Andrews. It was completed in 1964 by a USGS soil survey team and was available through the Andrews GIS data archive (FSDB). The 1964 survey includes map units of soil series, percent slope, and landform (USDA, 1964). This survey was largely based on aerial photo interpretation.

Additionally, an intensive soil survey was completed for the Andrews WS 1, 2 & 3 in the 1960's in conjunction with the beginning of the small watershed experiments (Dyrness, 1969). In order to create a dataset from the small watershed survey, the soil survey field map (Dyrness et al., unpublished) was digitized using ArcInfo 7.0.4 (ESRI, 1996). The small watershed survey includes map units of soil series, soil series phase (based on rock fragment), percent slope, and landform. Figure 2-7 shows maps of these attributes for the small watershed survey. This survey was based on soil profile and landform analysis. Soil series and soil phase profile summaries (Rothacher et al., 1967 & Dyrness, 1969) were used to develop the soil depth, percent rock fragment and texture percentages needed for the MAPSS-W datasets. Table 2-3 lists the soil series from these surveys and the soil attributes required by MAPSS-W. These soil attributes were added to the soil survey maps in ArcInfo 7.0.4 (ESRI, 1996) and each attribute layer was converted to a 30m grid using ArcGrid 7.0.4 (ESRI, 1996).

Three soil layers are represented in MAPSS-W. The first layer is .5m deep and supplies water to herbaceous and woody vegetation. The second layer is 1.0m deep and supplies water just to woody vegetation. Plant do not root in the third soil layer. This layer represents fractured bedrock and is the location of lateral water movement between grid cells (Daly, 1994).

#### **2.2.2.4 Vegetation**

Three vegetation lifeforms (trees, shrubs and herbs) are represented in MAPSS-W (Daly, 1994 & Neilson, 1995). These lifeforms are represented as grids of leaf area index (LAI) for each lifeform. An additional grid indicates whether the woody vegetation (trees & shrubs) is deciduous or evergreen. LAI is defined in MAPSS and MAPSS-W as a measure of the functional (transpiring) leaf area per unit of ground ( $m^2/m^2$ ) (Daly, 1994 & Neilson, 1995). For previous applications of MAPSS and MAPSS-W, functional LAI was

defined as all-sided LAI (Daly, 1994 & Neilson, 1995). For this application of MAPSS-W, functional LAI was defined as single-sided LAI. This definition was based on the observation that many of the dominant woody species in WS 1 & 2 have concentrations of stomata on one side of the leaf (Conard & Radosevich, 1981; Pezeshki & Hinkley, 1982; Johnson & Ferrell, 1983).

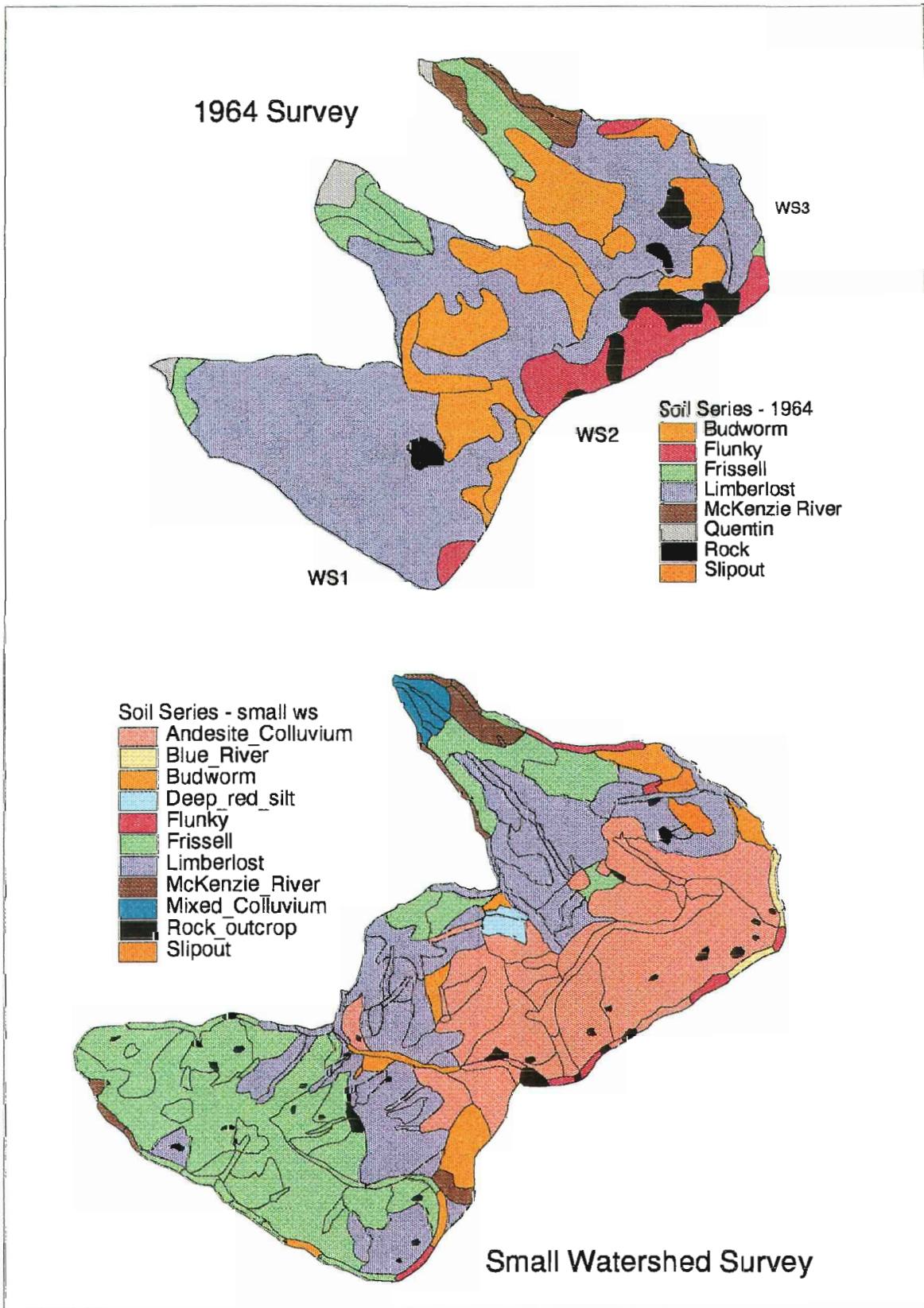
Two types of vegetation datasets were created for this study. The initial calibration and evaluation simulations were done using uniform vegetation grids, in which every grid cell had the same LAI values for trees (13), shrubs (1), and herbs (.2). These numbers were chosen from the reported values of tree and shrub LAI (between 3 and 22 for mature and old-growth conifer stands) and represent an average old-growth conifer stand in the western Cascades (Waring & Franklin, 1979). Additional vegetation datasets were developed based on aerial photo interpretation. These datasets were used to test hypotheses about vegetation-hydrology interactions and are discussed in chapter 4.

## **2.3 Results**

### **2.3.1 Spatially Distributed Data Layers**

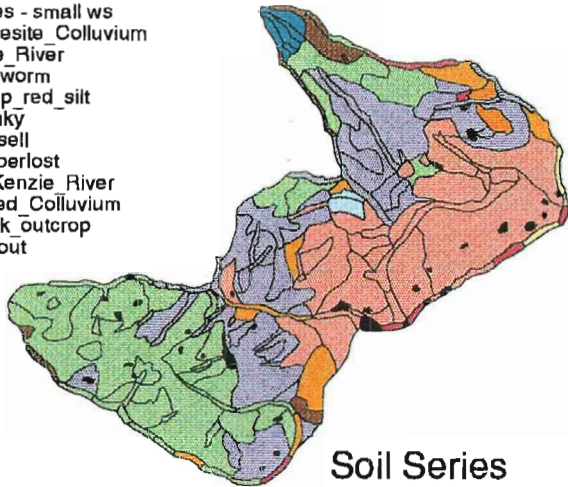
MAPSS-W uses three topographic data layers, four sets of monthly climate data layers (precipitation, temperature, vapor pressure, and wind speed), four soils data layers (soil depth, percent rock fragment, percent clay and percent sand), and four vegetation data layers (tree LAI, shrub LAI, herbaceous LAI and a deciduous-evergreen index). The 30m resolution data layers that were created for the Andrews application of MAPSS-W are listed in Table 2-4.

Figure 2-6: Soil Series Maps for the 1964 Soil Survey and the Small Watersheds Soil Survey



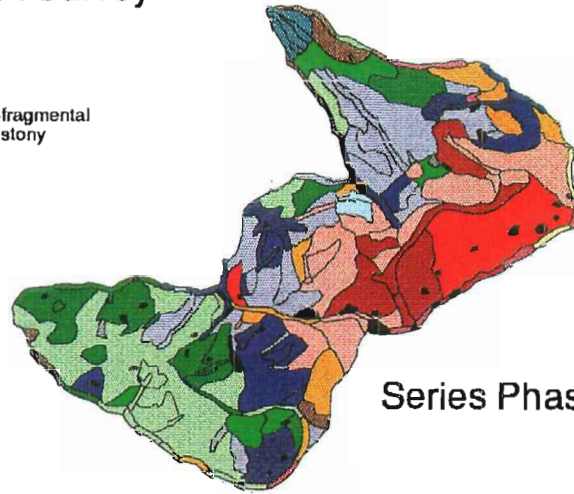
# Small Watersheds Soil Survey

- Soil Series - small ws**
- Andesite Colluvium
  - Blue River
  - Budworm
  - Deep\_red\_silt
  - Flunky
  - Frissell
  - Limberlost
  - McKenzie River
  - Mixed Colluvium
  - Rock\_outcrop
  - Slipout



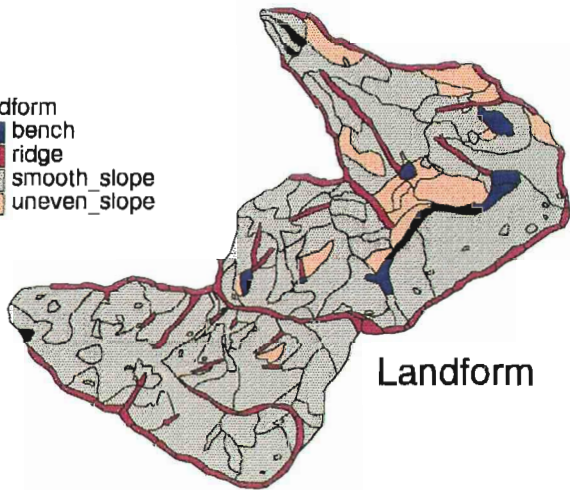
Soil Series

- Soil Series Phase**
- Andesite Colluvium
  - Andesite colluvium-fragmental
  - Andesite colluvium-stony
  - Blue River
  - Budworm
  - Deep\_red\_silt
  - Flunky
  - Frissell
  - Frissell-fine loam
  - Frissell-stony
  - Limberlost
  - Limberlost-fine loam
  - Limberlost-stony
  - McKenzie River
  - Mixed Colluvium
  - Rock\_outcrop
  - Sediment
  - Slide
  - Slipout



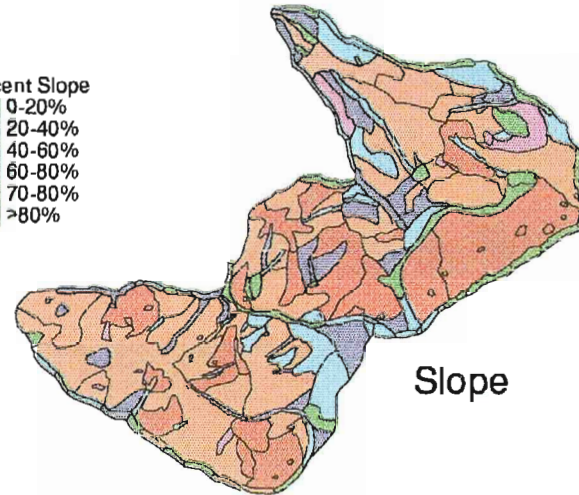
Series Phase

- Landform**
- bench
  - ridge
  - smooth\_slope
  - uneven\_slope



Landform

- Percent Slope**
- 0-20%
  - 20-40%
  - 40-60%
  - 60-80%
  - 70-80%
  - >80%



Slope

Figure 2-7: Small Watershed Soil Survey Maps Showing Soil Series, Soil Phase, Landform and Slope

**Table 2-3: H. J. Andrews Soil Attributes Used for MAPSS-W Soil Datasets**

Soil Phase	Soil Attributes									
	Depth	Percent Clay			Percent Sand			Percent Rock Fragment		
		layer 1	layer 2	layer 3	layer 1	layer 2	layer 3	layer 1	layer 2	layer 3
Andesite colluvium	1524	21	21	21	43	43	43	35	35	35
Andesite colluvium - fragmental	1524	21	21	21	43	43	43	75	75	75
Andesite colluvium - stony	1524	21	21	21	43	43	43	50	50	50
Blue river	1000	20	20	20	40	40	40	50	50	50
Budworm	1500	26	26	23	36	27	28	10	10	80
Deep red silt	2400	20	30	30	40	35	15	0	0	0
Flunky	584	20	16	16	34	54	54	65	50	50
Frissell	790	30	33	33	50	43	43	35	35	35
Frissell - finoam	790	30	33	33	50	43	43	25	25	25
Frissell - stony	790	30	33	33	50	43	43	50	50	50
Limberlost	1270	24	26	26	40	34	34	35	35	35
Limberlost - finoam	1270	24	26	26	40	34	34	25	25	25
Limberlost - stony	1270	24	26	26	40	34	34	50	50	50
Mckenzie river	1100	35	44	50	23	17	11	0	12	30
Mixed colluvium	1800	27	32	35	35	20	25	15	5	15
Rockland	1500	10	10	10	70	70	70	90	90	90
Sediment	1270	24	26	26	40	34	34	35	35	35
Slide	790	30	33	33	50	43	43	35	35	35
Slipout	1700	24	22	32	47	50	35	10	15	5

Table 2-4: MAPSS-W 30m resolution data layers (stored in IPW format)

30m Data Layer	File Name
<u>Topography</u>	
DEM	elev
Watershed Boundary	ws1mask, ws2mask
Lateral Flow	slope
<b>* Climate</b>	
<u>Monthly Precipitation Grids</u>	
nearest neighbor interpolation	n_ppt
cubic spline transformation	c_ppt
<u>Monthly Temperature Grids</u>	
adiabatic lapse rate	al_tmp
monthly lapse rate without inversion	ml_tmp
monthly lapse rate with inversion	il_tmp
<u>Monthly Vapor Pressure Grids</u>	
mean temperature	orig_vpr
minimum temperature	min_vpr
combination (mean during summer/ minimum during winter)	mix_vpr
<u>Monthly Wind Speed Grids</u>	
Primet wind speed	wnd_ap
Vanmet wind speed	wnd_av
Distributed wind speed	wnd_ad
<u>Soils</u>	
1964 survey	soil_64
(without rock fragment)	soil_64worf
small watershed survey	soil_d
(without rock fragment)	soil_dworf
<u>Vegetation</u>	
pre-harvest uniform vegetation	veg_13
pre-harvest aerial photo veg	veg_59
uniform vegetation for WS 1 - 1967	veg_67
aerial photo interpretation WS 1 - 1972	veg_72
aerial photo interpretation WS 1 - 1979	veg_79
aerial photo interpretation WS 1 - 1990	veg_90

\*Climate datasets were developed for each of the water years of interest: 1958-61, 1967, 1968, 1972, 1973, 1979, 1980, 1990, 1991

## 2.3.2 Data Comparisons

### 2.3.2.1 Topographic Resolution

Figure 2-5 shows the difference in DEM elevation and watershed boundaries between the 30m and 200m grid resolutions. The 30m resolution allows the stream channels to be distinctly represented in both watersheds. At 200m resolution the stream channels and watershed boundaries are less clearly defined. The 200m resolution represents some of the hillslopes as one or two cells, and the stream channel was enlarged to a width of 200m and shortened, represented by less than six grid cells. Increasing the grid resolution decreases the elevation, soils, vegetation and climate detail represented in the model. For example, the range of elevation was decreased in the 200m resolution DEM and this, in turn, decreases the temperature extremes. Table 2-5 summarizes the area, elevation and number of grid cells in each watershed for the two resolutions.

**Table 2-5 : WS 1 & 2 Topographic Resolution Statistics**

	<b>WS 1</b>		<b>WS 2</b>	
	<b>acre</b>	<b>ha</b>	<b>acre</b>	<b>ha</b>
Map Area	237	96	149	60.3
Simulated Area (30m)	256	103.5	148	60
Simulated Area (200m)	169	68.4	91	36.8
	<b># of grid cells</b>		<b># of grid cells</b>	
30m cells	1150		665	
200m cells	26		14	
	<b>minimum</b>	<b>maximum</b>	<b>minimum</b>	<b>maximum</b>
30m elevation (m)	440	1015	525	1070
200m elevation (m)	476	926	592	1025

### 2.3.2.2 Climate

This section describes the key differences between the various climate datasets. Comparisons of MAPSS-W simulation results, based on these alternative climate datasets, are presented in Chapter 3.

#### 2.3.2.2.1 Precipitation Interpolation

Two 30m precipitation datasets were created from the 100m precipitation distribution. The nearest neighbor interpolation maintained the spatial pattern of the 100m grid, and the cubic spline smoothed the spatial pattern. As a result of the cubic spline maximum precipitation was increased slightly in high elevations grid cells. This was most noticeable in the dry summer months.

#### 2.3.2.2.2 Temperature Lapse Rates

Three temperature datasets were created using elevation lapse rates. The seasonal pattern of the temperature lapse rates is illustrated in Figure 2-8. The monthly lapse rates (Rosentrater, 1997), increased the rate of temperature change above the adiabatic lapse rate ( $-6^{\circ}\text{C}/\text{km}$ ) during April and May. This caused the range in temperature extremes in the watershed to be greater. During the rest of the year the monthly rate of temperature change was less than the adiabatic lapse rate.

In the inversion layer dataset, temperatures at low elevations were cooler due to the cooling effect of the inversion zone. This led to lower maximum monthly temperatures throughout the year in comparison to the other two temperature datasets. The influence of the inversion zone is less pronounced in January, September and October. This is due to a similarity in lapse rates above and below the inversion height (Rosentrater, 1997).

Figure 2-8: Seasonal Pattern in Temperature Datasets

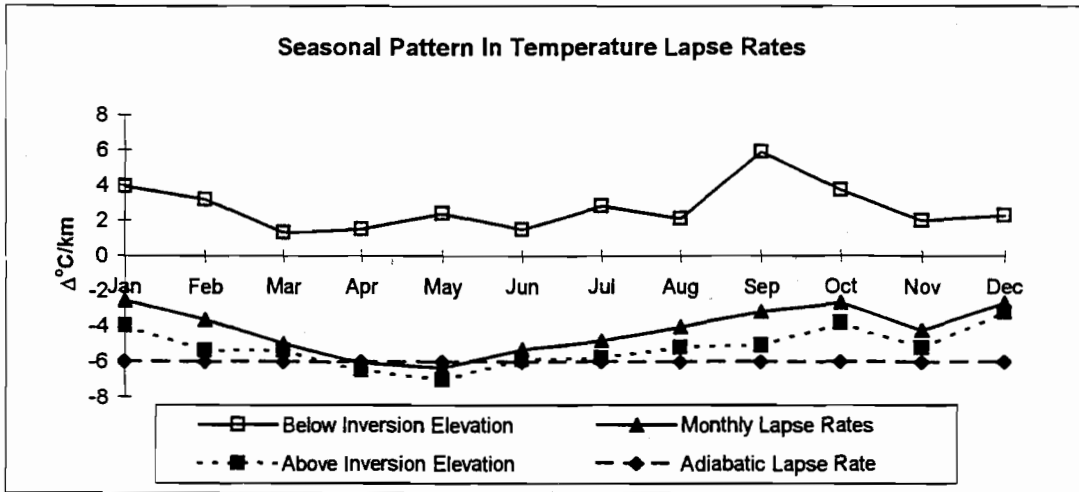


Figure 2-9: Seasonal Pattern in Vapor Pressure Datasets

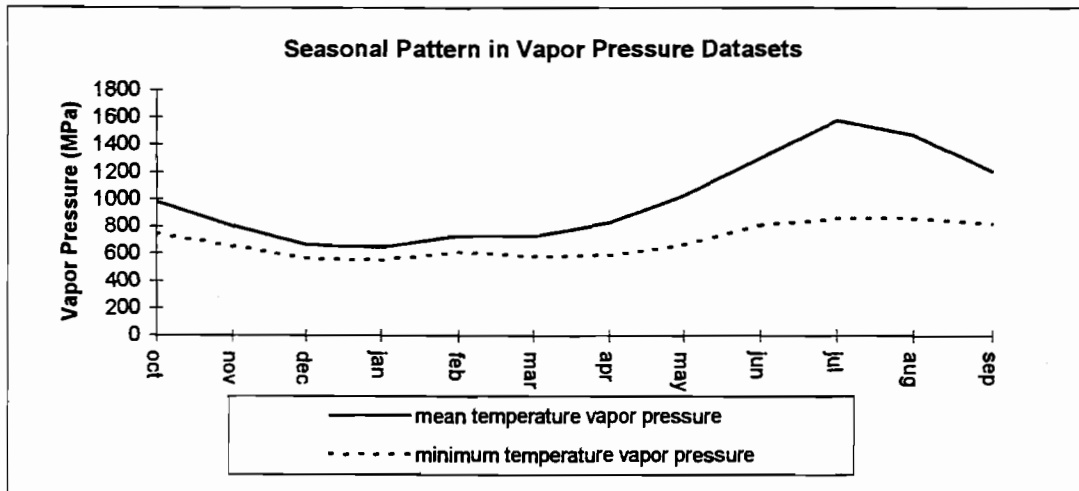
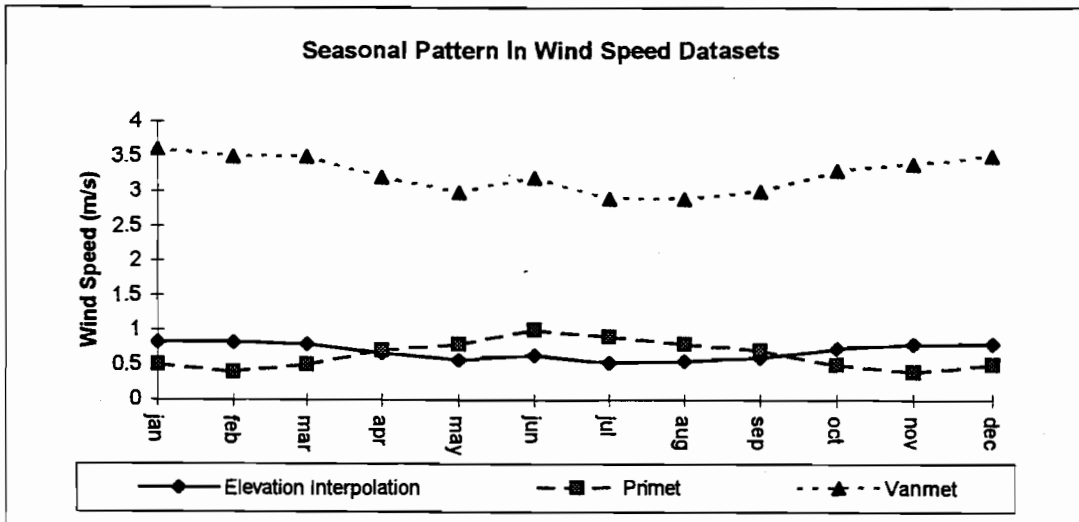


Figure 2-10: Seasonal Pattern in Wind Speed Datasets



#### 2.3.2.2.3 Vapor Pressure

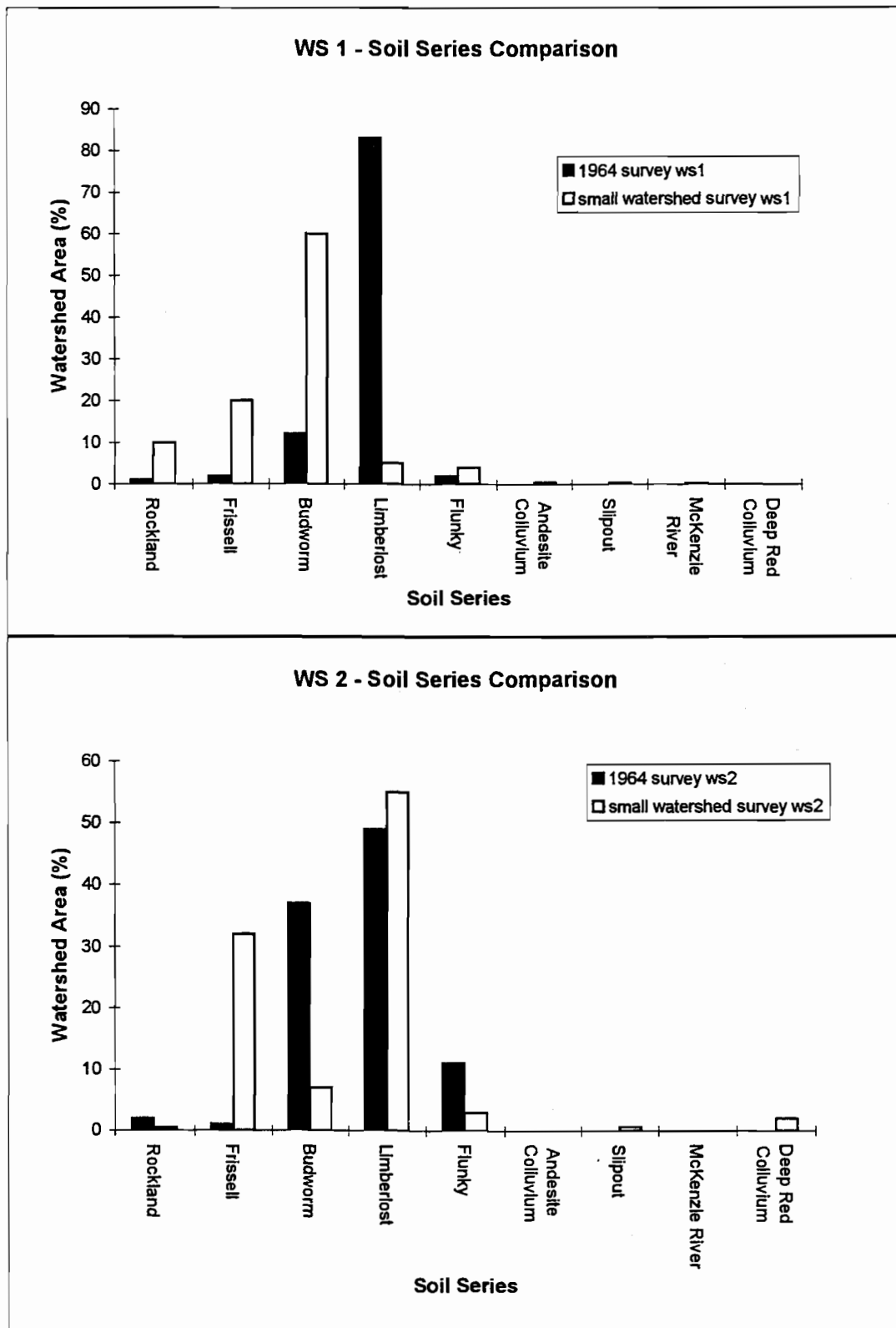
Two vapor pressure datasets were created. The first was based on mean temperatures and the second was based on minimum temperatures. The seasonal patterns of the vapor pressure datasets are illustrated in Figure 2-9. This graph presents the monthly means for each dataset from the monthly estimates for the 12 water years of interest. The vapor pressure based on mean temperatures was consistently higher than vapor pressure based on minimum temperatures. During the winter months the vapor pressure values are similar, but during spring and summer the mean temperature vapor pressure increases sharply as the diurnal temperature range increases.

The vapor pressure dataset that was used in the final calibration, evaluation and experimental model simulations was a combination of these two datasets. The minimum temperature vapor pressure grids were used during the winter (October-April), in order to increase winter potential evapotranspiration (PET), and the mean temperature vapor pressure grids were used during the summer (May-September), in order to maintain appropriate summer streamflow levels.

#### 2.3.2.2.4 Wind Speed

Three wind speed datasets were created based on average wind years. These wind years were developed from data collected at the Primet and Vanmet meteorological stations. The seasonal trends in wind speed are illustrated in Figure 2-10. The magnitude of the wind speed at Vanmet was consistently greater than the magnitude at Primet. Wind speeds at Primet were higher during the summer than during the winter. Conversely, wind speeds at Vanmet were higher during the winter than during the summer.

Figure 2-11 a & b:  
Soil series comparison: 1964 soil survey vs. small watershed survey



### 2.3.2.3 Soil Survey Map Units

Two soils datasets were developed. The first was based on the 1964 soil survey and the second was based on the small watersheds soil survey. The soil series map units for these surveys differ significantly for both WS 1 & 2. These differences are illustrated as a percentage of watershed area in Figure 2-11 a & b. The 1964 survey designated greater than 80% of WS 1 as Limberlost soils, in comparison, the small watershed survey designated 60% of WS 1 as Budworm soils. In WS 2, the 1964 survey designated 49% of the watershed area as Limberlost soils and 37% as Budworm soils. The small watershed survey designated 55% of WS 2 as Limberlost soils and 32% as Frissell soils.

The implications of these soil series differences are most apparent in the soil depth and rock fragment attributes. Differences in soil texture are limited because the soil series in WS 1 & 2 are predominantly loamy in texture. In WS 1 soil depth was greater in the 1964 survey, 90% of the watershed area has soil depths of 1270mm. In the small watershed survey, more than 60% of the watershed has soil depths less than 800mm. In WS 2, both surveys designate soil depths of 1270mm or greater in more than 90% of the watershed. These soil depths are based on soil profile measurements summarized in Dyrness (1969) and Rothacher et al. (1967), and do not account for the additional depth of unconsolidated materials and fractured bedrock assumed to underlie the surface soils (Rothacher et al. 1967). In order to represent the additional water holding capacity available in these underlying soils, it was necessary to adjust hydraulic conductivity parameters in MAPSS-W. The MAPSS-W soil hydrology parameters are discussed further in chapter 3.

Percent rock fragment is used to calculate effective depth in MAPSS-W. The map units of soil series phase designated in the small watershed survey are based on percent rock fragment measurements. Rock fragment measurements varied between 0 and 75% (Dyrness, 1969). Overall, percent rock fragment is higher in the small watershed survey compared to the 1964 survey. The 1964 survey designated more than 80% of WS 1 as 20% rock fragment, in comparison, the small watershed survey designated more than 80% of the watershed as 25-50% rock fragment. In WS 2, the 1964 survey designated more than 80% of the watershed area as 20% rock fragment or less, in comparison, the

small watershed survey designated more than 80% of the watershed area as 35% or more rock fragment.

## **2.4 Discussion**

### **2.4.1 Spatial Considerations**

The comparisons of 30m and 200m elevation datasets highlights the importance of choosing an appropriate resolution to represent the watershed of interest. Resolution and scale are integral to the representation of landscape heterogeneity. The 200m resolution does not provide much detail in WS 1 & 2. The distinction between hillslope and riparian areas were lost at this resolution. This distinction was key for the consideration of vegetation-hydrology interactions hypotheses. It should also be noted that spatially distributed watershed models implicitly integrate the small scale processes of water movement to create landscape scale patterns.

### **2.4.2 Data Extrapolation**

In order to model landscapes in a spatially explicit manner, environmental variables must be available as spatially distributed datasets. Environmental variables are generally measured as point measurements, which must be extrapolated to the landscape. Spatial distribution of point data is often performed based on the topographic variables; slope, elevation, and aspect. Data distributions are often performed as a linear or non-linear interpolation between two measurements sites based on one or more of these topographic variables.

The precipitation data for this application of MAPSS-W were distributed based on a multiple linear interpolation based on elevation and aspect. This interpolation was performed using PRISM (Daly et al., 1994). The temperature, vapor pressure and wind speed distributions were based on simple linear interpolations based on elevation. These

distributions could be improved by including aspect in a multiple linear interpolation, as this would adjust the data sets for the influences of solar radiation. In order to create these datasets measurements would need to be taken throughout the small watersheds or the distribution would need to be based on a network of sites surrounding the small watersheds.

## **2.5 Conclusions**

This chapter described the data sources and distribution methods used to create the gridded datasets required for MAPSS-W simulations. Multiple datasets were created for some climate and soils variables in order to improve the spatial representation of these variables. The differences between these alternative datasets were discussed and simulation results are presented and discussed in Chapter 3.

Comparison of 30m and 200m grid resolution provided insight into the importance of choosing a resolution that adequately represents the area of interest. WS 1 & 2 are small watersheds of 1km<sup>2</sup> and .6km<sup>2</sup> respectively. The 30m resolution allows these watersheds to be represented as distinct, well-defined areas with well defined stream channels. Increasing the resolution to 200m decreases the distinction between stream and hillslope areas. The size and topography of an area should be considered when grid cell resolution is chosen for spatially explicit modeling applications.

There were several key assumptions made in the development of these climate distributions, which introduce errors into the model results. The distributed temperature datasets were not corrected for the influence of solar radiation. In the Pacific Northwest radiation loads and temperatures are higher on south aspects than on north aspects (Cleary et al., 1978). WS 1 & 2 face north-northwest and have distinct solar radiation regimes on the north and south facing hillslopes. Additionally, the temperature measurements taken at CS2met represent the temperature within an old-growth forest gap. While this may be appropriate for the pre-harvest simulations, it is likely that the air temperature regime in post-harvest WS 1 was more extreme (higher and lower) than the temperatures recorded at CS2met.

The accuracy of the vapor pressure datasets was limited by the lack of correction for solar radiation in the temperature datasets. Temperature and relative humidity were measured in an old-growth gap. Like the temperature measurement, the measurement of relative humidity at CS2met is likely representative of pre-harvest WS 1, but the humidity regime in post-harvest WS 1 was likely more extreme (higher and lower) than the relative humidity values recorded at CS2met. Additionally, using a single relative humidity value for every grid cell, ignores the influence of aspect, slope location (riparian, mid-slope, or ridge), shading, and canopy cover on relative humidity values.

The wind speed datasets are based on the assumptions that wind patterns can be adequately represented by an average wind year. The correlation between wind speed and the other climate variables (precipitation, temperature and vapor pressure) is lost when average wind speed data are used. However, it was necessary to create an average wind year, because the available wind speed records are incomplete and begin in 1973. These wind speed datasets are also based on the assumption that measurements, taken at meteorological stations that are influenced by different landforms and aspects, will adequately represent wind speeds in the small watersheds. Primet and Vanmet are in locations where the wind patterns may be significantly different from those in WS 1 & 2. Primet is located in the Lookout Creek valley and protected by a ridge to the west. Vanmet is located in the upper elevations of the Lookout Creek drainage and faces south. WS 1 & 2 face north-northwest. The seasonal wind speed patterns and wind speed magnitudes are distinct at Primet and Vanmet. It is quite possible that the wind patterns in WS 1 & 2 are distinct as well.

As with any gridded representation of environmental variables, all of the distributed datasets created for this application of MAPSS-W assume homogeneity and pattern that are not realistic at finer resolutions. The 30m datasets provide substantial heterogeneity within the watershed areas. WS 1 was represented by 1150 grid cells and WS 2 was represented by 665 grid cells.

### **3. Chapter 3: Calibration and Evaluation of MAPSS-W for Application at the HJ Andrews Experimental Forest**

#### **3.1 Introduction**

The MAPSS-W (Daly, 1994) watershed model calculates site water balance and vegetation growth based on spatially distributed topography, climate, soils, and vegetation datasets and a number of adjustable environmental parameters. It is expected that different environments will require different environmental parameter values (Franks et al., 1997). Whereas, the current application of MAPSS-W is for watersheds in the western Cascades, the previous application of MAPSS-W was for the Upper Reynolds Creek basin in Idaho. These locations have distinct precipitation and snowpack regimes, and different soils and vegetation. Therefore, it was necessary to adjust a number of the environmental parameters in order to simulate the hydrologic response of watersheds 1 & 2 (WS 1 & 2) in the H.J. Andrews Experimental Forest.

MAPSS-W parameter values were based on measurements and estimates made at the Andrews. This chapter discusses the rationale for key parameter values and the simulation comparisons used to evaluate model function. In the process of calibrating MAPSS-W for the Andrews watersheds, sensitivity analyses were performed on single environmental parameters. Sensitivity analysis results are presented, along with the comparisons between the Andrews parameterization and the Reynolds Creek parameterization. Additionally, simulation results are presented for model runs which used the alternative climate and soils input datasets described in chapter 2.

#### **3.2 Background**

##### **3.2.1 Streamflow Measurements**

Concrete trapezoidal flumes, with cutoff walls to bedrock, were installed in WS1 & 2 in the fall of 1952 (Rothacher et al., 1967). Streamflow has been measured in these

watersheds continuously since flume installation. Streamflow is measured as gage height on a continuous-strip-chart recorder and converted to cubic feet per second (cfs), cubic feet per second per square mile (cfs/m) and area inches (Rothacher et al., 1967).

Annual streamflow patterns are closely related to annual precipitation patterns in these watersheds. Mean monthly streamflows in WS 1 & 2 reach maximum levels between December and March and are at a minimum in August. Monthly streamflow is highly variable between November and May, and is dependent on storm patterns. Monthly streamflow is relatively uniform during the lowflow period between June and September. These seasonal patterns are illustrated in Figures 3-1a & b. Figure 3-1a shows monthly streamflow from the four pre-harvest water years used for model calibration and evaluation. Figure 3-1b shows monthly streamflow from the twelve water years of interest used for model calibration and evaluation.

### **3.2.2 MAPSS-W**

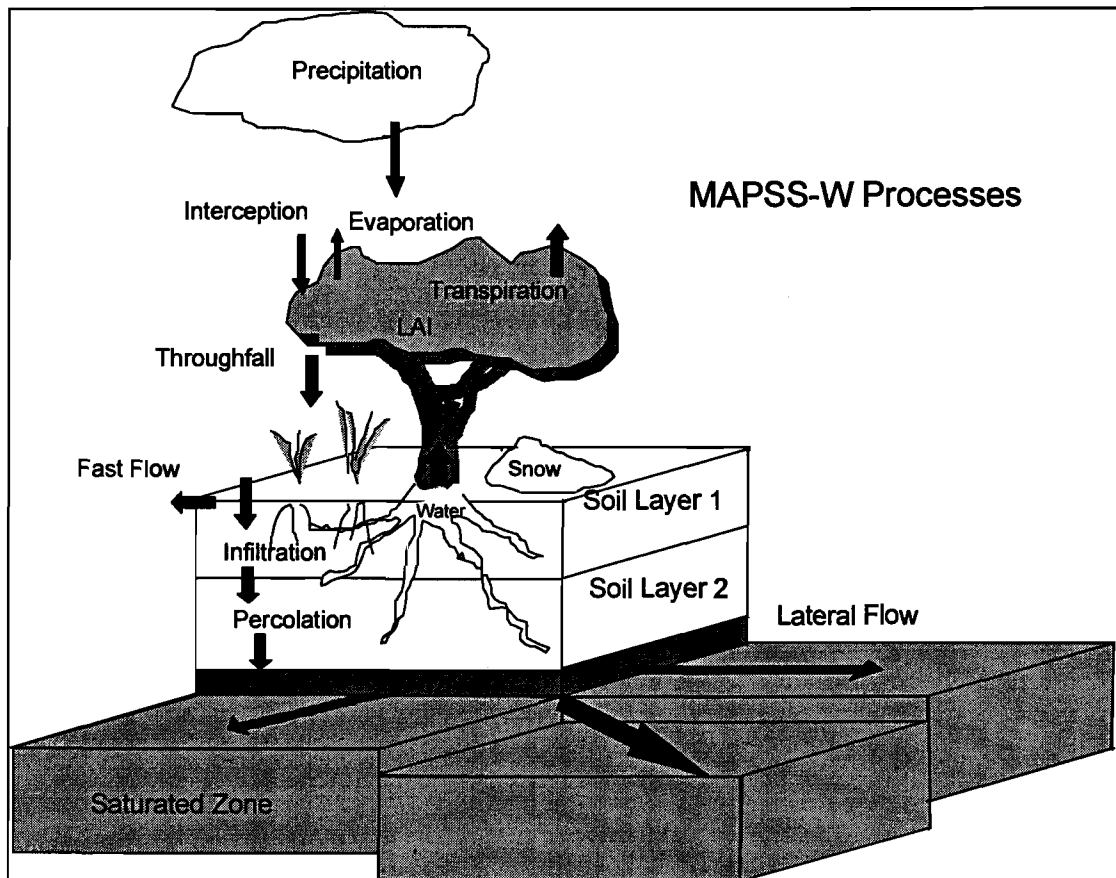
The spatially explicit, watershed model, MAPSS-W (Daly, 1994), simulates water balance processes and vegetation growth at a daily time-step. MAPSS-W (Daly, 1994) is a result of a linkage of the aboveground processes of the biogeography model, MAPSS (Mapped-Atmosphere-Plant-Soil-System) (Neilson, 1995), with the belowground processes of the watershed model, DHSVM (Wigmosta, 1994). The processes simulated by MAPSS-W are illustrated in Figure 3-2 and include: partitioning of precipitation between snow and rain, canopy interception and evaporation of rain, snowmelt, infiltration, percolation, competition for water and transpiration by woody and herbaceous vegetation, competition for light between woody and herbaceous vegetation, and lateral routing of water between grid cells.

MAPSS-W, like MAPSS, is based on the theory that maximum leaf area production is primarily a function of available soil moisture and plant water requirements (Woodward, 1987). Transpiration represents plant water use and is calculated as a function of potential evapotranspiration (PET) (Neilson, 1995). The turbulent transfer model (Marks, 1990) is used in MAPSS-W to calculate PET. This makes MAPSS-W sensitive to temperature gradients, humidity gradients, wind speed and surface



conditions. Actual transpiration(AT) is calculated as a function of PET, and is constrained by soil moisture, maximum stomatal conductance, and leaf area (Neilson, 1995). MAPSS-W simulates water balance processes and vegetation growth for a single water year. Antecedent soil moisture and vegetation conditions are calculated during model initialization (Daly, 1994).

**Figure 3-2 : Schematic of Processes Represented in MAPSS-W**



Adapted from Daly (1994)

Three vegetation lifeforms (trees, shrubs and herbs) are represented in MAPSS-W. Vegetation leaf area is represented by spatially distributed layers of leaf area index (LAI). LAI is defined in MAPSS and MAPSS-W as a measure of the functional (transpiring) leaf area per unit of ground ( $m^2/m^2$ ) (Daly, 1994 & Neilson, 1995). For previous applications

of MAPSS and MAPSS-W, functional LAI was defined as all-sided LAI (Neilson, 1995 & Daly, 1994). For this application of MAPSS-W, functional LAI was defined as single-sided LAI. This definition was based on the observation that most of the dominant woody species in WS 1 & 2 have concentrations of stomata on one side of the leaf (Conard & Radosevich, 1981; Pezeshki & Hinkley, 1982; Johnson & Ferrell, 1983).

Woody LAI is assumed to remain static throughout the water year and is provided to the model as two spatially distributed data layers (trees and shrubs). Woody LAI is a combination of both tree and shrub LAI. MAPSS-W uses one woody vegetation parameterization (tree or shrub) for each grid cell, based on a dual LAI threshold that designates the woody LAI as tree or shrub canopy. Woody vegetation can be parameterized as evergreen or deciduous in each grid cell, but the transpiration parameters are the same for each lifeform for the entire grid. This means that MAPSS-W only represents the difference in seasonal activity between evergreen and deciduous vegetation and does not represent differences in stomatal function.

In MAPSS-W, herbaceous vegetation is increased or decreased daily based on water balance calculations. These calculations include competition for water between herbaceous and woody vegetation in the top soil layer (0.5m). Woody vegetation access water from the top and middle soil layers to a maximum depth of 1.5m (Neilson, 1995). Competition for water from the top soil layer is calculated based on the proportion of woody to herbaceous canopy conductance and LAI.

The herbaceous growth rate is a function of temperature and available water. The seasonal presence or absence of herbaceous LAI is a function of soil moisture, frost, and snow cover (Daly, 1994). Maximum herbaceous LAI is an inverse linear function of woody LAI (Neilson, 1995).

Liquid water at the soil surface is partitioned to fast flow, which includes overland and macropore flow, or to infiltration and percolation through the soil layers (Neilson, 1995). Infiltrated water is available to plants, the water not transpired by the woody and herbaceous vegetation percolates to the third soil layer. The third soil layer represents a fractured bedrock layer and lateral flow occurs in the third soil layer (Daly, 1994). MAPSS-W incorporates the DHSVM lateral flow algorithms which are based on the assumption that downslope movement of water can be best described by surface topography, due to the dominant influence of gravitational potential in steep terrain

(Wigmosta, 1994). Lateral water routing is based on the differences in elevation and slope between each grid cell and the surrounding eight grid cells (Wigmosta, 1994).

### **3.3 Materials & Methods**

#### **3.3.1 HJA WS 1 & 2 Measured Streamflow**

Average daily and monthly streamflow records were obtained from the Forest Service Data Bank (FSDB). The area inch streamflow records were converted to area mm units for simulation comparison purposes. Calibration and evaluation comparisons of MAPSS-W simulated streamflow were made against monthly and daily total streamflow measurements. Twelve water years (October 1 - September 30) were used for MAPSS-W calibration and evaluation. The twelve water years of interest (1958-61, 1967, 1968, 1972, 1973, 1979, 1980, 1990, 1991) were chosen to correspond with the five distinct periods identified in the WS 1 streamflow record by Hicks et al (1991). The pre-harvest period was followed by a rapid rise in summer streamflow levels during harvest and an equally rapid decline once harvest was completed. The return to pre-harvest summer streamflow levels is followed by a period of summer streamflow deficits, which is followed by a second return to pre-harvest summer streamflow levels. These streamflow changes are discussed more extensively in Chapter 4.

#### **3.3.2 HJA - MAPSS-W Parameterization**

The previous MAPSS-W calibration was for the Upper Reynolds Creek Sub-basin of the USDA-Agricultural Research Service's Reynolds Creek Experimental Watershed (Daly, 1994). The climate, topography, soils, and vegetation at Reynolds Creek basin are quite different from those of the Andrews WS 1 & 2. Due to the environmental differences between Reynolds Creek and WS 1 & 2 at the Andrews, parameter adjustments were necessary for the current application of MAPSS-W.

This application of MAPSS-W was used to investigate successional vegetation influences on streamflow following timber harvest. In the process of developing this parameterization of MAPSS-W, sensitivity analyses were performed for key model parameters. Initial simulations using the Reynolds Creek parameters indicated that snow dynamics, soil hydrology, vegetation structure and transpiration parameters would need to be adjusted to adequately represent the Andrews WS 1 & 2. The Andrews parameterization of MAPSS-W was based on descriptive and quantitative information available for the snow dynamics, soil hydrology characteristics, and the structure and function vegetation in WS 1 & 2. Additional parameter adjustments were made based on comparisons of simulated streamflow to measured streamflow records. Table 3-1 summarizes the parameter changes made for the Andrews simulations.

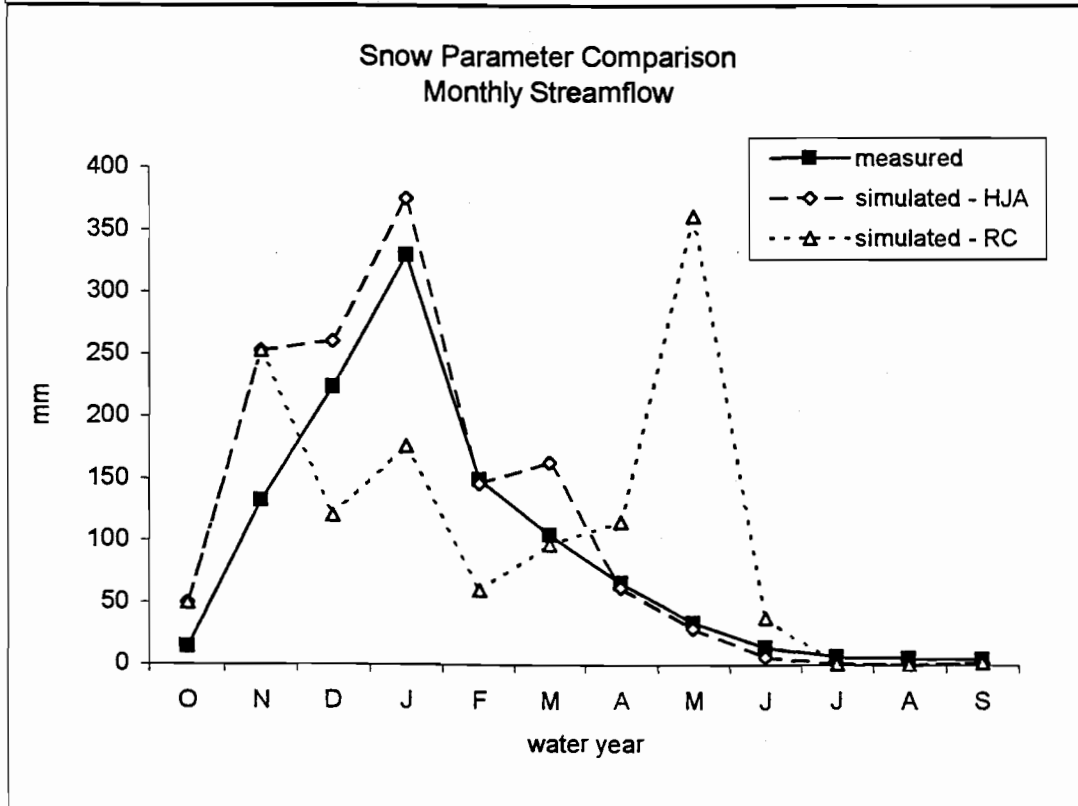
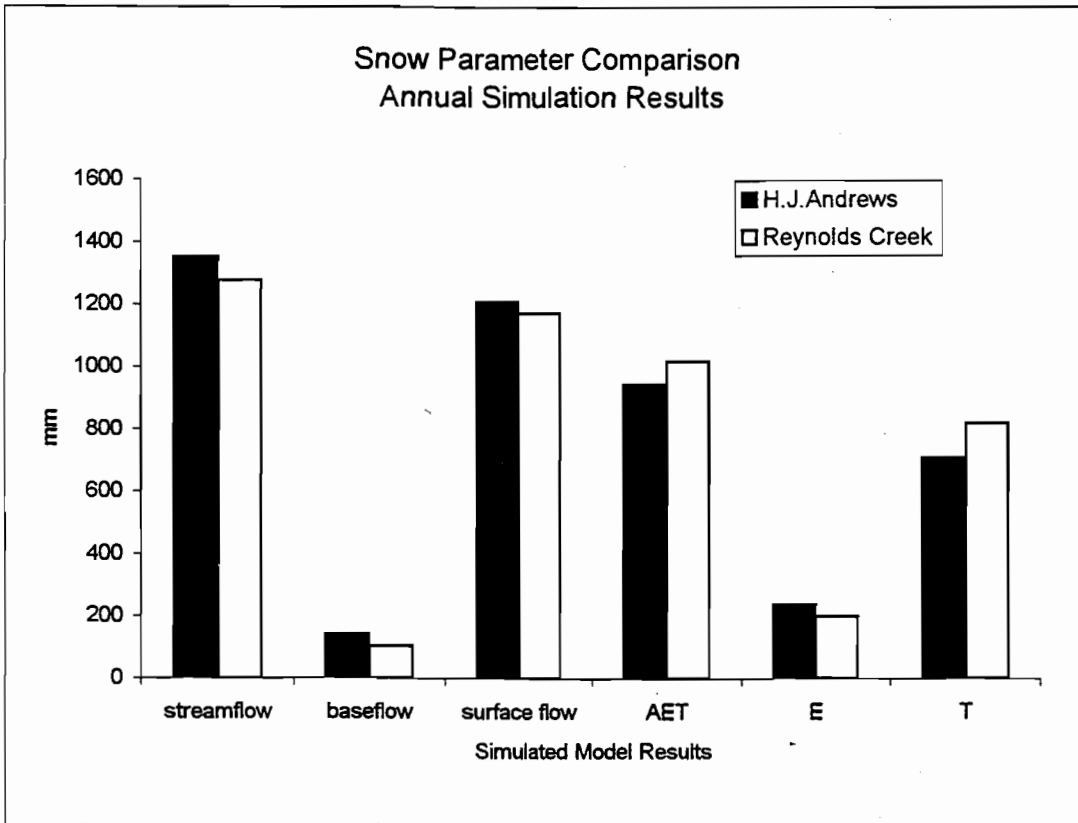
After the Andrews calibration was completed, comparisons of model output variables were made between the Reynolds Creek parameterization, and the Andrews parameterization. Following calibration and evaluation, experimental simulations were run to explore hypotheses about the hydrologic influences of vegetation on streamflow during post-harvest vegetation succession. The experimental runs will be discussed in Chapter 4.

Once it was determined that a new parameterization was necessary for the Andrews WS 1 & 2, water year 1959 (WY 59) was chosen for preliminary calibration. Calibration of all watershed characteristics simultaneously (snow, soil hydrology and vegetation) proved difficult and calibration was simplified using water year 1967 (WY 67) for WS1. This simplified the system by removing the vegetation, as water year 1967 is the first year following the 100% clear-cut and broadcast burn in WS1. Once the parameters for snow dynamics and soil hydrology were adjusted, the calibration was completed for vegetation parameters using WY 59. Evaluations of the Andrews parameters were performed for both watersheds using data from pre-harvest water years 1958, 1960, and 1961. Additional evaluation simulations were performed for WS 2 using data from water years 1968, 1972, 1973, 1979, 1980, 1990, and 1991. These simulations were also used in the experimental comparisons discussed in Chapter 4.

**Table 3-1: Key MAPSS-W Parameters (Reynolds Creek & H.J. Andrews values)**

	RC	HJA	Parameter	name in parameter file	units	description
<b>Snow</b>						
	3.0	1.0	$T_u$	snow0	°C	Temperature above which snowfall fraction equals 0
	1.0	-1.0	$T_l$	snow1	°C	Temperature below which snowfall fraction equals 1
	2.5	0.0	$T_{nm}$	no_melt	°C	Temperature below which snow does not melt
	3.0	16.0	$k_m$	melt_slope	mm/°C	Coefficient for snow melt rate
<b>Soil Hydrology</b>						
	3.8	1.5	$k_{surf}$	k_surfrun	-	Coefficient for surface runoff/macropore flow
	0.063	0.010	$k_{s_{vert}}$	ks_vertical	mm/hr	Saturated vertical hydraulic conductivity
	0.012	0.002	$k_{s_{lat}}$	ks_lateral	mm/hr	Saturated lateral hydraulic conductivity
	5.0	3.0	f	lateral flux coefficient	-	Coefficient for decrease if lateral flux with depth
	0.49	0.55	p	porosity	percent	Soil porosity
<b>Seasonality</b>						
	7.0	3.0	$T_f$	frost	°C	Temperature below which grass and deciduous woody LAI are set to zero
<b>Leaf Area</b>						
	15.0	20.0	$LAI_{max}$	max_LAI	m <sup>2</sup> /m <sup>2</sup>	Maximum LAI for AT normalization
	0.3	5.0	$LAI_i$	interc_LAI	mm	maximum precipitation interception per day
	5.0	15.0	$LAI_{full}$	full_atten_LAI	m <sup>2</sup> /m <sup>2</sup>	Woody LAI for full light attenuation
<b>Transpiration</b>						
	2.0	12.0	$Z_{g,t,s}$	z(G,T,S)	m	wind speed measurement height
	0.0005	0.0050	$z0_g$	z0(G)	-	roughness length coefficient(herbaceous)
	0.0100	0.2000	$z0_t$	z0(T)	-	roughness length coefficient(tree)
	0.0010	0.0100	$z0_s$	z0(S)	-	roughness length coefficient(shrub)
	1.0	1.0	$Co_s \min_g$	cond_min (G)	mm/sec	Minimum stomatal conductance for grass
	1.5	1.0	$Co_s \min_t$	cond_min (T)	mm/sec	Minimum stomatal conductance for trees
	0.8	0.8	$Co_s \min_s$	cond_min (S)	mm/sec	Minimum stomatal conductance for shrubs
	3.5	3.5	$Co_s \max_g$	cond_max (G)	mm/sec	Maximum stomatal conductance for grass
	2.5	3.5	$Co_s \max_t$	cond_max (T)	mm/sec	Maximum stomatal conductance for trees
	1.5	5.0	$Co_s \max_s$	cond_max (S)	mm/sec	Maximum stomatal conductance for shrubs
	-1.5	-2.0	$wp_g$	wp(G)	MPa	permanent wilting point for grass
	-1.5	-2.2	$wp_t$	wp(T)	MPa	permanent wilting point for trees
	-1.5	-5.0	$wp_s$	wp(S)	MPa	permanent wilting point for shrubs

Figure 3-3 a & b: Snow Parameters Comparison Annual & Monthly Results



### 3.3.2.1 Snow Dynamics

An initial MAPSS-W simulation using the Reynolds Creek parameters with the Andrews datasets produced an annual streamflow value close to the measured value, but examination of the total monthly streamflows showed that there was too much streamflow during April and May and not enough during the winter months (Figure 3-3a & b). These results were caused by the snow parameter values.

MAPSS-W partitions precipitation to rain or snow based on a dual temperature threshold (Neilson, 1995). All precipitation falls as snow when temperatures are below the lower temperature threshold ( $T_l$ ) and as rain when temperatures are above the upper temperature threshold ( $T_u$ ). Precipitation is proportioned between rain and snow when the temperature is between the upper and lower temperature thresholds. Snowmelt is based on a single temperature threshold ( $T_{nm}$ ) and the rate of snow melt is regulated by a snowmelt coefficient ( $k_m$ ) (Neilson, 1995). It was necessary to decrease the temperature thresholds and increase the snowmelt coefficient in order to simulate the transient snow dynamics which occur in WS 1 & 2.

The lower elevation areas of the Andrews have been described as having a transient snow regime. Snow generally lasts 3-4 days and is patchy, persisting longer on north-facing slopes (Rothacher, 1963). Monthly snow observations taken along the ridges and at the stream gages of WS 1 & 2, in 1958-61, 1967, 1968, 1972, 1973, describe patchy snow accumulation in clearings, ephemeral snow pack conditions and little snow under the old-growth canopy (snow data, FSDB). Measurements of snow moisture have are taken at two meteorological stations in the Andrews, Vanmet and Uplmet, but both are located above the maximum elevation of WS 1 & 2. Both develop substantial snowpacks during the winter. The average snow water equivalent for these sites is 450mm (snow data, FSDB). The National Resource Conservation Service snow telemetry data base was also examined for appropriate snow comparison sites, but all surrounding measurement sites are located above the maximum elevation of the transient snow zone (1100m a.m.s.l.). Due to these snow data limitations for the WS 1 & 2 elevation range (450-1100m a.m.s.l.), the snow parameters were calibrated based on comparisons of simulated and measured streamflow.

### 3.3.2.2 Soil Hydrology

The key soil hydrology parameters in MAPSS-W are saturated vertical and lateral hydraulic conductivity ( $k_{\text{vert}}$  and  $k_{\text{lat}}$ ), the surface-baseflow coefficient ( $k_{\text{surf}}$ ), the lateral flux coefficient ( $f$ ), and porosity ( $p$ ). The MAPSS-W saturated vertical and lateral hydraulic conductivity parameters were set to represent low hydraulic conductivity rates, contrary to the high rates of hydraulic conductivity measured in WS 1, 2, & 10 (Dyrness, 1969; Harr, 1977). This was necessary in order to represent the true soil depths in the watershed. MAPSS-W limits soil depth to 1.5m, but the soils and fractured bedrock in WS 1 & 2 may extend to a depth of 16m (Dyrness, 1969). In order to represent this water storage capacity in MAPSS-W it was necessary to decrease the rate of water movement through the soil.

The surface-baseflow coefficient and the lateral flux coefficient values were based on comparisons of measured and simulated streamflow. The surface-baseflow and lateral flux coefficients were adjusted to increase baseflow and decrease surface flow. These adjustments also increased MAPSS-W soil water storage. The porosity parameter value was based on measurements of at least 50% pore space in undisturbed soils in WS 1, 2 & 10, to a depth of at least 1.5m (Dyrness, 1969; Harr, 1977).

### 3.3.2.3 Seasonality

The temperature threshold that determines the deciduous and herbaceous vegetation growing season was decreased to 3°C in order to extend the simulated growing season. The Reynolds Creek parameter value of 7°C limited the growing season to May-October. The growing season in WS 1 & 2 is generally March-December (Rothacher et al., 1967). Extending the simulated growing season allowed deciduous and herbaceous vegetation to take advantage of available soil moisture during the mild spring and fall months.

### 3.3.2.4 Leaf Area

The MAPSS-W leaf area index (LAI) parameters were adjusted to better represent the dense, multi-layered forest canopy in WS 1 & 2. The LAI values measured in the western Cascades are some of the highest in the world (Gholz et al., 1976). LAI estimates for conifers in the Pacific Northwest range between 3 and 19  $\text{m}^2/\text{m}^2$  and may reach 22  $\text{m}^2/\text{m}^2$  in dense stands (Waring & Franklin, 1979). These high LAI values have substantial influence on the interception and evaporation of precipitation, and the distribution of understory vegetation. The maximum LAI parameter ( $\text{LAI}_{\text{max}}$ ) was increased to accommodate the regions high LAI values.

The high LAI values in conifer stands are due to the clustering effect of the needles along the branches. This allows deep penetration of light into the stand (Schulze, 1982). The full attenuation parameter ( $\text{LAI}_{\text{full}}$ ) was set at 15 to allow some herbaceous growth under the conifer canopy. This parameter setting was based on observations of herbaceous vegetation communities in old-growth Douglas-fir stands (Rothacher et al., 1967; Dymess, 1973).

The rainfall interception parameter ( $\text{LAI}_i$ ) was increased to represent the large amount of interception that occurs in Pacific Northwest forests. Under dense stands of old-growth Douglas-fir, in western Oregon, interception averages 24% of summer precipitation and 14% of winter precipitation (Rothacher, 1963). High leaf area and dense communities of epiphytes account for this high interception rate. The interception capacity of fir trees, in Russia, has been estimated to be 2.8 - 4.6mm per event, and may be as high as 6 - 8mm per event in dense stands (Shiklomanov & Kretovsky, 1988). In the Pacific Northwest, Douglas-fir storage has been measured to be 2.5mm per event, and was estimated to capture 10-35% of the total annual precipitation (Waring & Schlesinger, 1985). The Reynolds Creek parameters allocated less than 5% of the annual precipitation to interception evaporation. Increasing the interception value to 5mm per day allocates approximately 10% of annual precipitation to evaporation.

### 3.3.2.5 Transpiration

The parameters involved in the calculation of potential evapotranspiration (PET) and actual evapotranspiration (AET) are the basis for water balance calculations in MAPSS-W. Values for roughness length ( $z_0$ ), maximum and minimum stomatal conductance ( $Co_s$  max,  $Co_s$  min), and wilting point (wp) were determined from calculations based on reference stand canopy heights (Hawk et al., 1978) and literature values available for the dominant canopy species. Conifer stands are estimated to have a maximum daily transpiration of 6mm per day (Waring & Schlesinger, 1985). Total annual mature stand transpiration is estimated to be 300-600mm/year for conifers, 500-800 mm/year for deciduous broadleaf and 400-500 mm/year for sclerophylls (Larcher, 1995).

Roughness length is a measure of the aerodynamic roughness of the canopy surface and is one of the key parameters used to explore the hydrologic influences of vegetation in WS 1 post-harvest. The tree roughness length for pre-harvest simulations was calculated based on mean tree height measured in reference stands surrounding WS 1 (Hawk et al., 1978) and vegetation plots in WS2 (Halpern, unpublished). Reference stands 1,7,8,15,and 16 were chosen for their close proximity to WS 1. Additional tree height measurements have been taken in WS2 (Halpern, unpublished). These forest stands have similar vegetation to the pre-harvest vegetation in WS 1 (Hawk et al., 1978). The mean conifer canopy height is 35m (+/- 17m) in these stands. Using the Jarvis et al ( 1976) equation for coniferous forest roughness length,  $z_0$  was calculated to be 2.6m. Shrub and grass roughness lengths were increased due to the topographic roughness created by the steep slopes and the complex canopy structure. Tree roughness length was decreased from the calculated value of 2.6m to better match the summer streamflow levels.

Minimum stomatal conductance, maximum stomatal conductance, and wilting point values were based on literature values for the dominant species in each of the hydrologic functional groups (conifers, evergreen broadleaf, deciduous broadleaf, and herbs). These functional groups are described in greater detail in Chapter 4. Table 3-2 summarizes these transpiration and LAI values by hydrologic functional group based on data from Conard (1986), Larcher (1995), Pezeshki & Hinkley (1982), Running et al.

(1986), Schulze (1982), Shainsky et al. (1994), Waring & Schlesinger (1985), Waring & Franklin (1979), and Smith & Clark (1990).

**Table 3-2: Hydrologic Functional Groups - Vegetation Parameters**

	<b>conifer</b> (Douglas-fir)	<b>deciduous broadleaf</b> (red alder)	<b>evergreen broadleaf</b> (snowbrush)	<b>herbaceous</b>
Minimum Stomatal Conductance (mm/s)	1	1	.8	1
Maximum Stomatal Conductance (mm/s)	4	10	7	3.5
Permanent Wilting Point (MPa)	-2.2	-2.5	-5	-2.5
Range of reported single-sided LAI (m <sup>2</sup> /m <sup>2</sup> )	4 - 23	3 - 15	4 - 12	2 - 5

### **3.3.3 Sensitivity Analysis**

Throughout the process of model calibration, sensitivity analyses was performed on the MAPSS-W parameters described above. Snow dynamics and soil hydrology streamflow simulations results were assessed and adjustments to parameter values were made based on daily and monthly streamflow measurements from WS 1 & 2. These analyses focused on the annual and monthly simulation results of streamflow, baseflow, surface flow, and AET. The leaf area and transpiration variables were not assessed, because they were modified to test hypotheses about hydrologic mechanisms in the experimental simulations (Chapter 4).

### **3.3.4 Resolution & Parameterization Comparison**

Initial MAPSS-W simulations, using 30m datasets for WS 1 & 2, produced an annual streamflow surplus of 1000mm. These initial simulations indicated that model parameters would need to be adjusted to adequately represent watershed function in the western

Cascades. The resolution of the datasets in this application of MAPSS-W was a confounding factor in the assessment of model function, because the previous application of MAPSS-W used 200m resolution datasets. In order to determine if the dataset resolution had a significant influence on model results a comparison was made between simulations using 30m input datasets and 200m input datasets. These comparisons of dataset resolution were made for both watersheds using datasets for two pre-harvest water years (WY59 & WY60). The comparison was performed for both the Reynolds Creek parameterization and the Andrews parameterization. These comparisons were run using the default soil setting with a sandy loam texture and a uniform vegetation dataset, in which all grid cells have the same LAI values (trees (13), shrubs (1), herbs (.2)).

### **3.3.5 Data Comparisons**

Following the calibration and evaluation of MAPSS-W for WS 1 & 2, comparisons were made of simulation results from model runs based on the alternative climate and soils datasets developed in Chapter 2. These comparisons were made in order to establish model sensitivity to different climate and soils distributions. These comparisons focus on annual and monthly streamflow, and transpiration results.

## **3.4 Results**

Model output variables include daily and monthly total streamflow, baseflow, surface flow, potential evapotranspiration (PET), evaporation, transpiration, snowfall, snowpack and snowmelt. MAPSS-W also produces spatially distributed maps of surface runoff, baseflow, water table depth, lateral flow, soil water content in soil layers 1 & 2, snowpack water equivalent, functional herbaceous and woody LAI, herbaceous and woody stomatal conductance, and effective soil depth. Sensitivity analysis and data comparison results are presented as the differences between total annual streamflow, baseflow,

surface flow and AET. Additional monthly comparisons of streamflow, baseflow, surface flow and AET are presented for some comparisons.

### **3.4.1 Calibration - Single Parameter Sensitivity Analysis**

It should be noted that the simulation results presented for the single parameter sensitivity analyses are not based on the final Andrews parameter calibration. These comparisons are meant to show the relative difference between parameter values and were performed throughout the calibration process. For this reason these results are not compared to the measured streamflow values.

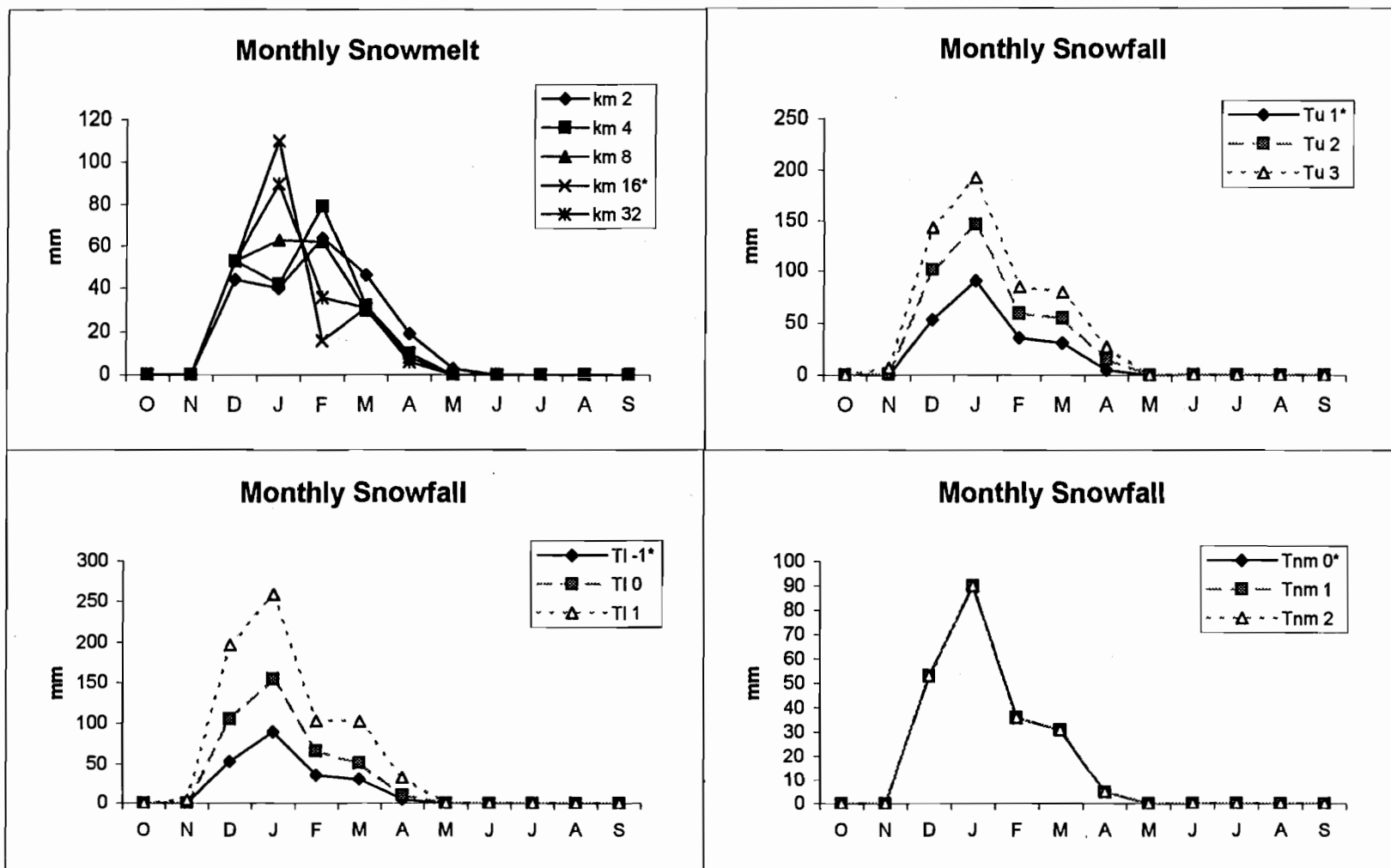
#### **3.4.1.1 Snow Dynamics**

While changes to snow parameters created less than 10mm difference in annual streamflow, changes in the snow formation thresholds caused substantial differences in monthly snowfall and snowmelt (Figure 3-4a,b,c,d). Changes in the snowmelt coefficient ( $k_m$ ) changed monthly snowmelt, these changes did influence the rate of snowmelt and the persistence of the snowpack. Snowmelt happened more slowly with lower snowmelt coefficient values. The timing of snowmelt was also influenced by the snowmelt temperature threshold ( $T_{nm}$ ), decreasing the threshold increased the rate of snowmelt. Snowfall increases when the snow formation thresholds ( $T_u$  &  $T_l$ ) are increased. For WS 1 & 2, these parameters were set to simulate a transient snowpack by lowering the snow formation thresholds and the snowmelt threshold and by increasing the snowmelt coefficient.

#### **3.4.1.2 Soil Hydrology**

Increasing the values of vertical and lateral saturated hydraulic conductivity increased streamflow, by increasing the rate of water flow through the system.

Figure 3-4a,b,c,d: Snow Parameter Comparison - Sensitivity Analysis Results



\*HJA parameter value

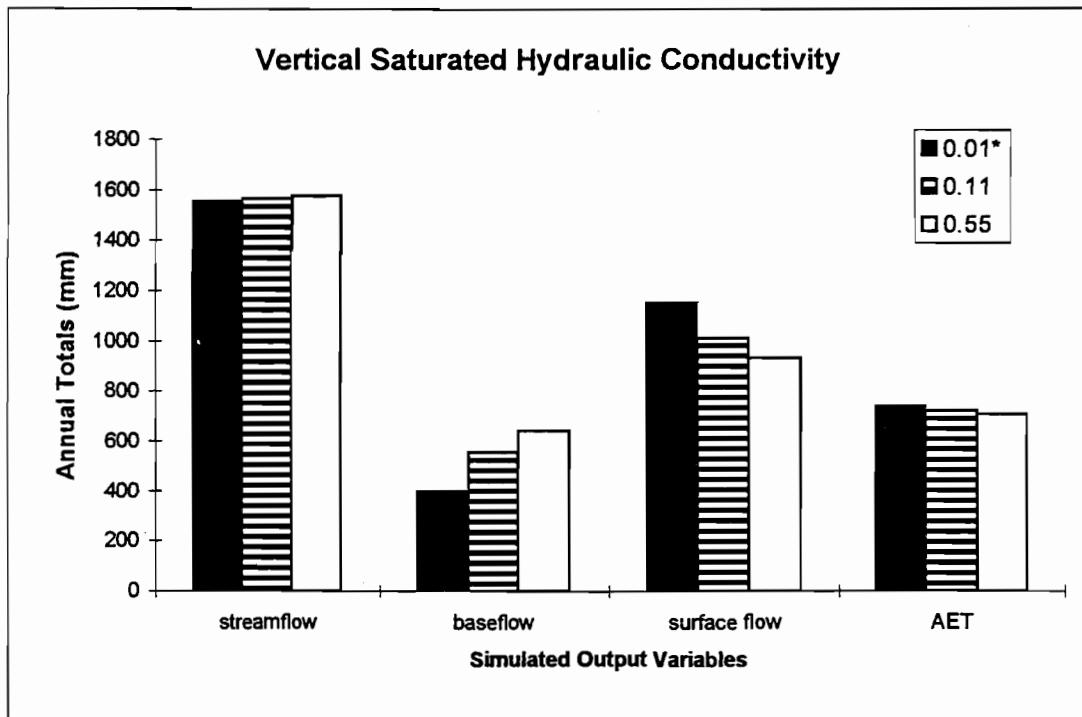
Increasing vertical and lateral saturated hydraulic conductivity values also increased baseflow and decreased surface flow. The annual differences in streamflow, baseflow, surface flow and AET are illustrated in Figure 3-5 & 3-6. Increasing the values of vertical and lateral saturated hydraulic conductivity increased streamflow in the fall and decreased streamflow in the winter. Changes in the patterns of baseflow and surface flow are most noticeable during the high precipitation, winter months. AET increased during the early summer when vertical saturated hydraulic conductivity was decreased. This increase in AET is due to an increase in the amount of water held in the soil when saturated hydraulic conductivity values are low. The patterns of monthly streamflow, baseflow, surface flow and AET are illustrated in Figures 3-7a,b,c,d & 3-8a,b,c,d.

Increasing the surface-baseflow coefficient decreased annual streamflow and increased AET. The maximum difference in annual streamflow is 50mm. The baseflow and surface flow patterns are more complex, the highest baseflow and lowest surface flow were simulated at a surface-baseflow coefficient setting of 2. The annual differences in streamflow, baseflow, surface flow, and AET are illustrated in Figure 3-9. Increasing the surface-baseflow coefficient increased baseflow and decreased surface flow in the early fall. Conversely baseflow was decreased and surface flow was increased during the winter, once saturated soil conditions were reached. The patterns of monthly streamflow, baseflow, surface flow and AET are illustrated in Figure 3-12a,b,c,d.

Increasing the lateral flux coefficient decreased annual streamflow and baseflow, and increased surface flow and AET. The annual differences in streamflow, baseflow, surface flow, and AET are illustrated in Figure 3-10. Increasing the lateral flux coefficient increased streamflow in the winter and decreased streamflow during the summer months. Monthly baseflow decreased and surface flow increased with an increase in the lateral flux coefficient. Monthly AET increased during the early summer with an increase in the lateral flux coefficient. These monthly streamflow, baseflow, surface flow, and AET patterns are illustrated in Figures 3-13a,b,c,d.

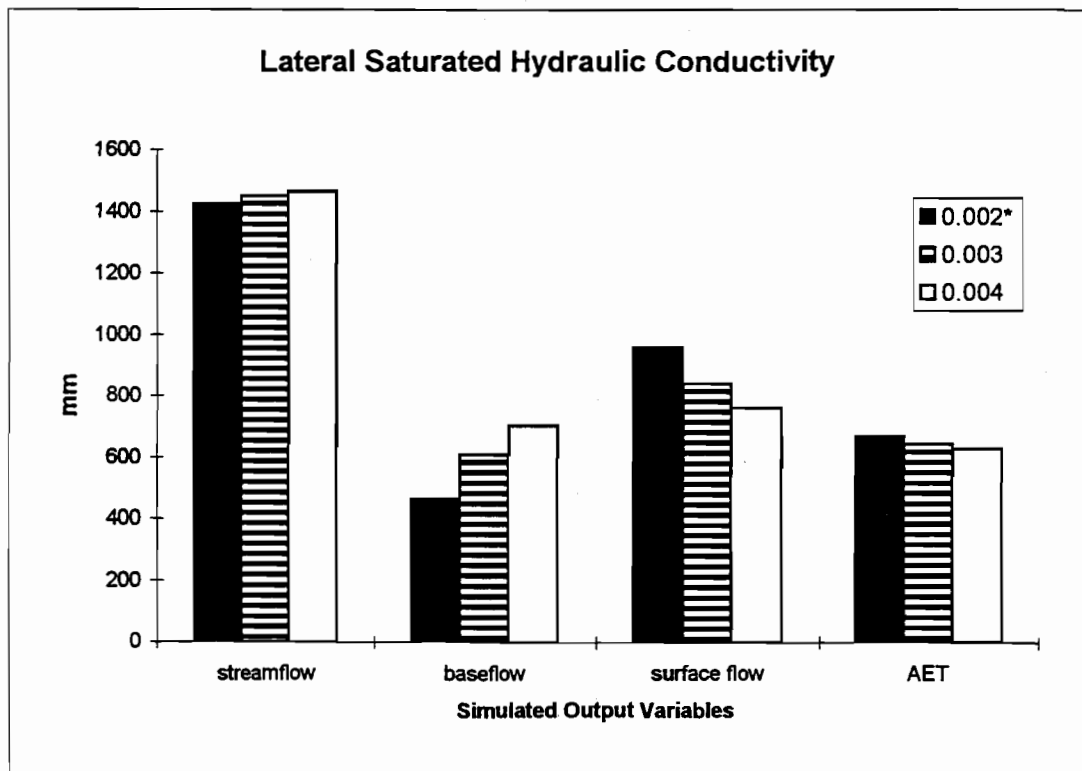
Increasing porosity decreased annual streamflow and baseflow and increased surface flow and AET. The annual differences in streamflow, baseflow, surface flow, and AET are illustrated in Figure 3-11. Increasing porosity decreased streamflow in the fall and spring. Baseflow was decreased and surface flow was increased throughout the year. An increase in porosity resulted in increased AET in the spring. These

Figure 3-5: Vertical Saturated Hydraulic Conductivity - Annual Results



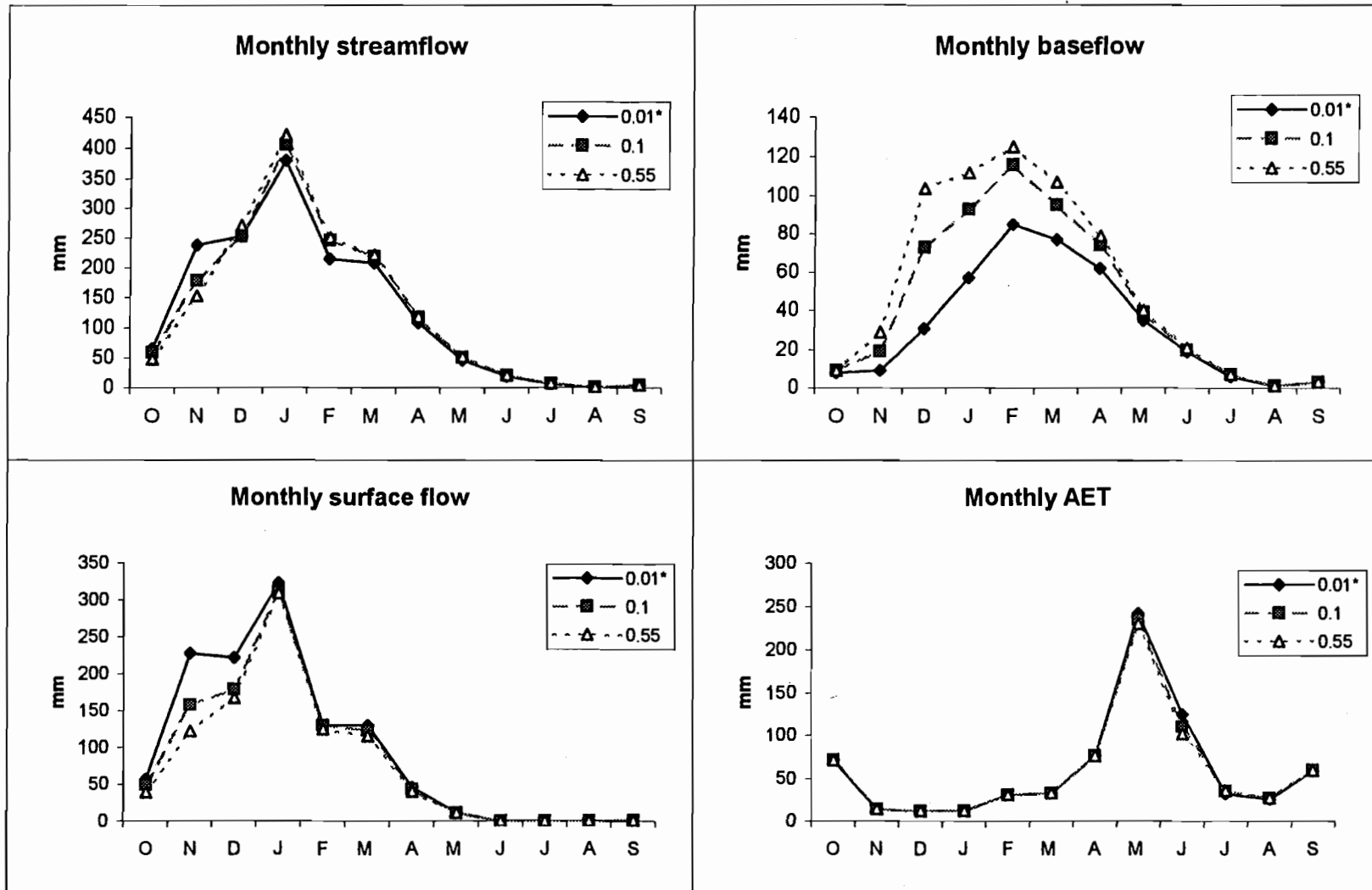
\*HJA parameter value

Figure 3-6: Lateral Saturated Hydraulic Conductivity - Annual Results



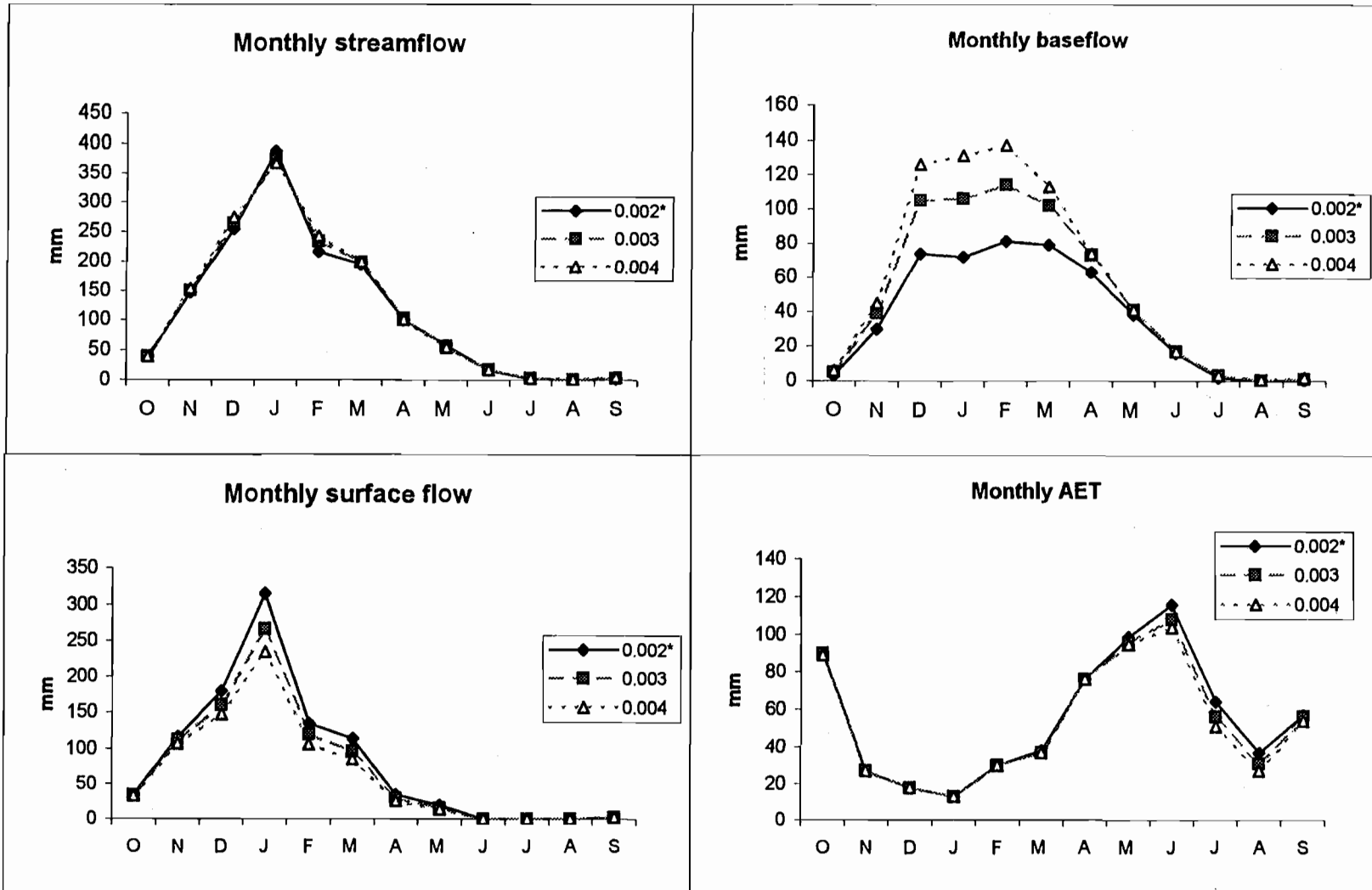
\*HJA parameter value

Figure 3-7a,b,c,d: Vertical Saturated Hydraulic Conductivity - Monthly Results



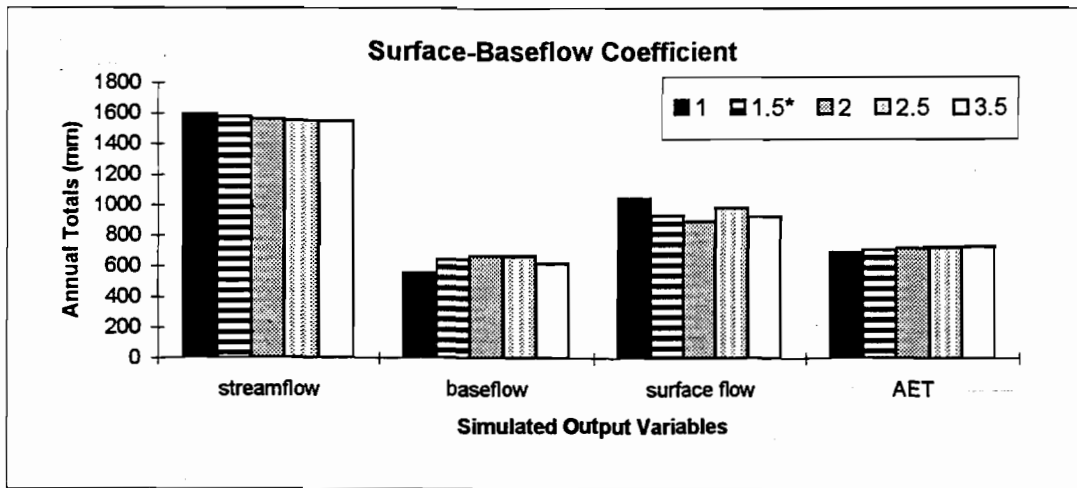
\*HJA parameter value

Figure 3-8a,b,c,d: Lateral Saturated Hydraulic Conductivity - Monthly Results



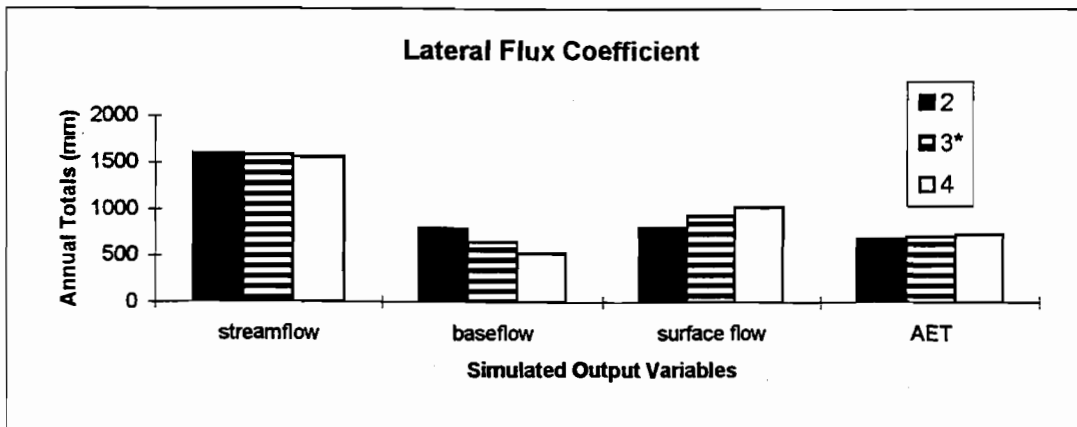
\*HJA parameter value

**Figure 3-9: Surface-Baseflow Coefficient - Annual Results**



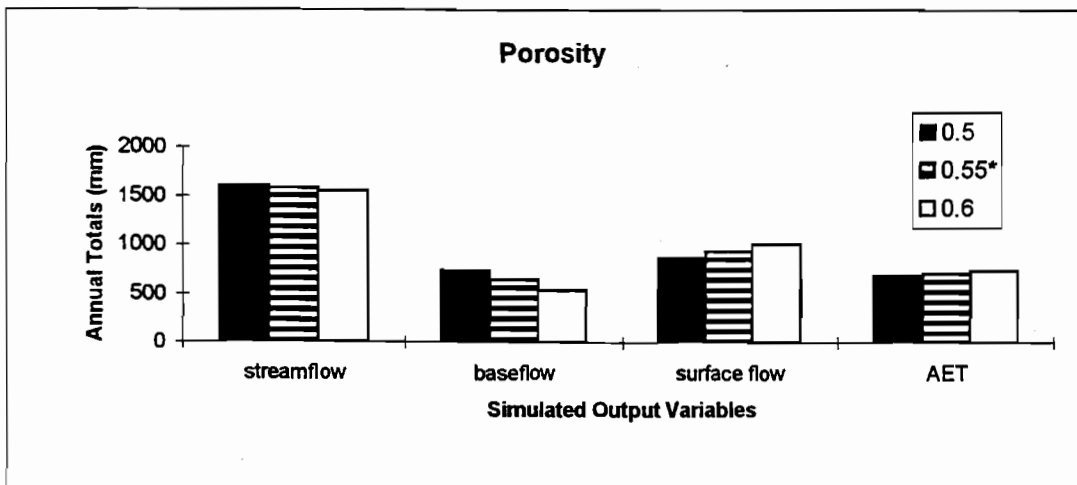
\*HJA parameter value

**Figure 3-10: Lateral Flux Coefficient - Annual Results**



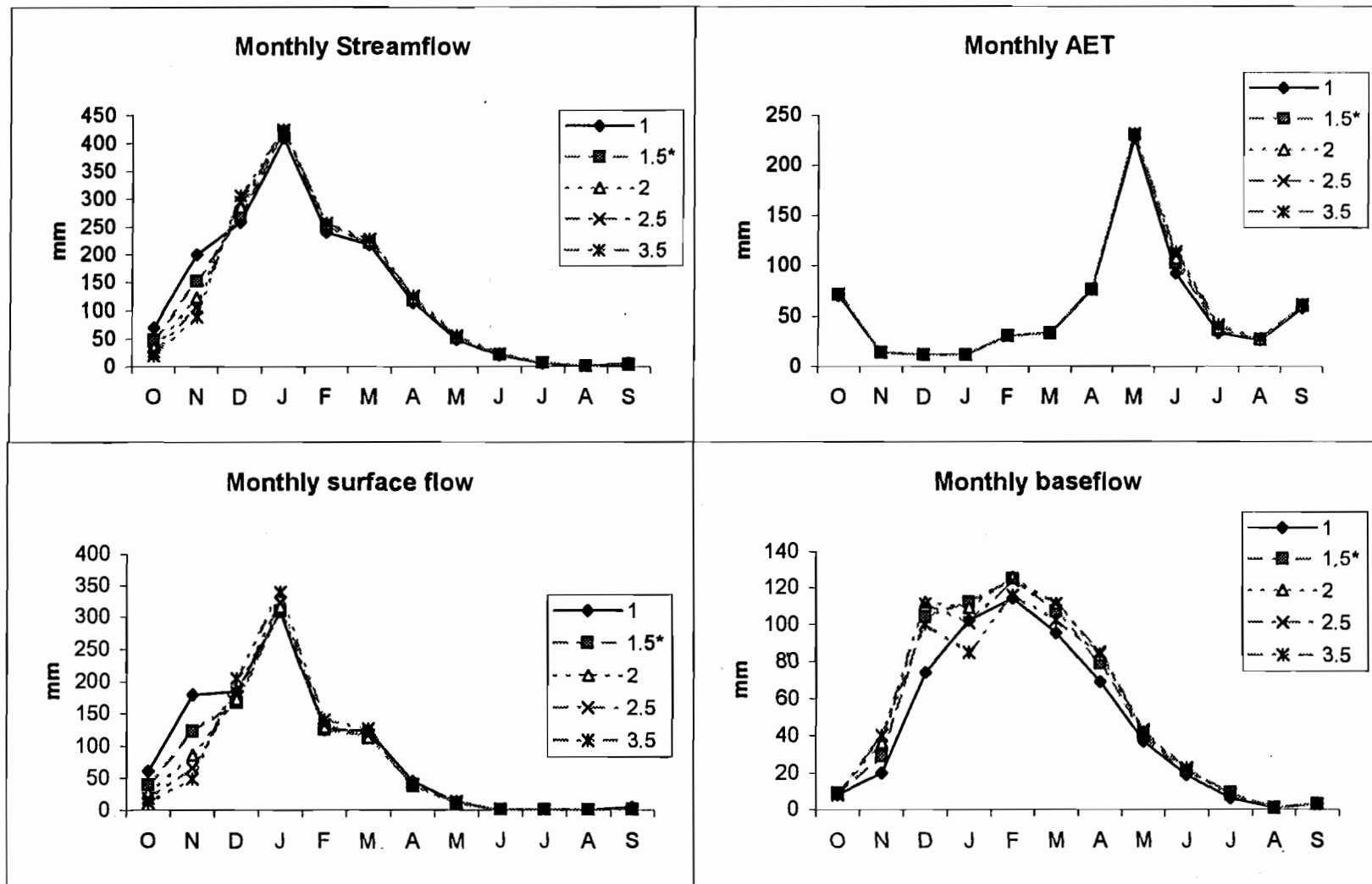
\*HJA parameter value

**Figure 3-11: Porosity - Annual Results**



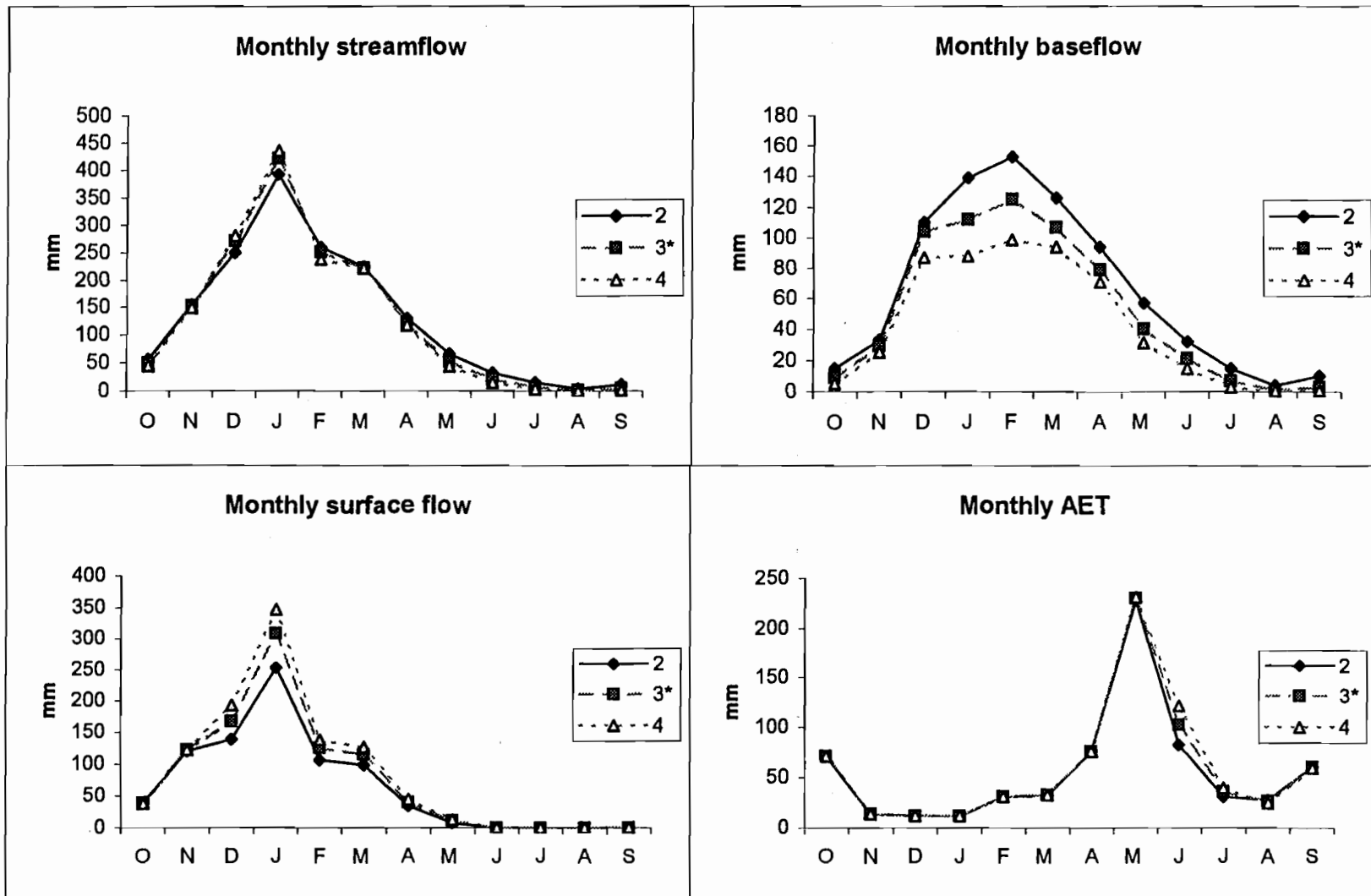
\*HJA parameter value

Figure 3-12a,b,c,d: Surface-baseflow coefficient - Monthly Results



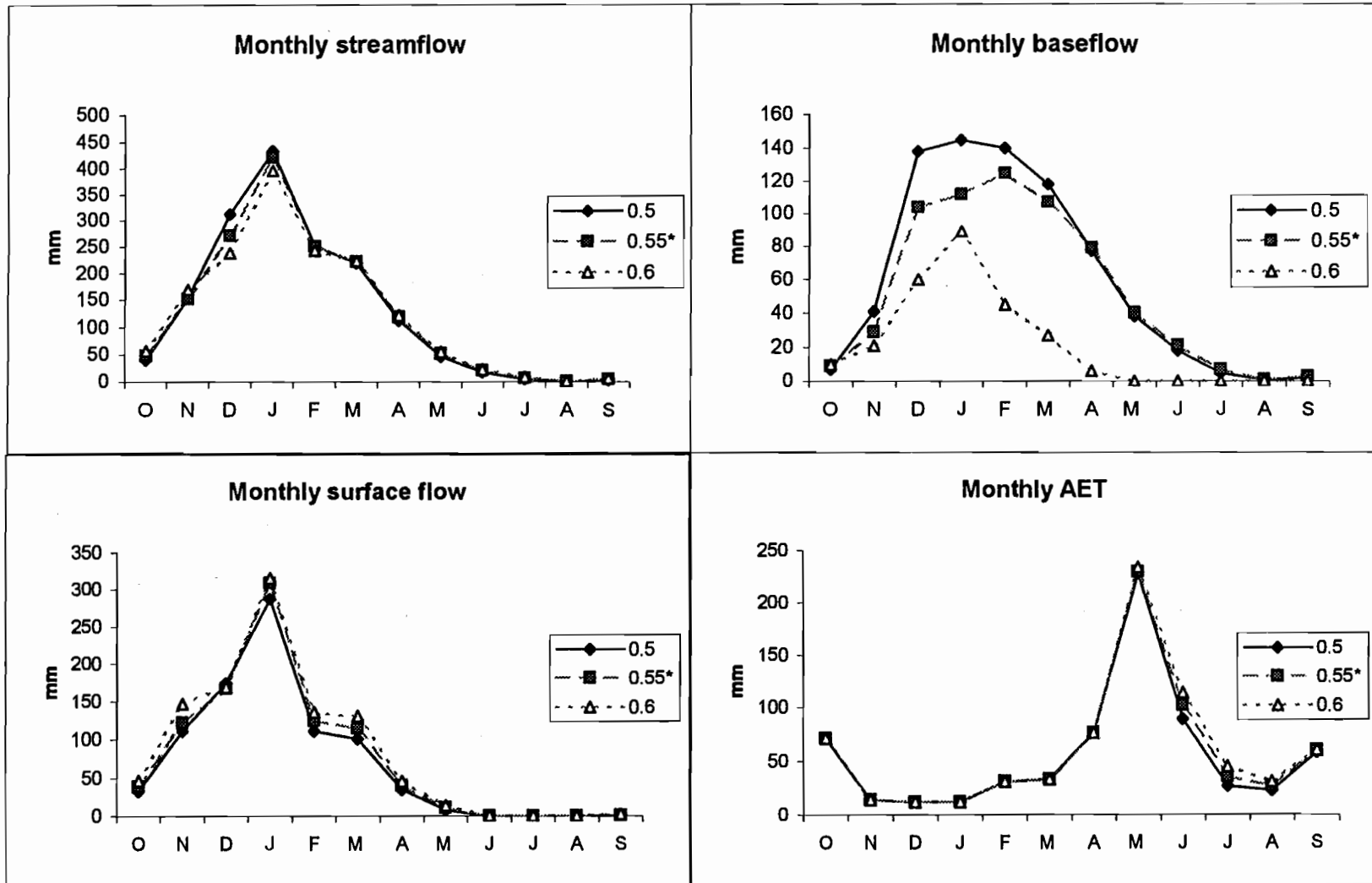
\*HJA parameter value

Figure 3-13a,b,c,d: Lateral flux coefficient - Monthly Results



\*HJA parameter value

Figure 3-14a,b,c,d: Porosity - Monthly Results



\*HJA parameter value

monthly streamflow, baseflow, surface flow, and AET patterns are illustrated in Figures 3-14a,b,c,d.

### **3.4.2 Evaluation - Variation Between Simulated Water Years**

Water years 1959 & 1967 were used to calibrate the MAPSS-W parameters for WS 1 & 2. Pre-harvest water years 1958, 1960, & 1961 were used to evaluate MAPSS-W streamflow simulations for both watersheds. Additionally, water years 1968, 1972, 1973, 1979, 1980, 1990, & 1991 were used to evaluate MAPSS-W streamflow simulations for WS 2. The WS 1 simulations for the post-harvest water years were used for vegetation-hydrology hypothesis testing and are discussed in Chapter 4.

The monthly and daily streamflow results from these simulations are presented in Figures 3-16a - i. Figures 3-16b and 3-16e illustrate the monthly and daily streamflow results for the calibration years (1959 & 1967). The pre-harvest (1958-61) streamflow simulations for both WS1 & 2 averaged within 3% of the measured annual streamflow. It was expected that the post-harvest WS 2 simulations would also be within 5% of the measured annual streamflow, since there was no watershed treatment in WS 2. However, the post-harvest WS2 streamflow simulations averaged 21% greater than measured streamflows. This increase in simulated streamflow variation indicates that MAPSS-W did not represent vegetation or soil function in WS 2 as accurately after harvest in WS 1. The vegetation datasets used for all WS2 simulations were identical. The post-harvest experimental streamflow simulations for WS 1 averaged 13% greater than measured streamflows. All summer streamflow simulations are within 4% of the measured streamflows.

Other researchers have noted this discrepancy between estimated streamflow and measured streamflow in WS 2. Several explanations have been suggested, but currently these explanations are speculative. Speculations include measurement error, climatic variation and changes in vegetation function. Measurement errors may include inaccuracy in the gage calibration, or leaky bedrock under the gage or elsewhere in the watershed. However, recent analysis of the small watersheds suggests that there is no leak out of WS 2 (Post, personal communication).

Recent analysis of precipitation and streamflow in WS 2 suggest that the discrepancy between measured and simulated streamflow may be due to seasonal changes in precipitation. Since the beginning of the climate and streamflow record for WS 2, fall and winter precipitation has decreased by approximately 5% and spring and summer precipitation has increased by approximately 5% (Post, personal communication). This decrease in fall and winter precipitation and increase in spring and summer precipitation is correlated with a decrease in fall and winter streamflow and a minimal increase in spring and summer streamflow. This lack of increase in spring and summer streamflow likely results from the vegetation capture and use of this additional precipitation.

It is also possible that changes in WS 2 vegetation contribute to this discrepancy between simulated and measured streamflow. WS 2 is a mixed old-growth/mature Douglas-fir stand which has continued to grow through the period of record. Additionally, harvest along the ridge between WS 1 & 2 may have produced changes in WS 2 vegetation function. Increased wind speed, incident solar radiation, temperature, and decreased relative humidity may have increased the transpirational demand on the vegetation along this ridge. It is unlikely that this edge effect would be sufficient to produce the large discrepancy between simulated and measured streamflow, and it is possible that several mechanisms are functioning in WS 2.

Monthly simulated streamflow shows a fairly consistent streamflow surplus in March. MAPSS-W show that least accuracy in streamflow pattern during the fall. These streamflow patterns suggest that the antecedent conditions from the preceding year are particularly important in the fall. Since the antecedent moisture conditions for MAPSS-W are based on the year being modeled, rather than the true conditions of the preceding year, the fall is difficult to simulate accurately.

### **3.4.3 Resolution and Parameterization Comparison**

After the calibration of MAPSS-W parameters were completed, comparisons were made between two dataset resolutions (30m & 200m) for both the Reynolds Creek parameterization and the Andrews parameterization. These simulations were all run

Figure 3-15 a-l: Daily and Monthly Streamflow Comparisons for WS 1 & 2.  
Figure 3-15a: WY 1958

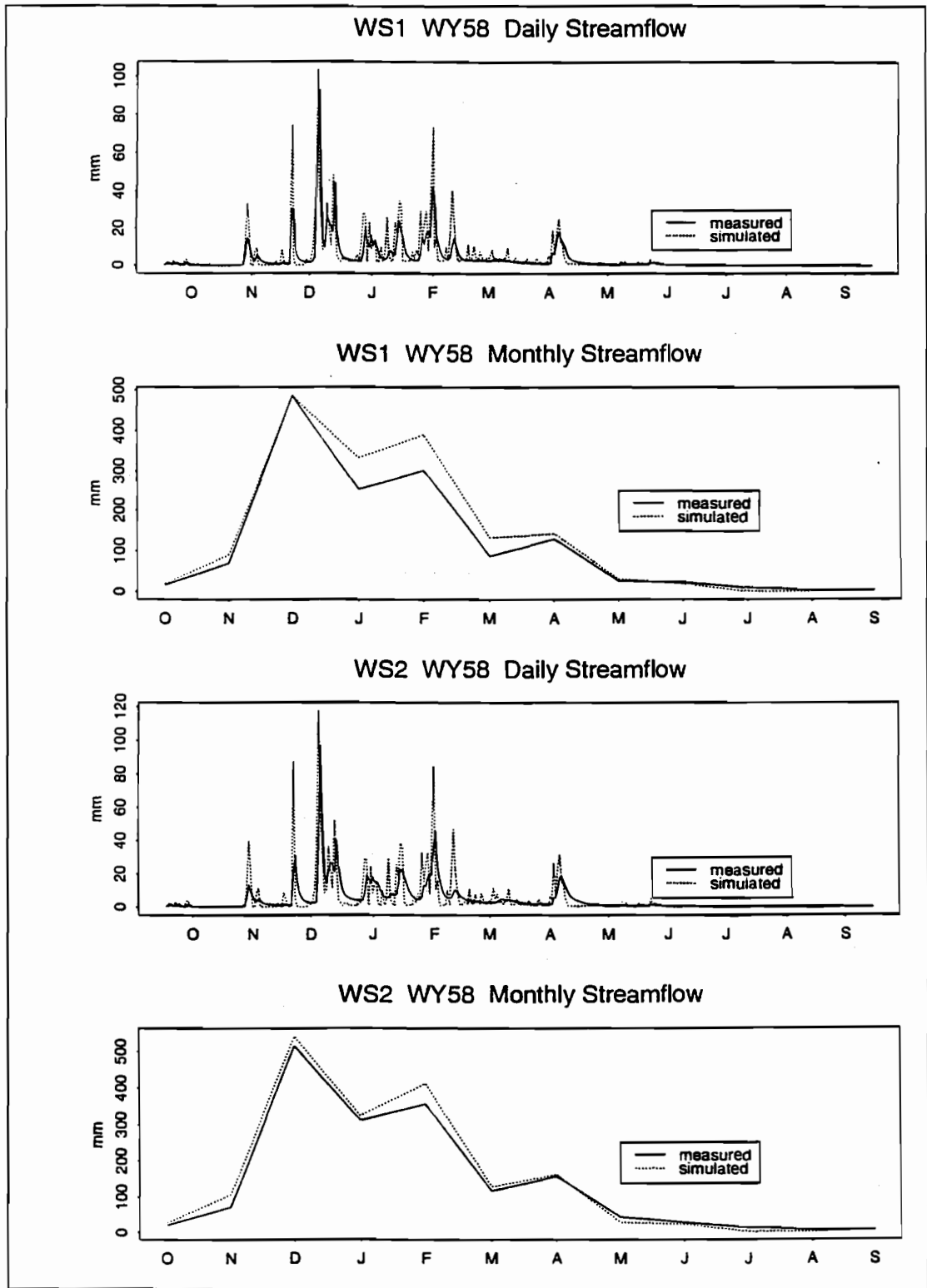


Figure 3-15b: WY 1959

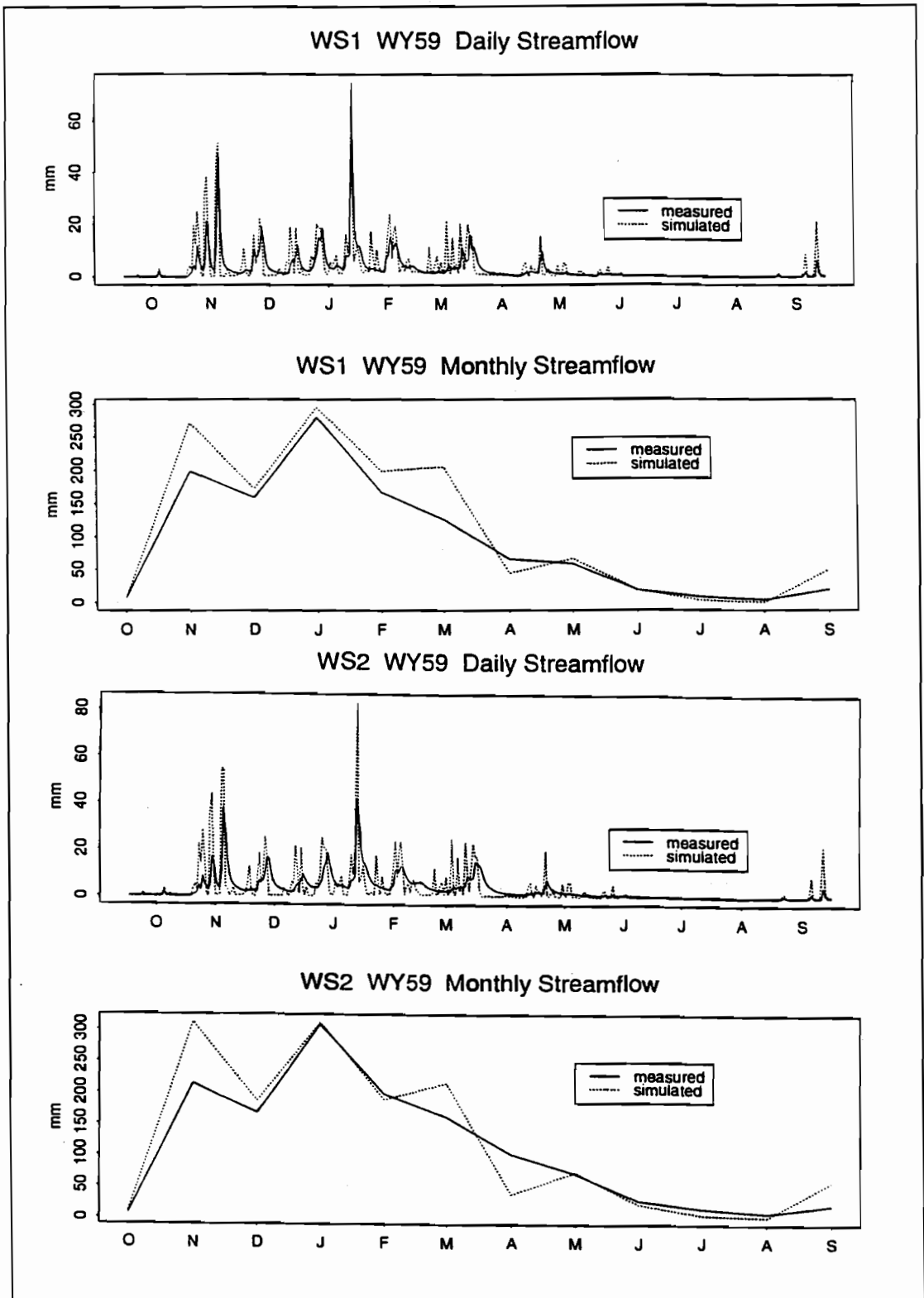


Figure 3-15c: WY 1960

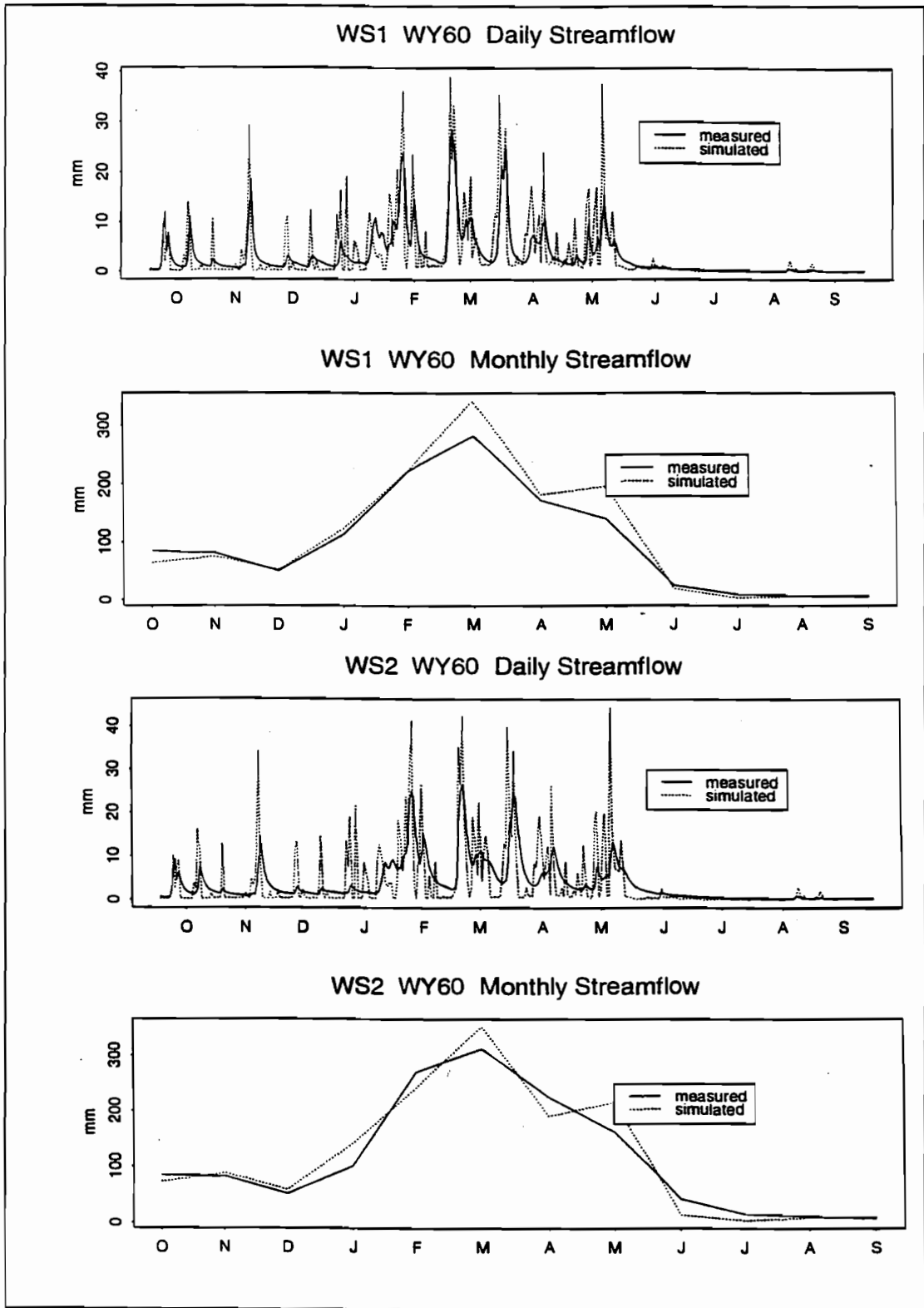


Figure 3-15d: WY 1961

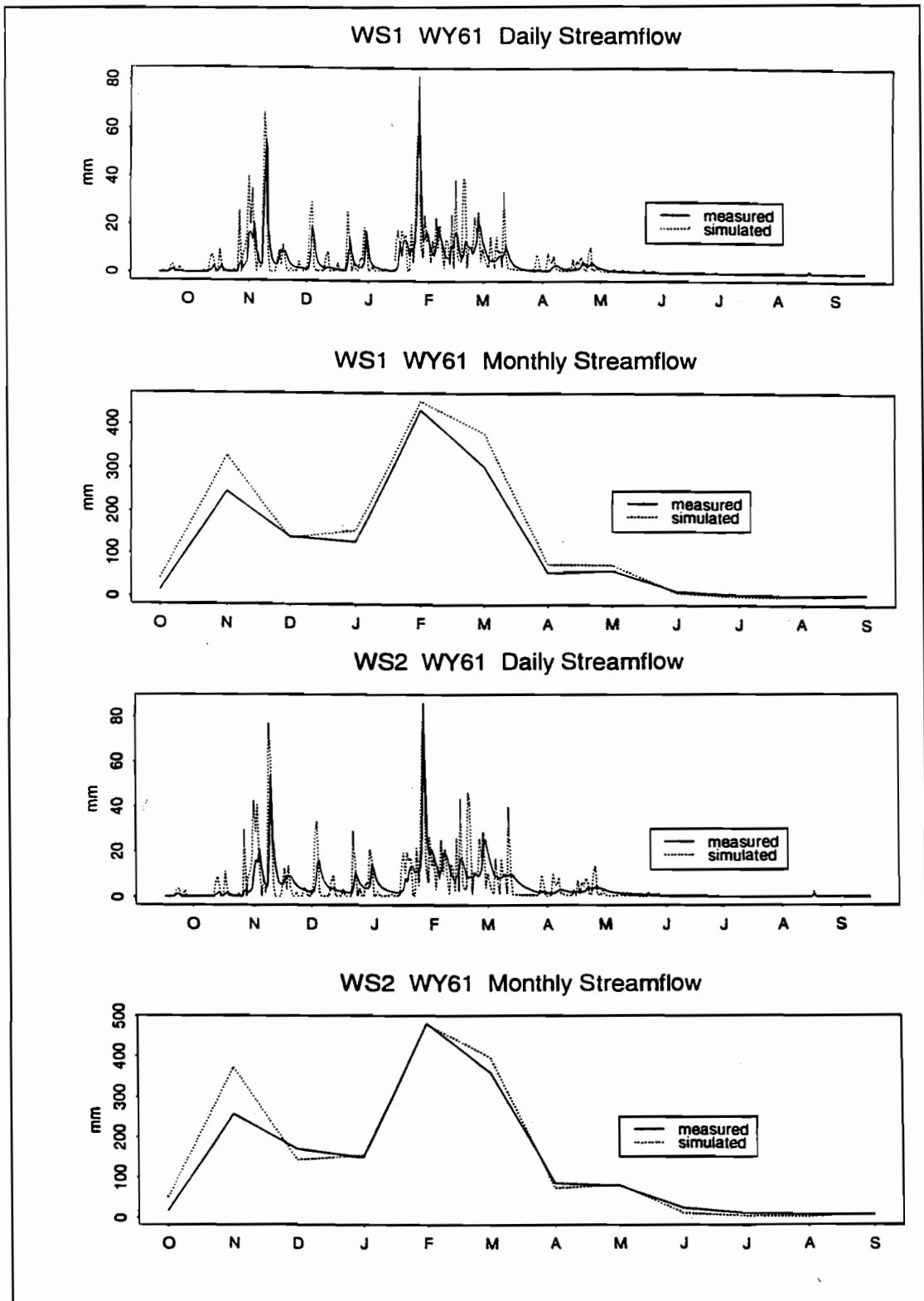


Figure 3-15e: WY 1967

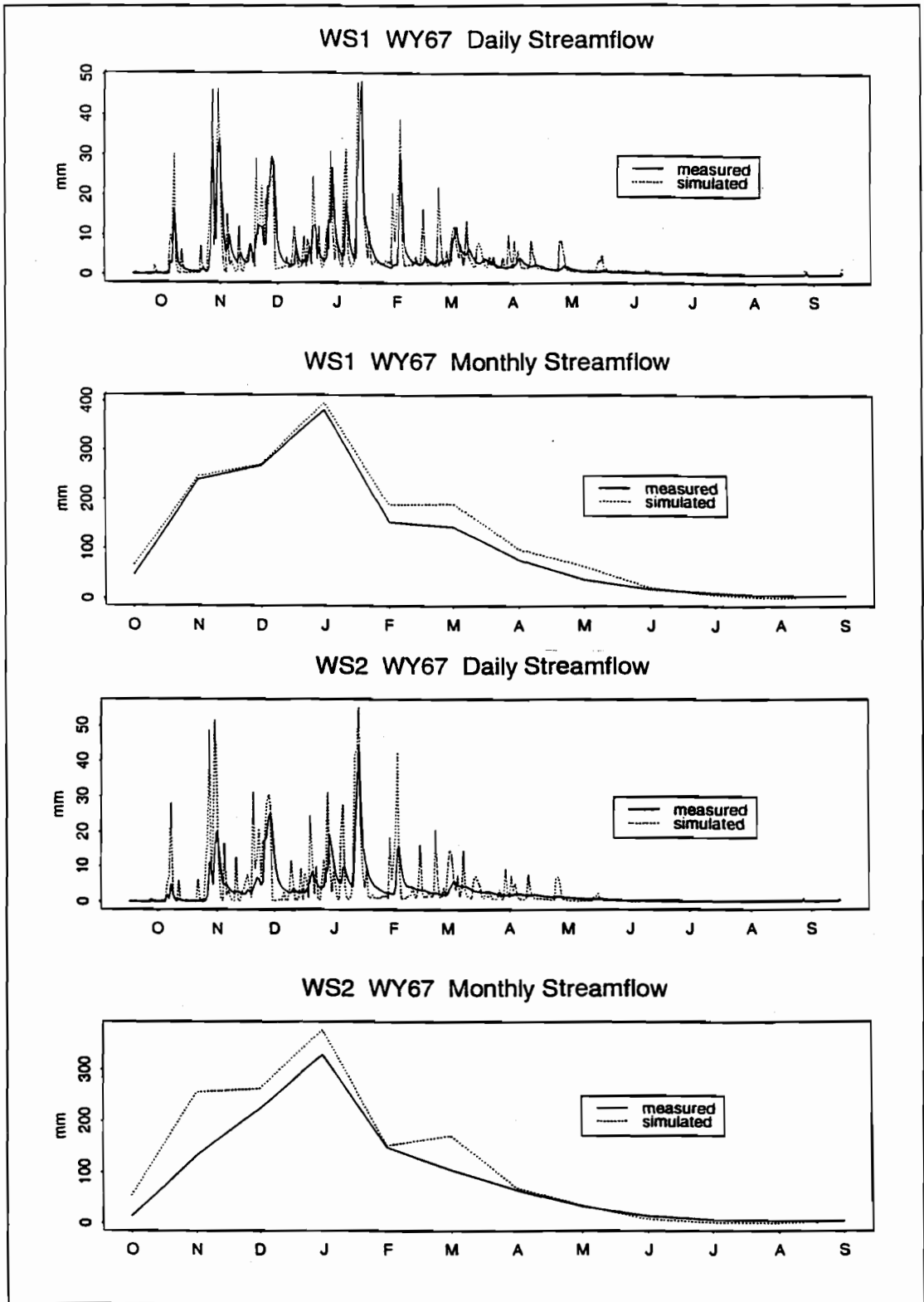


Figure 3-15f: WY 1968

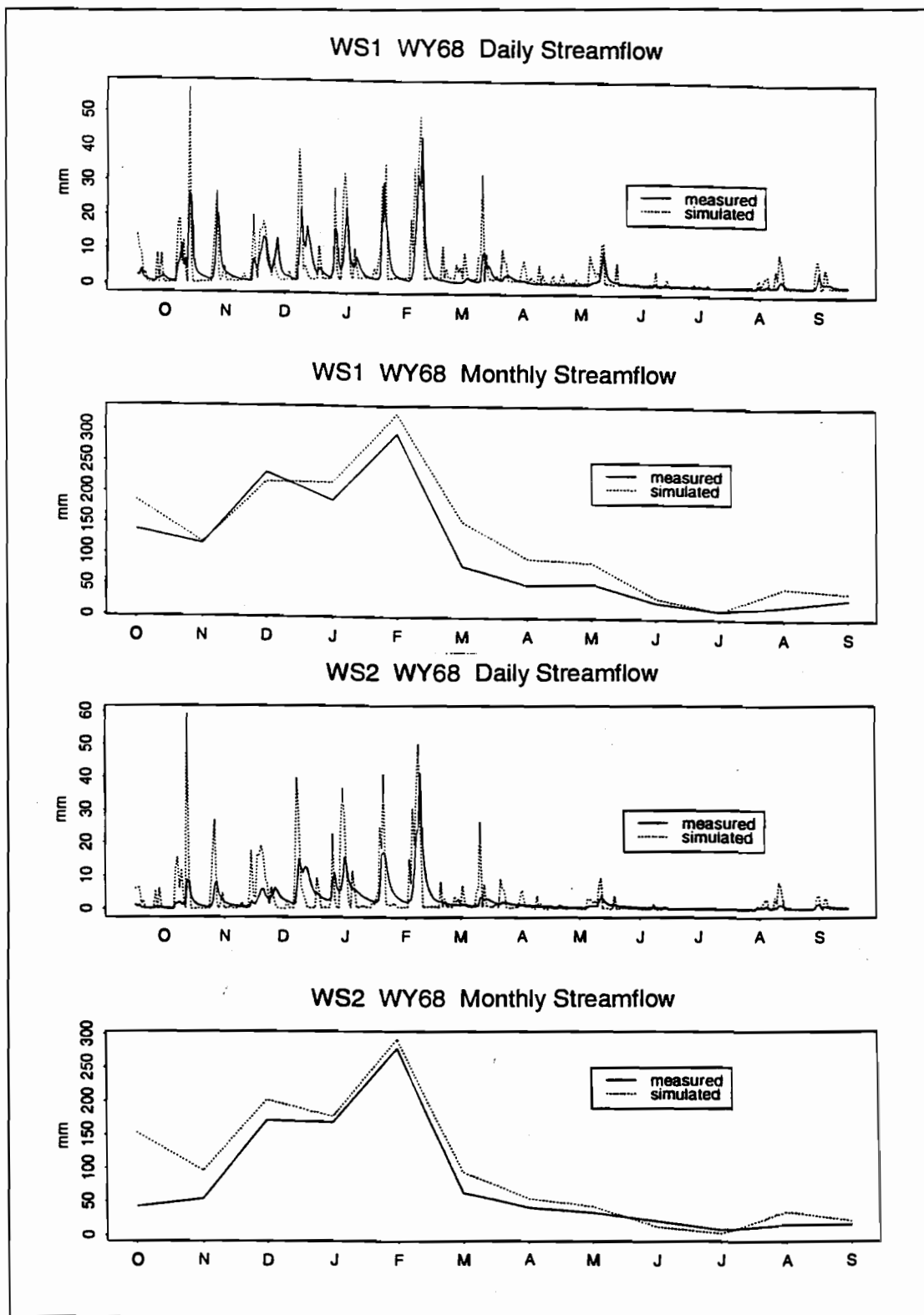


Figure 3-15g: WY 1972

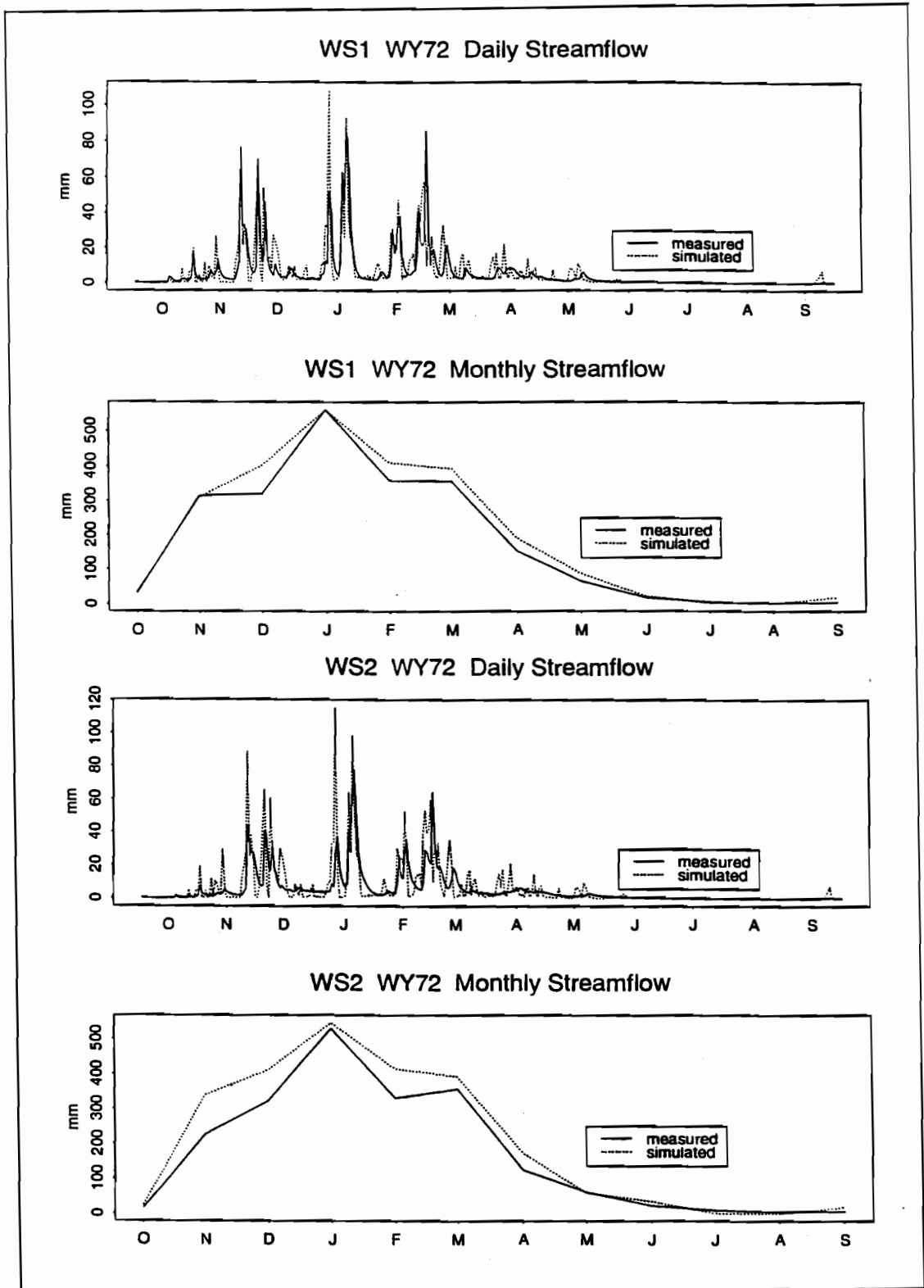


Figure 3-15h: WY 1973

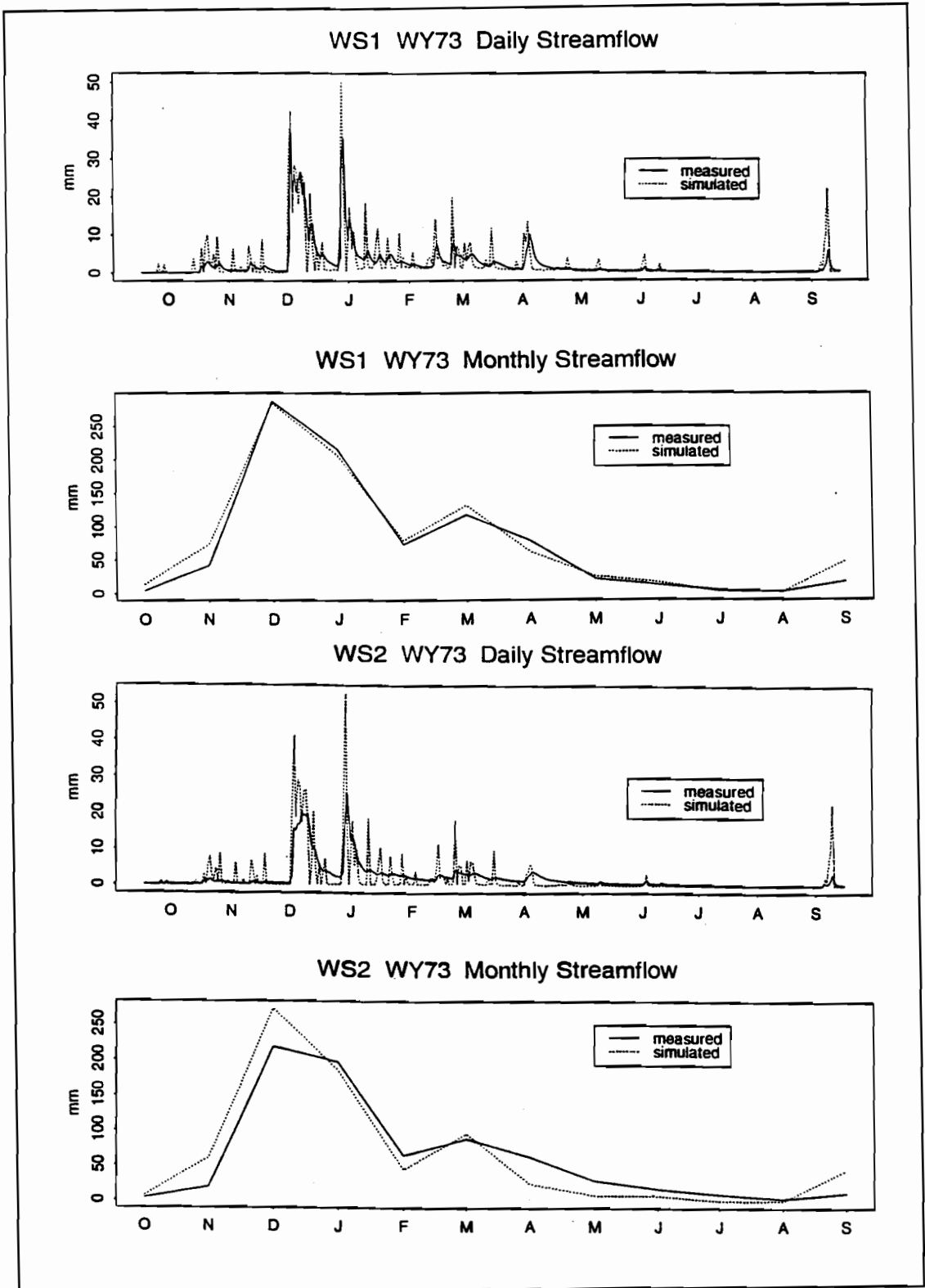


Figure 3-15i: WY 1979

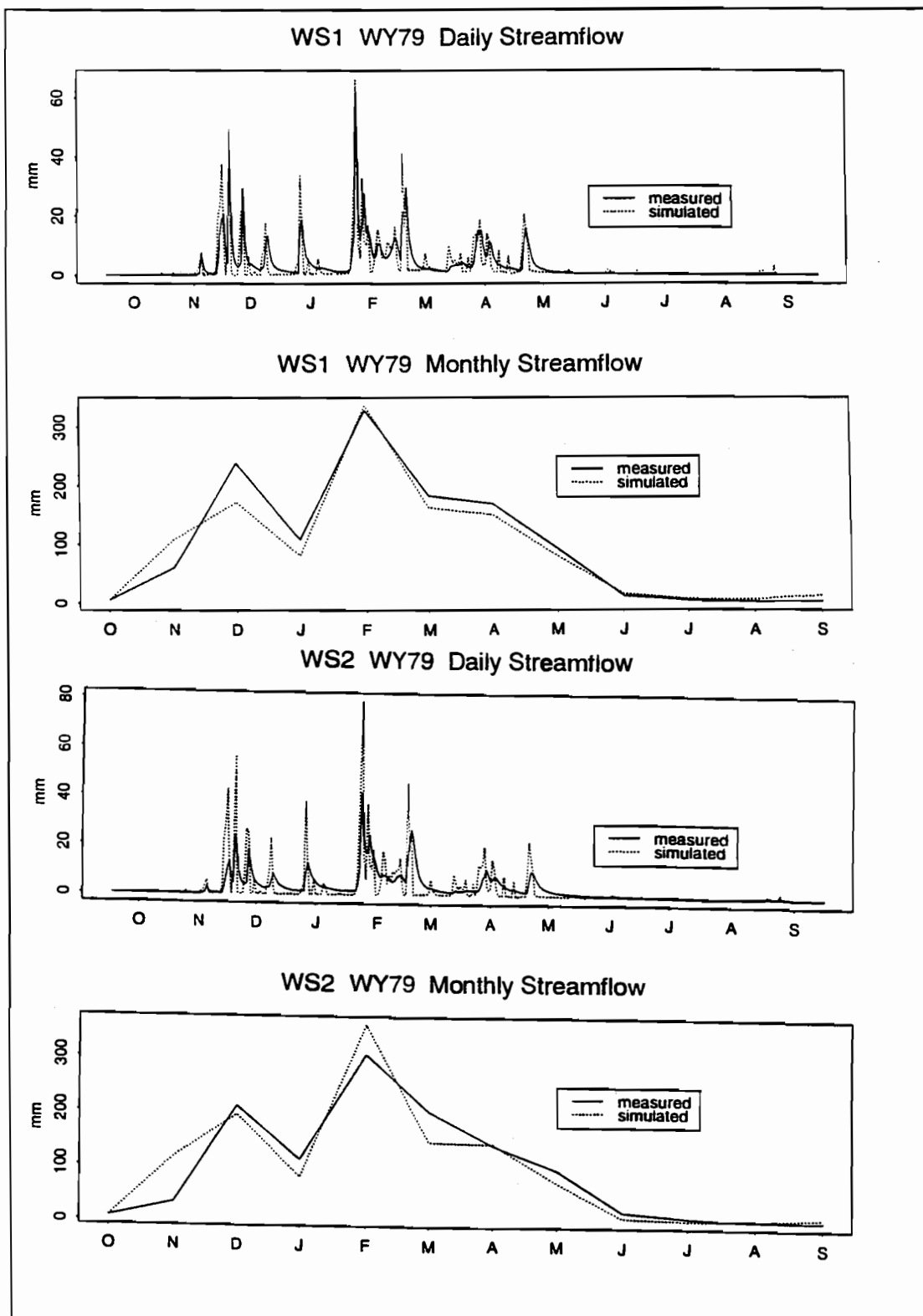


Figure 3-15j: WY 1980

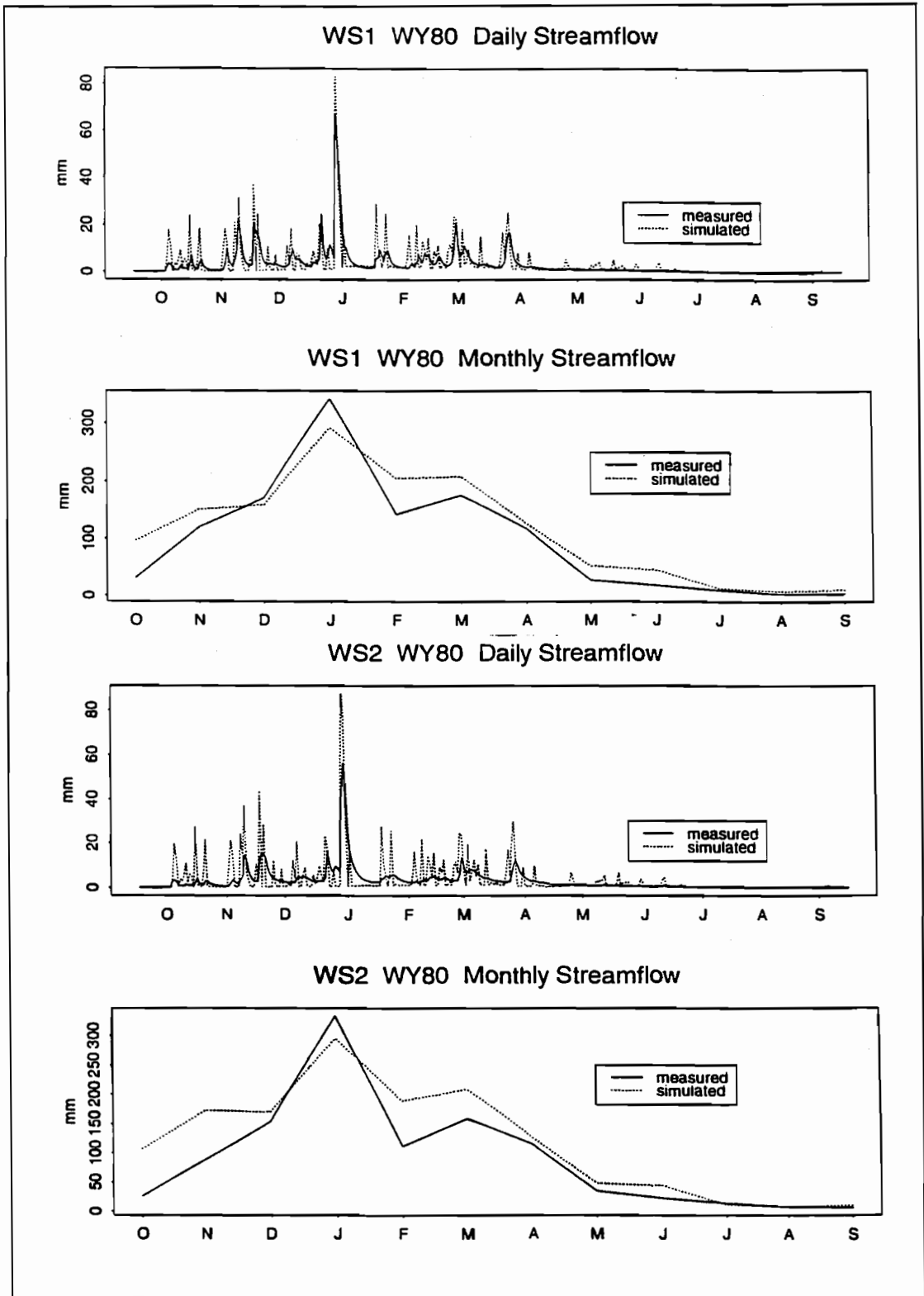


Figure 3-15k: WY 1990

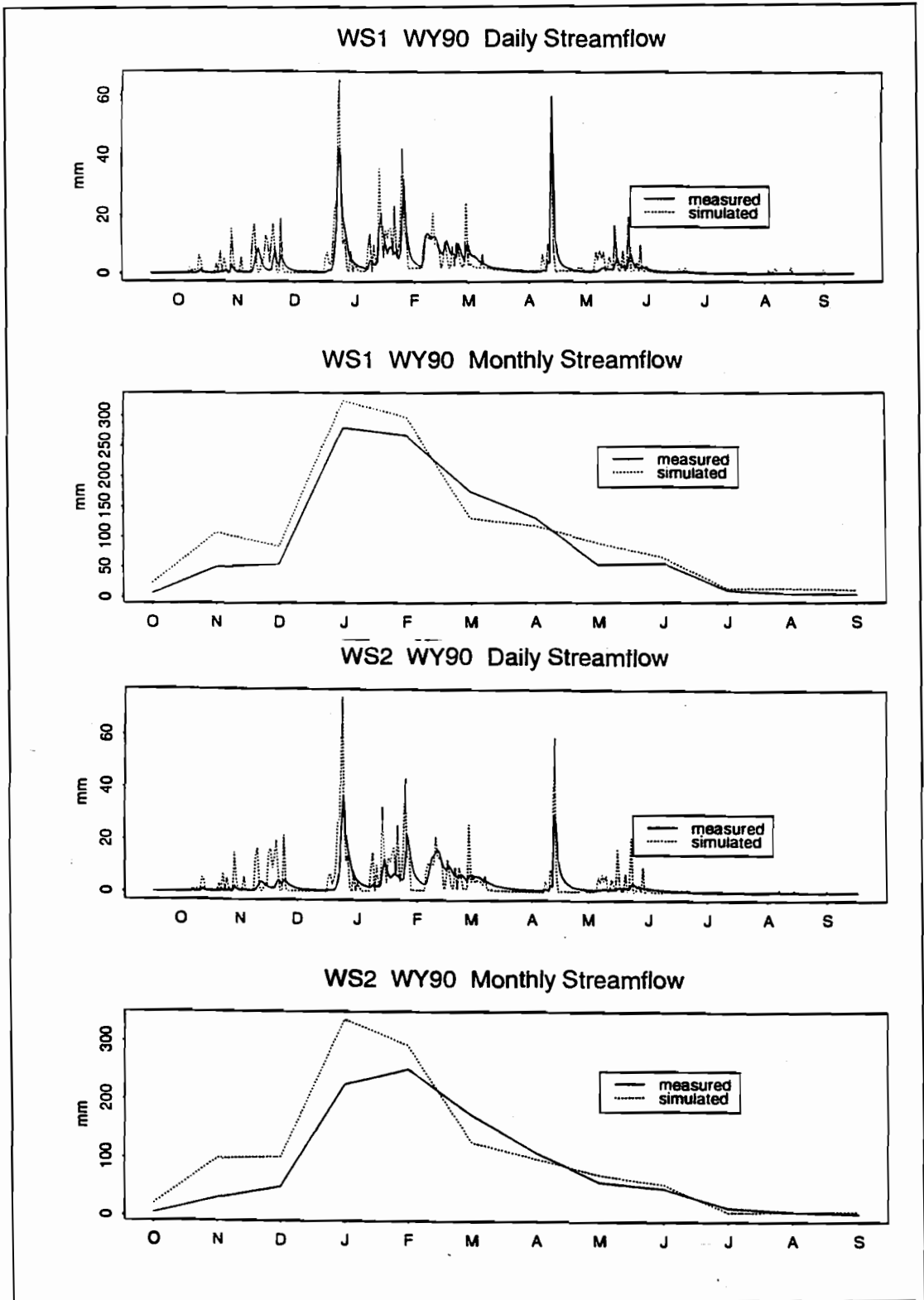
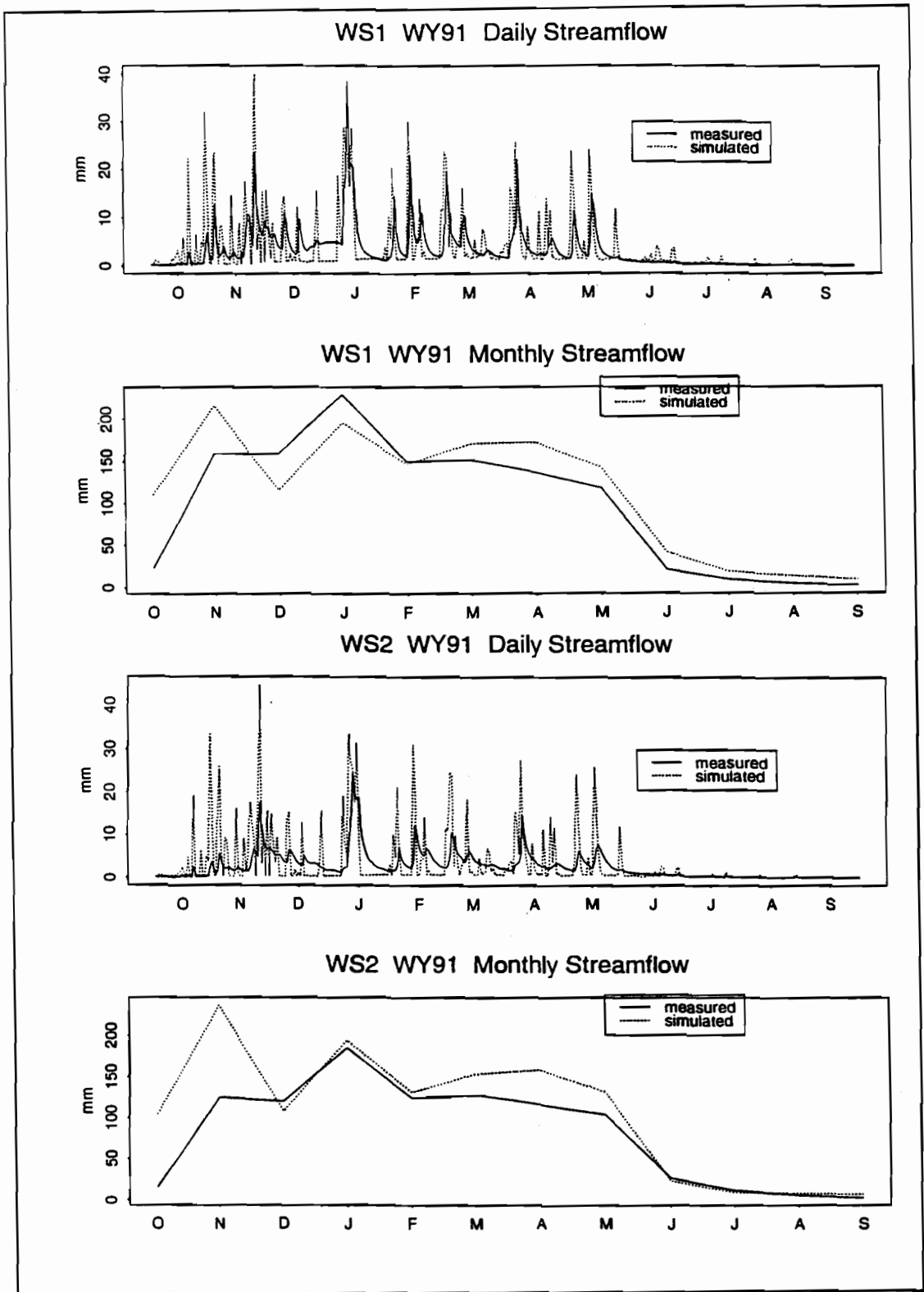


Figure 3-15I: WY 1991



using datasets for the Andrews WS 1 & 2. References to the Reynolds Creek simulations indicate the simulations based on the Reynolds Creek parameter values.

Figures 3-16a & b illustrate the simulated annual precipitation, streamflow, baseflow, surface flow, and AET results for these comparisons of dataset resolution and model parameterization. The 200m precipitation dataset produced slightly more precipitation than the 30m dataset. However, the 30m simulations resulted in higher streamflow levels for the Andrews simulations. The Reynolds Creek parameterization resulted in higher streamflow for the 30m simulation for WS1, but a slightly higher streamflow level for the 200m simulation for WS2. Baseflow was very low in the 200m simulations. Baseflow increased more significantly in the 30m simulations for Reynolds Creek than in the Andrews simulations. This is due to the soil hydrology parameterization for the Andrews, which was based on a clay loam/ loam soil texture, rather than the default, sandy loam used for these comparisons. The response of surface flow is also related to the soil hydrology parameter settings for Reynolds Creek and the Andrews. While the Reynolds Creek simulations had lower surface flow values for the 30m simulations, the Andrews simulations surface flow values were similar for both resolutions. AET did not change in the Reynolds Creek simulations and decreased in the 30m Andrews simulation. The Reynolds Creek AET was constrained by low roughness lengths and maximum AET was simulated for both resolutions.

Figures 3-17a,b,c,d & 3-18a,b,c,d illustrate the monthly streamflow, baseflow, surface flow and AET patterns for WS 1 & 2 comparisons, respectively. The monthly results indicate that environmental parameter values are more critical than resolution; however, the choice of dataset resolution does influence simulation results. Both HJA simulations using Reynolds Creek parameterizations produced too much streamflow in the spring and not enough streamflow in the fall and winter. This pattern is also illustrated by the monthly surface flow results. Baseflow was the variable most affected by resolution.

Figure 3-16a & b: Resolution & Parameterization Comparison  
Annual Results

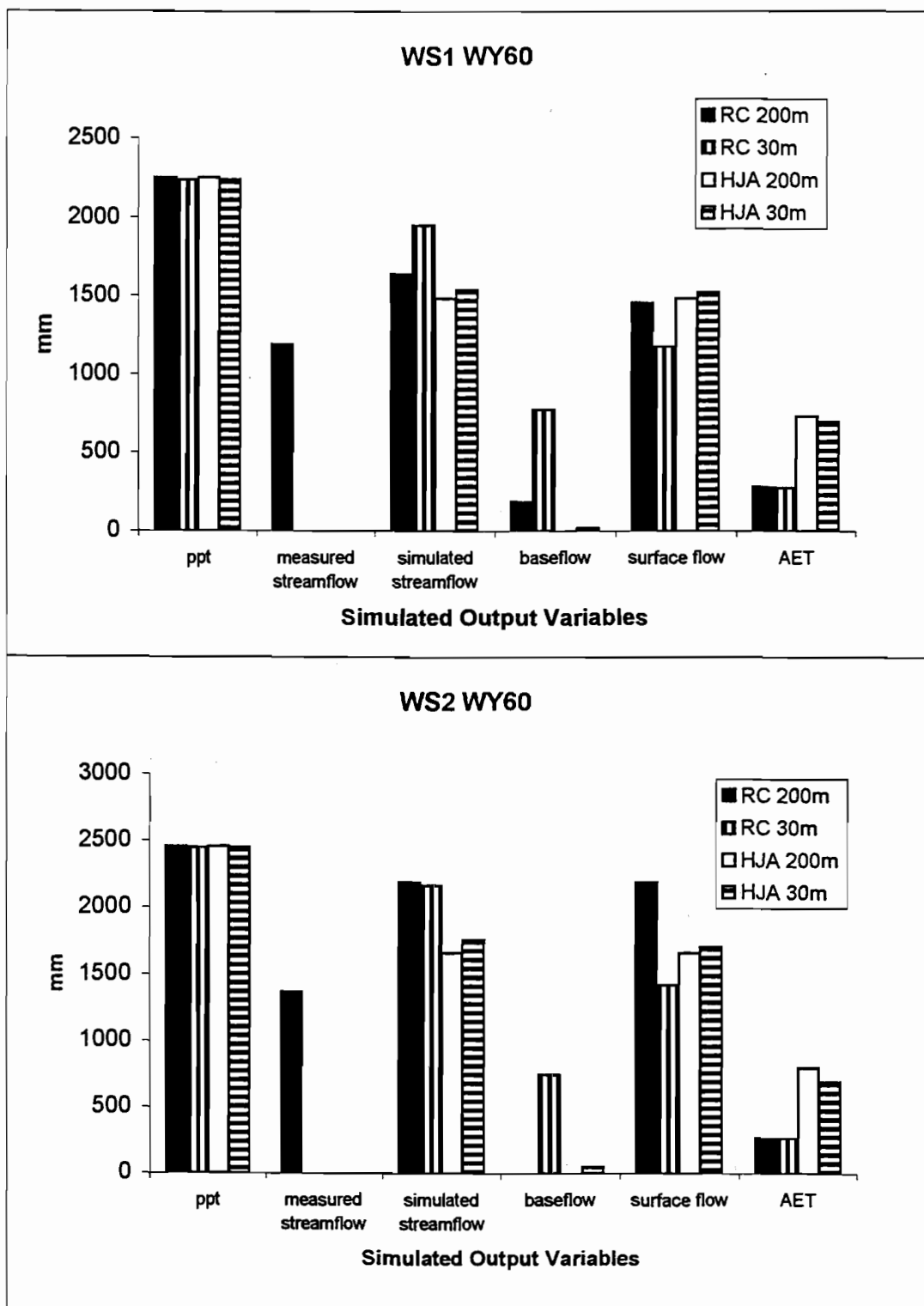


Figure 3-17a,b,c,d: Resolution & Parameterization - WS 1 Monthly Results

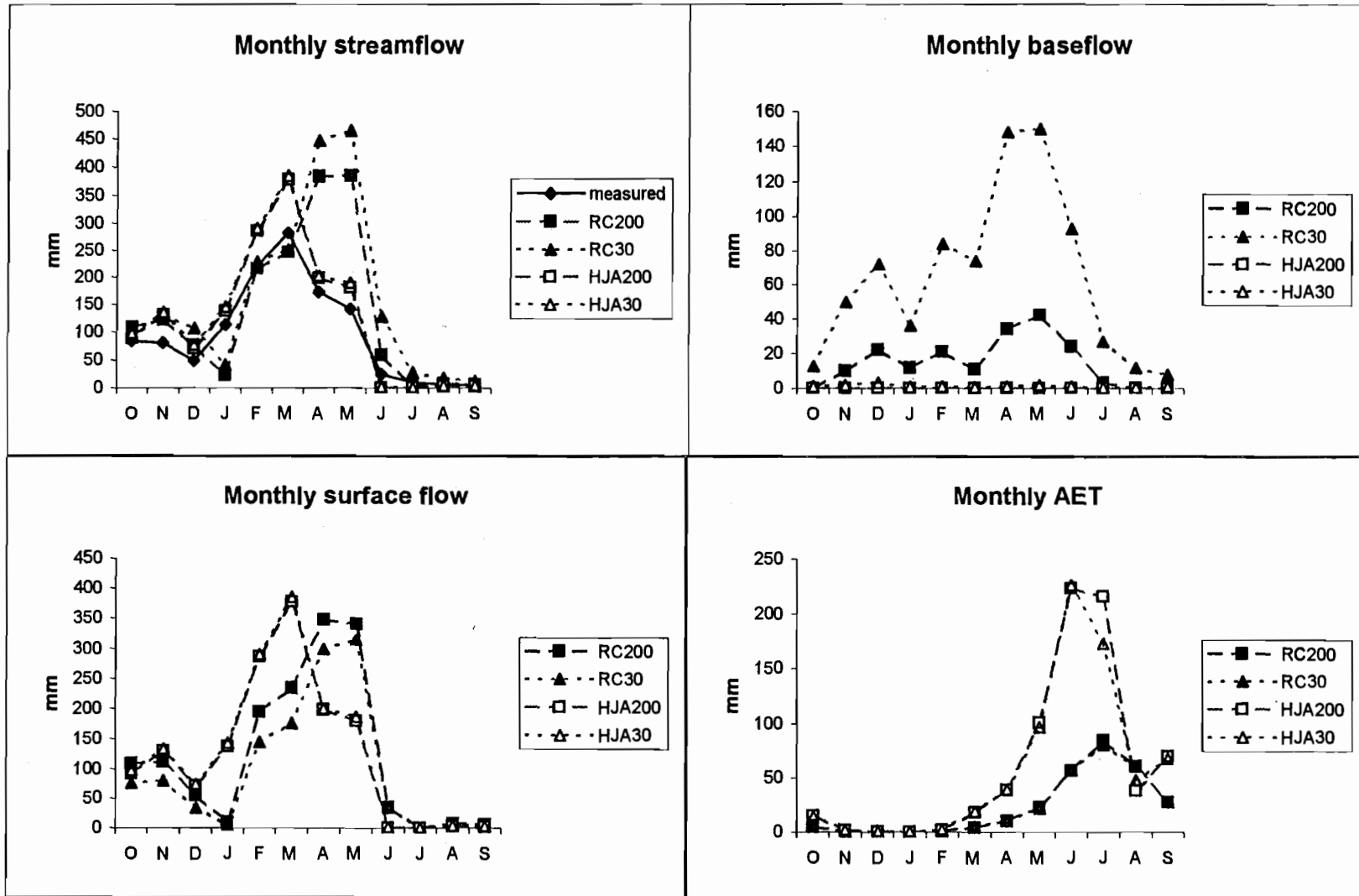
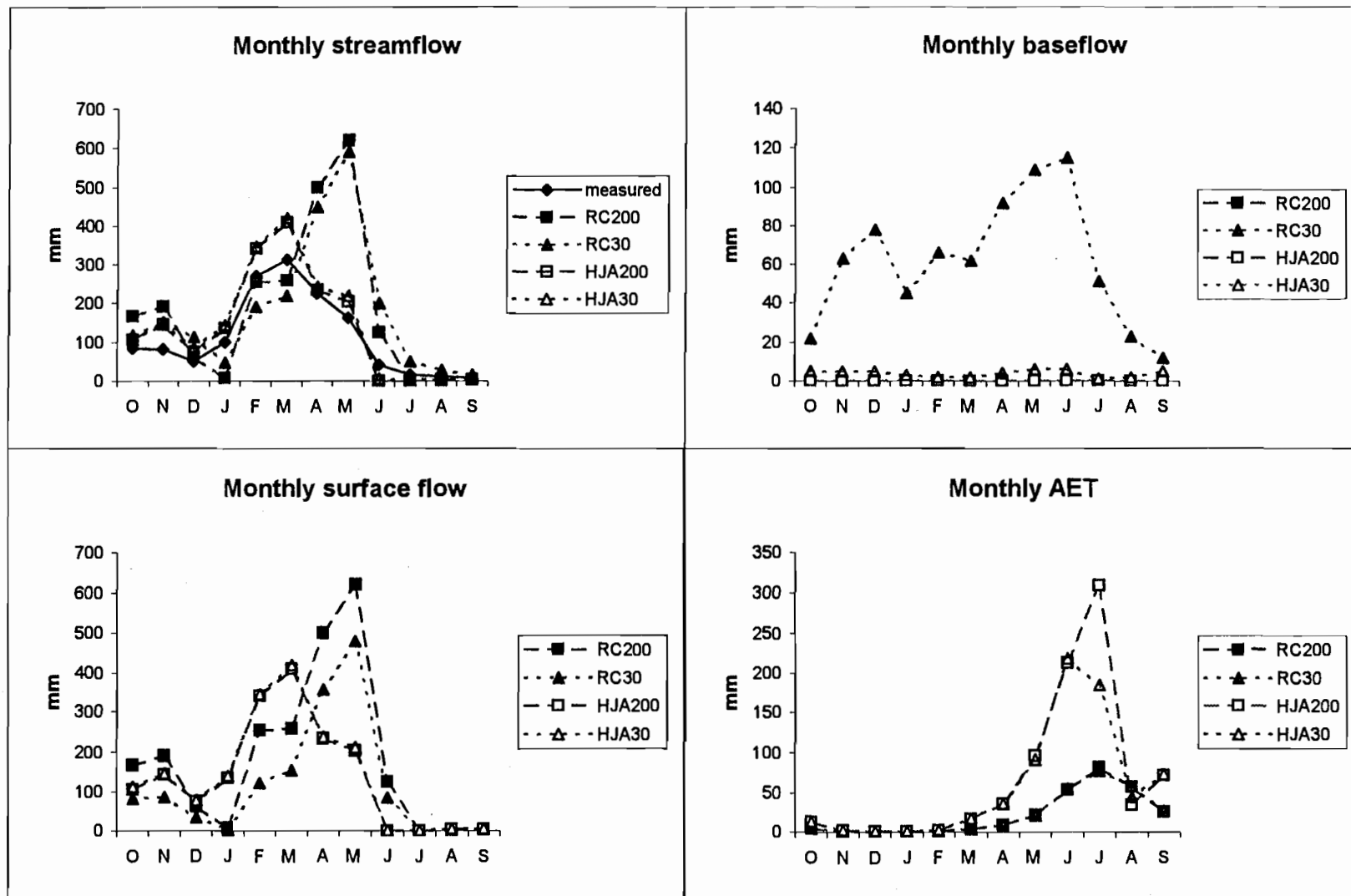


Figure 3-18a,b,c,d: Resolution & Parameterization - WS 2 Monthly Results



### **3.4.4 Climate Comparisons**

Comparisons were made of simulations which were run for alternative climate datasets for water year 1959, the small watershed soils dataset, and the uniform forest canopy dataset.

#### **3.4.4.1 Precipitation**

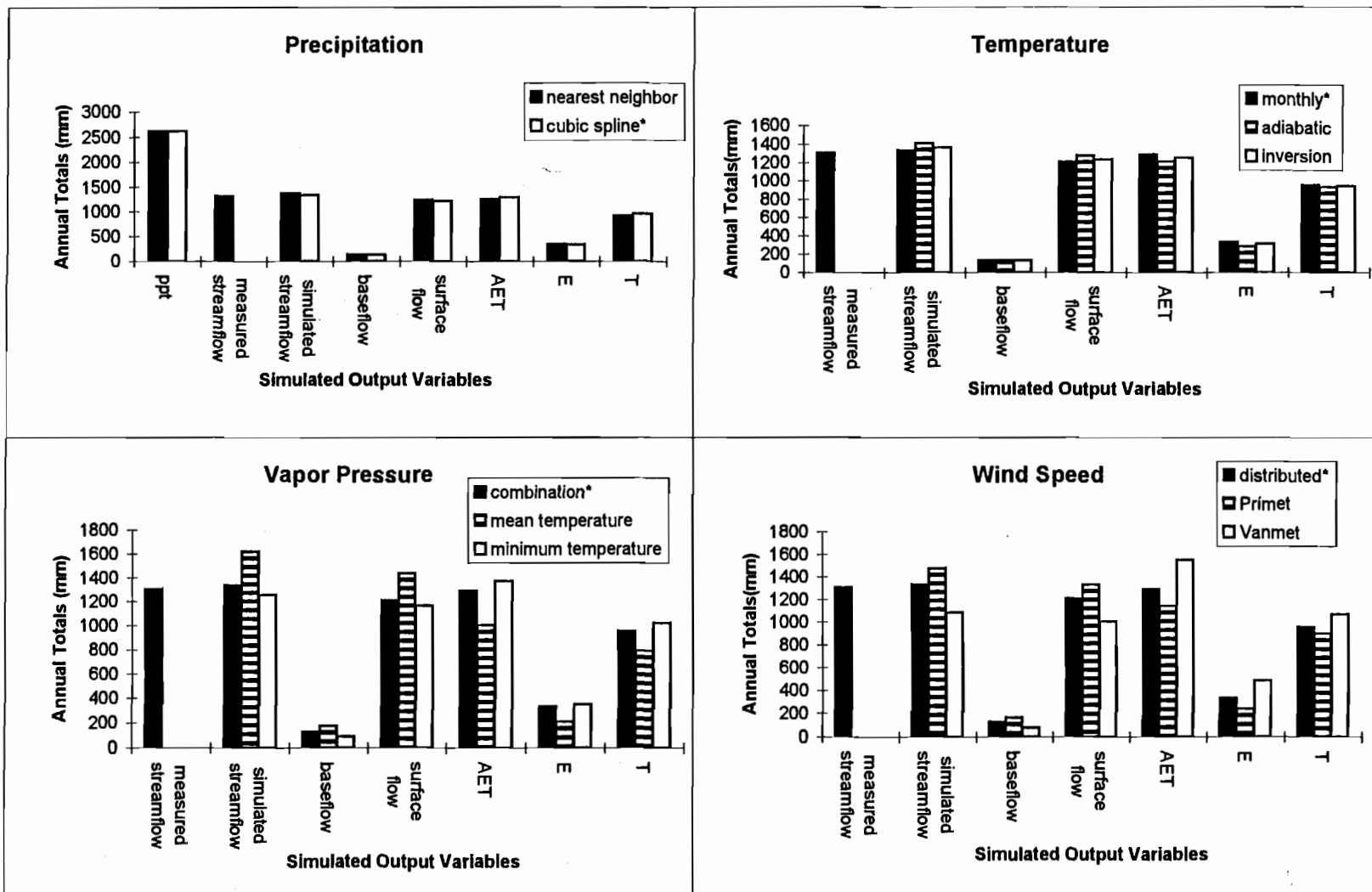
Figure 3-19a illustrates the annual precipitation, streamflow, baseflow, surface flow AET, evaporation (E), and transpiration (T) results for simulations comparing the precipitation datasets developed from the nearest neighbor interpolation method and the cubic spline interpolation method. The nearest neighbor interpolation resulted in slightly higher annual precipitation, streamflow, baseflow, surface flow, and evaporation, and lower AET and transpiration values. The difference in annual streamflow between these simulations was small (35mm); and the difference in the mean annual precipitation was 13mm. The cubic spline datasets were used for the evaluation and experimental simulations.

#### **3.4.4.2 Temperature**

Figure 3-19b illustrates the annual streamflow, baseflow, surface flow, AET, evaporation and transpiration results for simulations comparing the three temperature lapse rate datasets. The adiabatic lapse rate dataset overestimated annual streamflow by 100mm. The inversion height lapse rate dataset overestimated annual streamflow by 60mm. The monthly lapse rate dataset overestimated annual streamflow by 30mm.

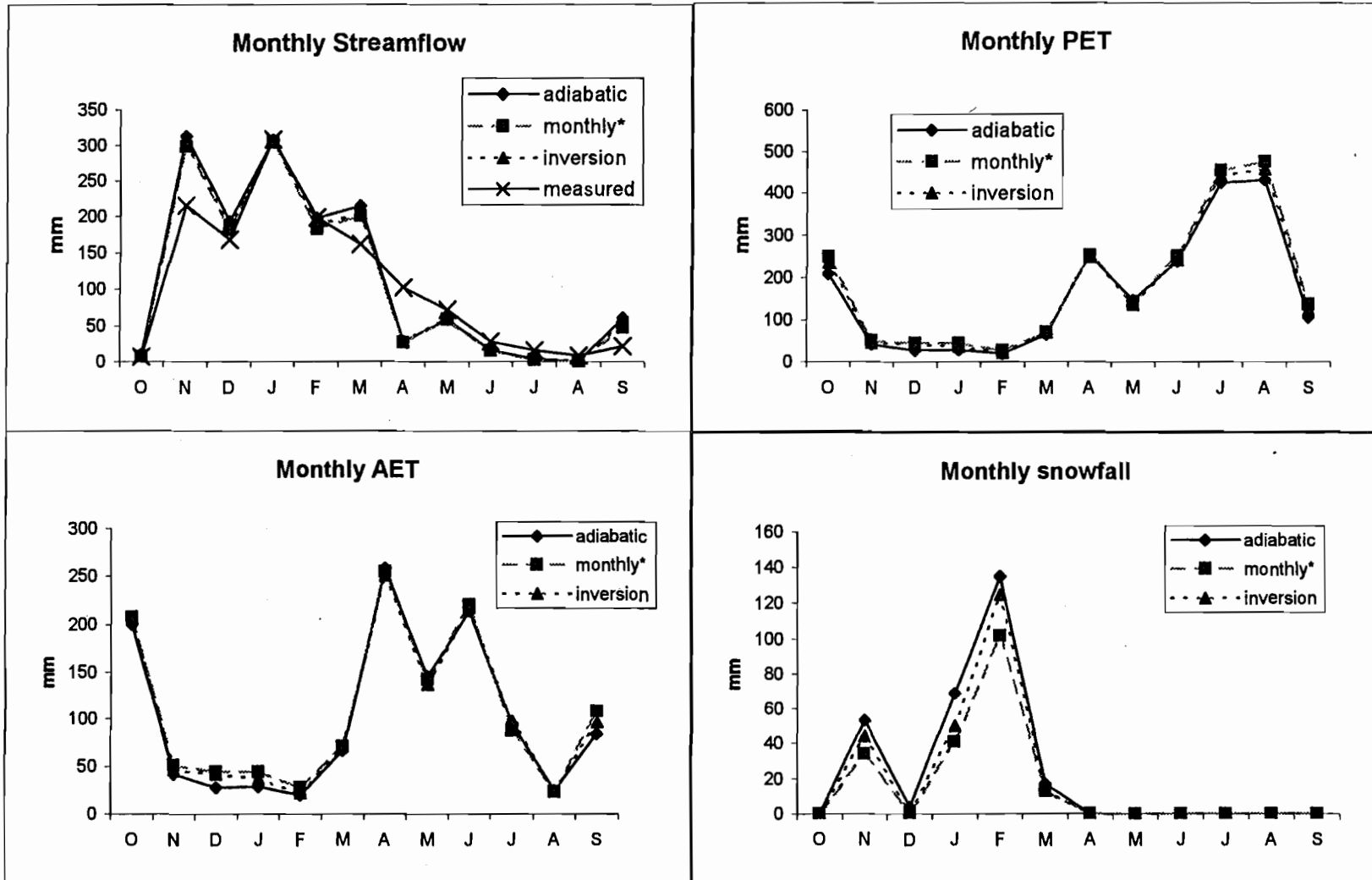
Figures 3-20a.b.c.d illustrate the simulated monthly streamflow, PET, AET and snowfall results for these three temperature datasets. The three temperature simulations resulted in similar monthly streamflow patterns. The monthly lapse rate dataset increased winter AET and summer PET the most. Snowfall was also influenced by the differences in minimum temperature in these three datasets. The adiabatic

Figure 3-19a,b,c,d: Climate Dataset Comparisons - Annual Results



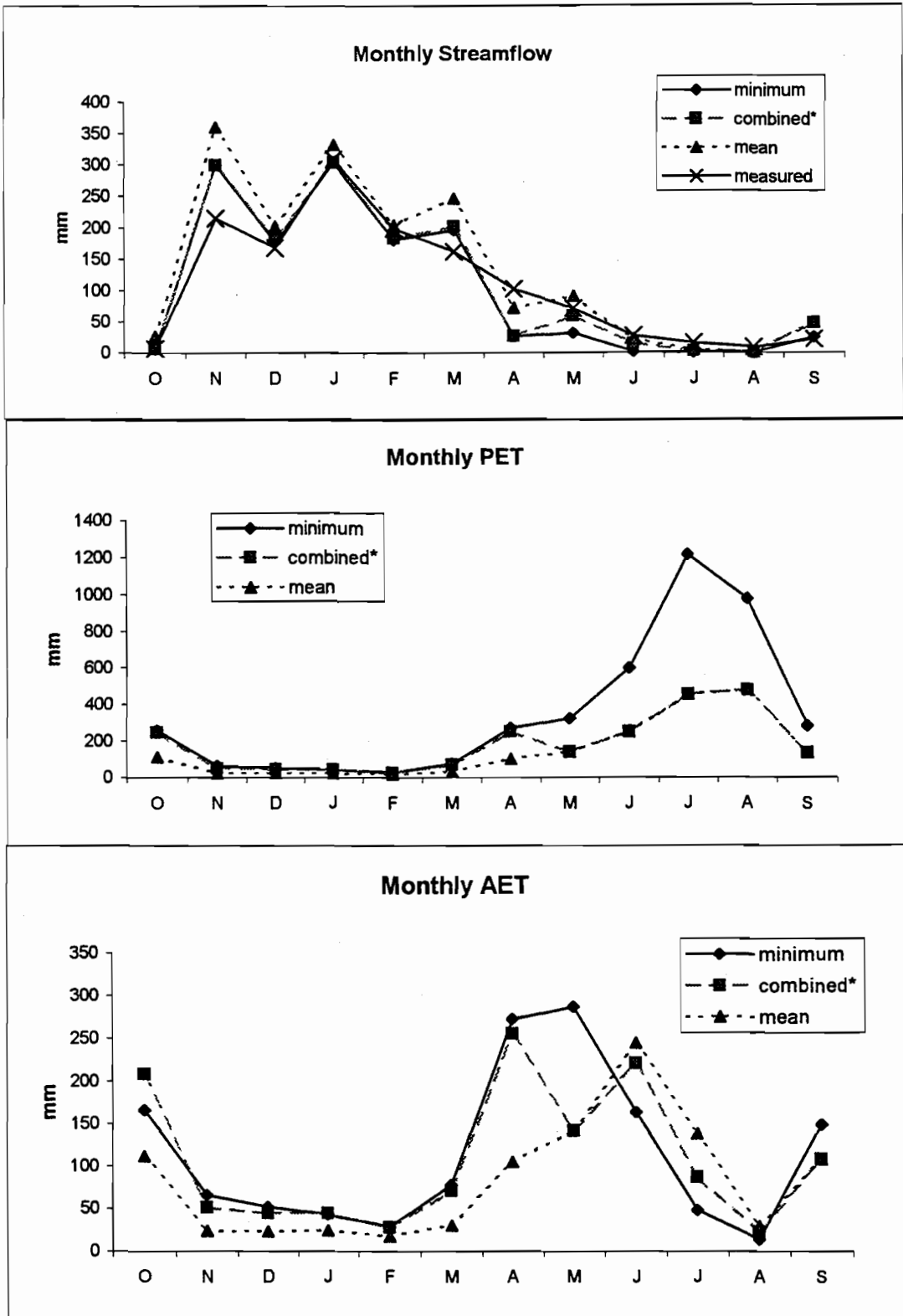
\*Dataset used in calibration, evaluation & experimental simulations

Figure 3-20a,b,c,d: Temperature Dataset Comparison - Monthly Results



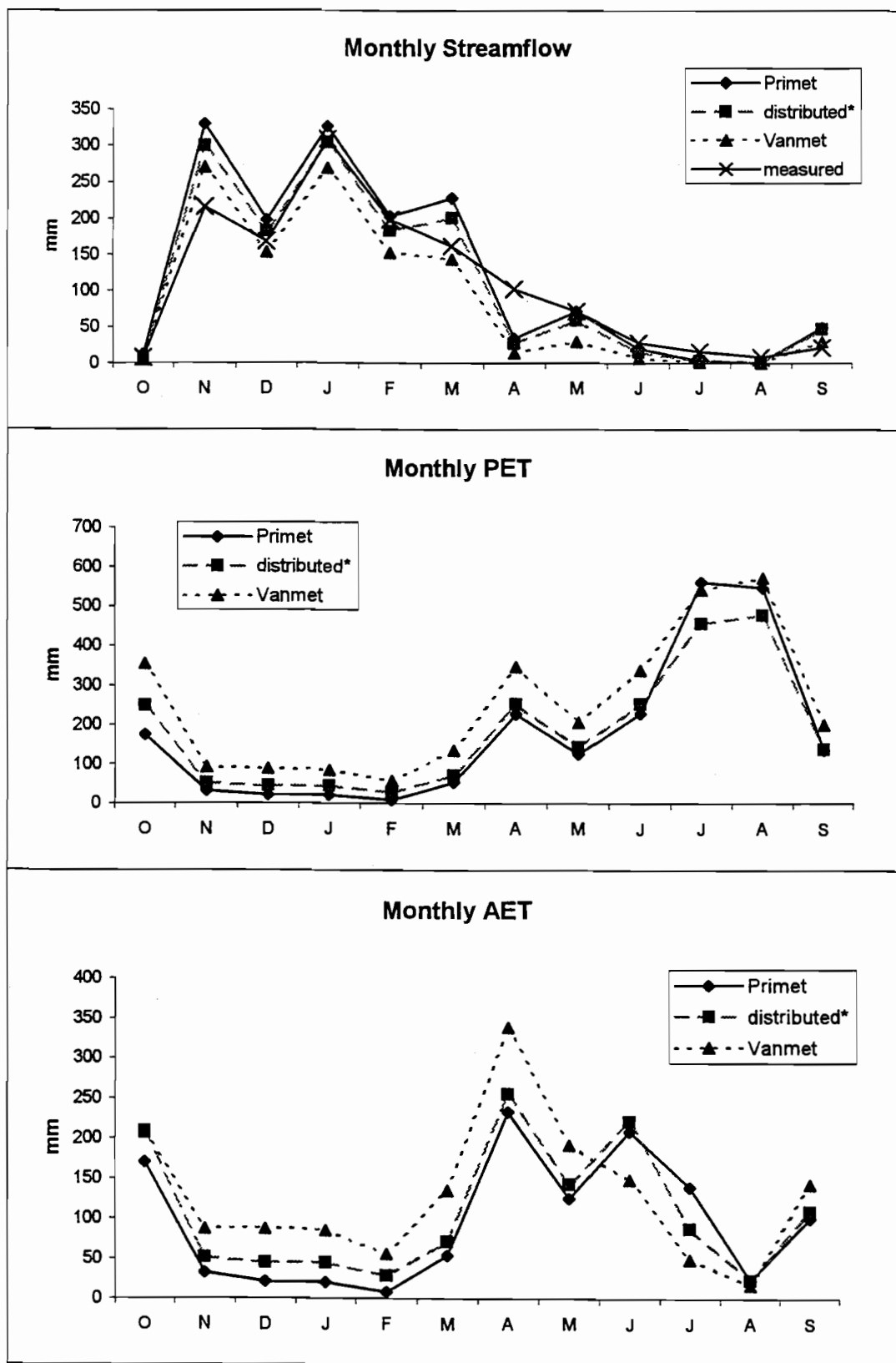
\*Dataset used in calibration, evaluation & experimental simulations

Figure 3-21a,b,c: Vapor Pressure Dataset Comparison  
 Monthly Results



\*Dataset used in calibration, evaluation & experimental simulations

Figure 3-22a,b,c: Wind Speed Dataset Comparison - Monthly Results



\*Dataset used in calibration, evaluation & experimental simulations

dataset produced 280mm of snow; the inversion height lapse rate produced 234mm of snow; and the monthly lapse rate produced the least snowfall (192mm). The evaluation and experimental simulations used the monthly lapse rate datasets for each water year of interest.

#### **3.4.4.3 Vapor Pressure**

Figure 3-19c illustrates the annual streamflow, baseflow, surface flow, AET, evaporation and transpiration results for simulations comparing the three vapor pressure datasets. The mean temperature vapor pressure dataset overestimated annual streamflow by 300mm. The minimum temperature dataset underestimated annual streamflow by 50mm. The combined vapor pressure dataset, which combines the minimum temperature grids from October-April with the mean temperature grids from May-September, overestimated annual streamflow by 30mm.

Figures 3-21a,b,c illustrate the simulated monthly streamflow, PET, and AET results for these vapor pressure datasets. The three vapor pressure simulations resulted in similar monthly streamflow patterns. The mean temperature vapor pressure dataset produced the highest winter streamflow levels. While winter PET and AET are within 100mm for all simulations, summer PET is much higher for the minimum temperature vapor pressure dataset. The results for the combined vapor pressure dataset shows the periods of mean temperature vapor pressure and minimum temperature vapor pressure. The evaluation and experimental simulations used the combined vapor pressure datasets for each water year of interest, because this dataset produced the closest streamflow simulation result.

#### **3.4.4.4 Wind Speed**

Figure 3-19d illustrates the annual streamflow, baseflow, surface flow, AET, evaporation and transpiration results for simulations comparing the three wind speed

datasets. The Primet dataset overestimated annual streamflow by 470mm. The Vanmet dataset underestimated annual streamflow by 220mm. The distributed wind speed dataset, produced a simulated streamflow which overestimated measured streamflow by 30mm.

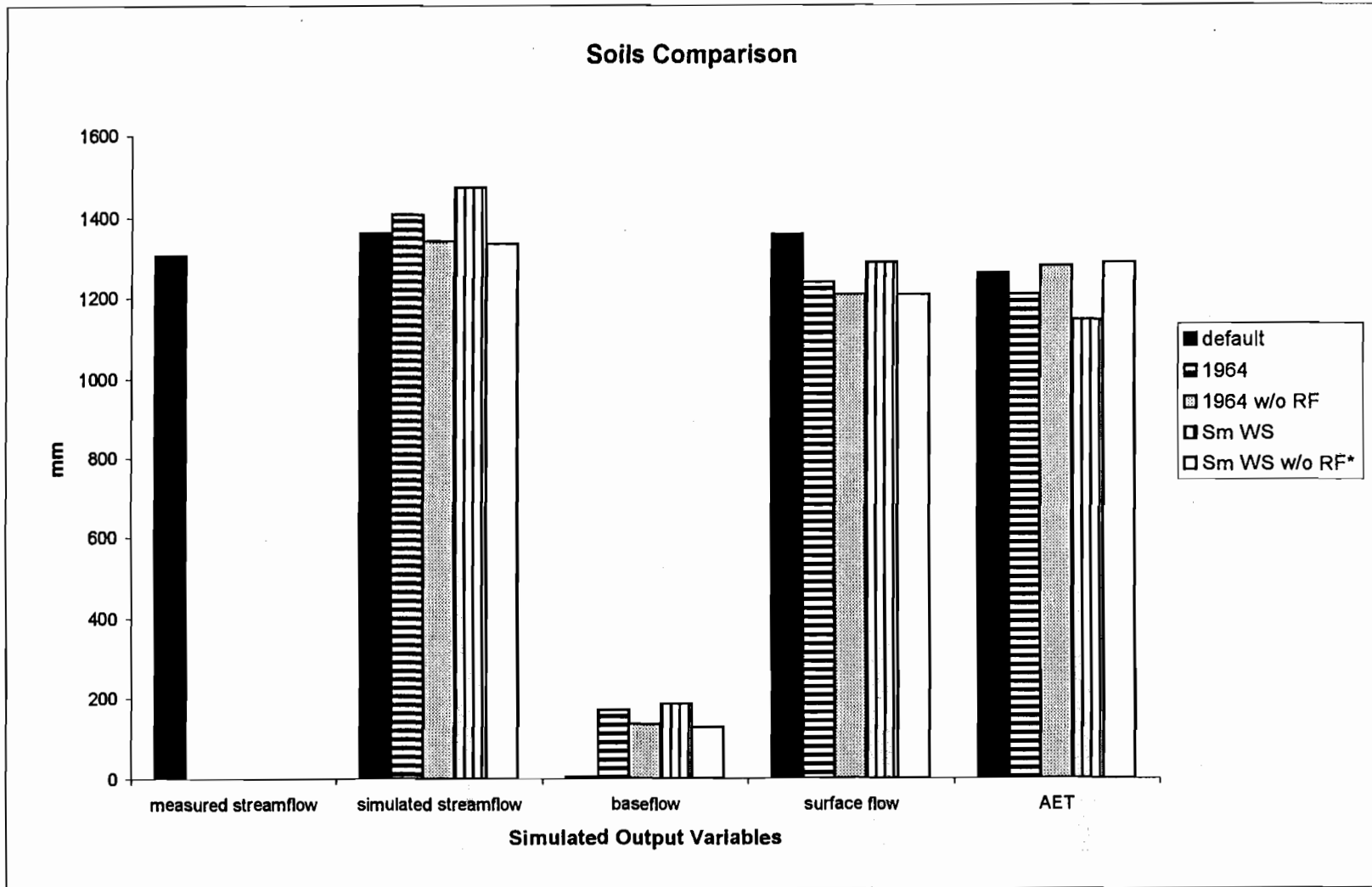
Figures 3-22a,b,c illustrate the simulated monthly streamflow, PET, and AET results for these wind speed datasets. The three wind speed simulations resulted in similar monthly streamflow patterns. The Primet dataset produced the highest winter streamflow levels. The Vanmet dataset produces an early spring peak in AET. The Primet and distributed datasets have two AET peaks. This appears to be an artifact of the vapor pressure datasets and these peaks were not seen in other years. The evaluation and experimental simulations used the distributed wind speed datasets for each water year of interest.

### **3.4.5 Soils Comparisons**

Figure 3-23 illustrates the annual streamflow, baseflow, surface flow, and AET results for simulations comparing the MAPSS default (sandy loam) soil setting against the two soil survey datasets with and without rock fragment. The soil survey datasets were created with and without rock fragment, because the calculation of effective soil depth decrease as rock fragment increases. The small watershed dataset with rock fragment overestimated annual streamflow by 200mm. The 1964 dataset with rock fragment overestimated annual streamflow by 120mm. The default soil setting overestimated annual streamflow by 55mm. The soil survey datasets without rock fragment values produced the closest annual streamflow results, overestimating measured streamflow by 35mm. Texture differences between the sandy loam of the default soil setting and the clay loam/ loam soils of the Andrews soils datasets made the largest difference in the amount of baseflow and surface flow. The sandy loam soil texture of the default soil setting produced almost no baseflow, when used in combination with the soil hydrology parameter setting for the Andrews soils.

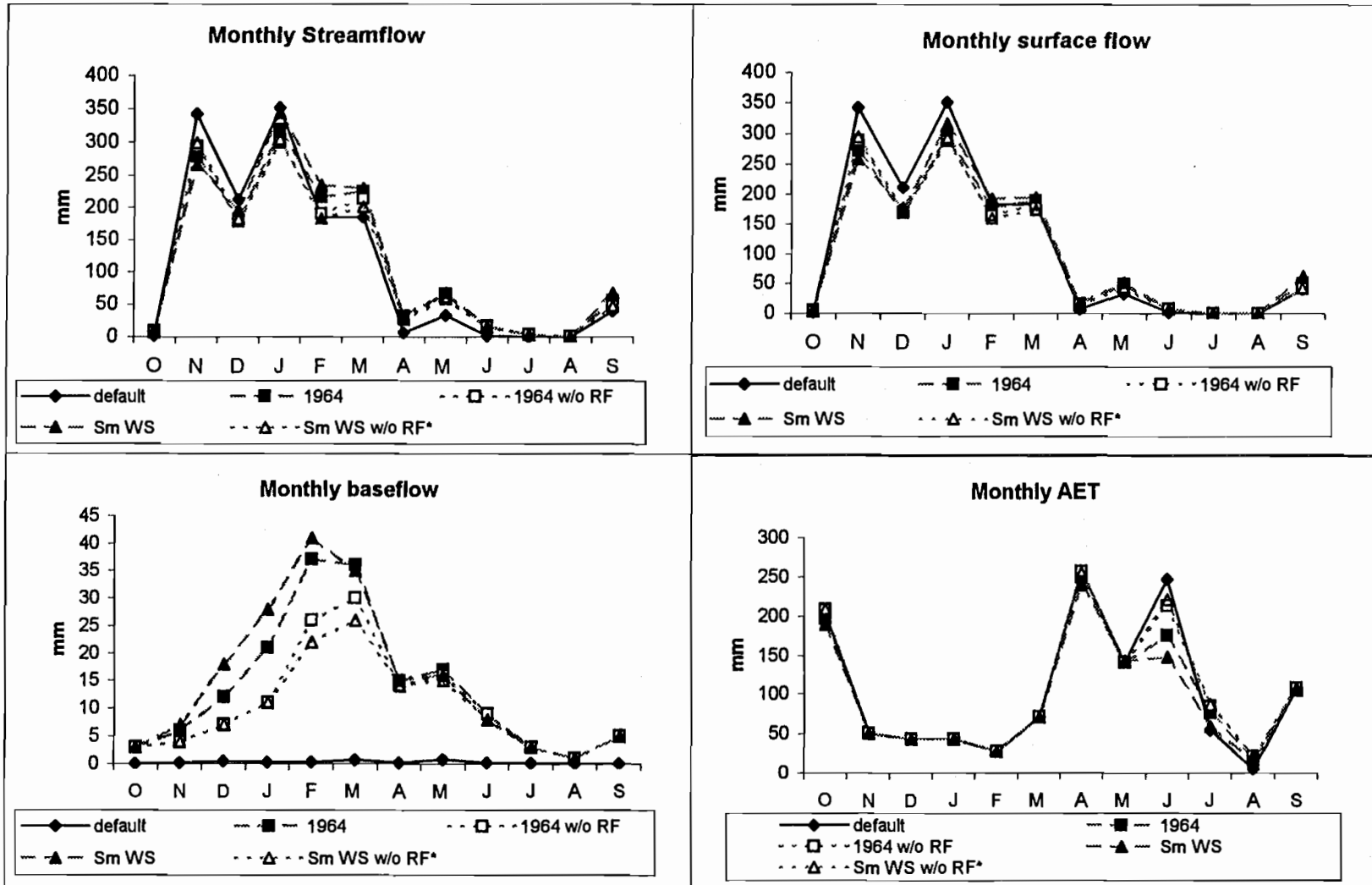
Figures 3-24a,b,c,d illustrates the monthly streamflow, baseflow, surface flow and AET results for these soils dataset comparisons. The default soil setting produced the

Figure 3-23: Soil Dataset Comparisons - Annual Results



\*Dataset used in calibration, evaluation & experimental simulations

Figure 3-24a,b,c,d: Soil Dataset Comparisons - Monthly Results



\*Dataset used in calibration, evaluation & experimental simulations

highest winter and lowest summer streamflows. The importance of rock fragment is most clearly seen in the monthly baseflow curves (Figure 3-25c).

## **3.5 Discussion**

### **3.5.1 Streamflow Simulations**

In the process of calibrating MAPSS-W for WS 1 & 2 at the Andrews, it was helpful to simplify the system by simulating the clear-cut watershed, WS1, for the first post-harvest water year (1967). These calibration simulations were run based on the assumption that there was a very limited woody vegetation LAI in the watershed during this year, thus limiting vegetation effects on the water balance. This was an important step in adjusting the soil hydrology parameters. Once the snow dynamics and soil hydrology parameters were adjusted to closely simulate the monthly and daily streamflow pattern for WS1, the model was run for WS2 changing only the necessary canopy vegetation parameters.

The accuracy of the MAPSS-W streamflow simulations relies on appropriate calibration of snow dynamics, soil hydrology, and vegetation parameter values. The difference in accuracy between the pre-harvest and post-harvest simulations indicate that MAPSS-W is sensitive to changes in local climate conditions which were not represented in the datasets developed for WS 2.

Given the assumptions made in climate dataset development, MAPSS-W does a reasonable job of representing daily, monthly and annual streamflow for WS 1 & 2. The wind speed dataset was based on averaged wind speed data. This means that the actual wind speed values were likely very different from those supplied to MAPSS-W. The vapor pressure datasets do not incorporate spatial variation in relative humidity. Differences in relative humidity may influence the vegetation on different slopes and in canopy gaps. The temperature datasets do not incorporate the influence of solar radiation, which may have substantial influences on the vegetation on the north and south aspects of the watershed. These climate variables all play significant roles in the

calculation of evaporation and transpiration, and thus influence the calculation of streamflow in MAPSS-W.

Calibration to a single water year, in this case water year 1967, may tune the model to conditions that are peculiar to that year. The calibration for 1967 appeared to capture fit the pre-harvest water years fairly well. The post-harvest simulations for WS 2 indicate that there were changes in the function of WS 2 which were not represented in the MAPSS-W simulations. WS 2 is the control watershed and was not treated directly; however, it appears that WS 2 was affected by the harvest of the vegetation in WS 1. The south edge of WS 2 borders WS 1, which was 100% clear-cut. Timber harvest along the south edge of WS 2 altered the local climate along the edge of WS 2. Plants along the edge of the watershed are likely influenced by increased turbulence, increased advection, and increased solar radiation.

The monthly streamflow results illustrate significant variability in the simulation of fall streamflow and a consistent streamflow surplus in March. The inconsistency of MAPSS-W in the fall appears to be related to the difference between modeled antecedent conditions and the true antecedent conditions for each water year of interest. The simulated streamflow surplus in March appears to be related to a deficit in simulated transpiration.

### **3.5.2 Model Generalization**

Given the differences between the climate, soils, and vegetation at Reynolds Creek and at the Andrews, it is not surprising that MAPSS-W parameter values had to be adjusted to accurately simulate the streamflow in WS 1 & 2. The most significant parameters adjustments were the ones made on snow thresholds. While streamflow dynamics at Reynolds Creek are dominated by a heavy winter snowpack and a period of spring snowmelt, streamflow dynamics in WS 1 & 2 are dominated by winter rains and summer drought.

The adjustments made to the soil hydrology parameters illustrate the importance of soil depth. In order to represent the deep soil water storage which occurs in WS 1 & 2, it was necessary to set the hydraulic conductivity values much lower than measured

values. These settings forced MAPSS-W to retain more water in the soil, which served as a surrogate for deeper soils.

The adjustments made to the vegetation parameters illustrate the importance of canopy structure. Increasing the maximum LAI threshold and light attenuation threshold allowed simulations to better represent the overstory and understory vegetation in WS 1 & 2. Adjustments were made to roughness length to increase PET and AET. Roughness lengths for the overstory conifer canopy are high due to tree height and canopy roughness.

### **3.5.3 Model Assumptions**

There are several assumptions made in MAPSS-W that hinder the model's functionality for the western Cascades. The primary assumption of MAPSS-W is that vegetation growth is limited by water. While precipitation is limited in the western Cascades during the summer, the vegetation is adapted to take advantage of the high moisture regime during the fall, spring and mild winters (Waring & Franklin, 1979). It is likely that, during the fall, winter and spring, the primary limitation to vegetation growth in this system is energy, but the watersheds do experience summer drought conditions. From a hydrological perspective the changes in LAI during succession should have a large effect on summer streamflow levels.

#### **3.5.3.1 Soils**

MAPSS-W limits functional soil depth to a maximum of 1.5m. In order to simulate adequate soil water storage, hydraulic conductivity parameters were adjusted to hold water in soil. Even with these adjustments the simulation of daily streamflow is quite flashy. This limitation to functional soil depth also eliminates root expansion beyond 1.5m.

### 3.5.3.2 Vegetation

MAPSS-W uses a turbulent transfer equation to calculate PET. This calculation of PET assumes that the vegetation acts as a single large leaf surface and the calculation is driven by wind speed, vapor pressure, and temperature. The accuracy of this equation is hindered by data limitations. Daily wind speed data is the key variable for this equation and the least well developed climate variable at the Andrews. The measurement locations and dates are not directly representative of WS 1 & 2. The single wind speed dataset which was developed for all water years of interest probably significantly hinders the ability to replicate streamflow patterns, because the temporal correlation between daily wind speed and the other climate variables has been lost. While the MAPSS-W PET calculation does not directly include a radiation term, the temperature dataset could have been adjusted to represent the influence of solar radiation. This adjustment was not included in the temperature data development and likely contributes to the errors in streamflow patterns as well.

MAPSS-W does not represent vegetation water storage mechanisms such as sapwood storage. In forest systems, such as WS 1 & 2, sapwood storage has been estimated to be as high as 250m<sup>3</sup>/ha. This is enough to supply half of the daily water budget (Waring & Franklin, 1979). This storage mechanism likely buffers some of the daily streamflow variation.

MAPSS-W makes several limiting assumptions about vegetation function. It is assumed that each lifeform (trees, shrubs, and herbs) is limited to a single set of transpiration parameter values. Each grid cell is designated as shrub or tree vegetation depending on the total woody LAI value. This means that trees and shrubs are not simulated in the same grid cell, which eliminates potential competition between woody lifeforms. Since each lifeform is limited to a single set of transpiration parameters, only one functional vegetation group can be represented for each lifeform per simulation. In order to perform experimental simulations comparing the hydrologic function of the vegetation functional groups, it was necessary to perform multiple simulations.

### **3.6 Conclusions**

This chapter presents the calibration and evaluation of MAPSS-W for WS 1 & 2 at the H.J. Andrews Experimental Forest. The process of calibration included single parameter sensitivity analysis of key snow dynamics and soil hydrology parameters. The evaluation process included comparisons between simulated and measured streamflow, and dataset comparisons.

The calibration of MAPSS-W for WS 1 & 2 highlighted the importance of snow dynamics, soil depth, and canopy parameters. The parameterization of snow thresholds was the most important adjustment for correct simulation of monthly streamflow patterns. Parameterization of hydraulic conductivity values to increase soil water storage as a surrogate for increasing soil depth was the key to correctly simulating baseflow levels. Roughness length parameterization was the most important adjustment for increasing PET and transpiration.

## **4. Chapter 4: An Investigation of Early Successional Vegetation Influences on Summer Streamflow Following Clear-Cut Harvest in the Western Cascades**

### **4.1 Introduction**

For management purposes, it would be useful to be able to predict the hydrologic response of unmonitored small basins. Developing an understanding of the hydrologic behavior of vegetation groups in terms of measurable characteristics such as leaf area, soil moisture, and potential transpiration may aid in efforts to predict streamflow responses in unmonitored watersheds. Human landuse practices are often correlated with alterations in streamflow quantity, quality and timing (Swank & Johnson, 1994). Paired watershed studies are based on hypotheses about the influence of landuse changes on streamflow. Landuse practices frequently alter soil structure and vegetation structure and communities. These studies examine the hydrologic function of soils and vegetation in an effort to understand the key hydrologic processes influencing streamflow. The quantity, quality and timing of streamflow is important for the plants and animals of the stream and riparian ecosystems, and influences the water resources available for human communities and recreation uses.

In the Pacific Northwest, low streamflows occur during the summer, coinciding with the period of greatest biological activity. Decreased water yield may lead to increased water temperatures which affects water chemistry, particularly the quantity of dissolved oxygen (Hicks et al., 1991). Lower water levels can affect the availability of rearing and spawning habitat for fish species (Hicks et al., 1991).

Timber harvest is the primary human landuse activity in many of the small mountain watersheds in the Pacific Northwest and has significant impacts on water yield and water quality. A paired watershed study was established in Watersheds 1 & 2 (WS 1 & 2) in the H.J. Andrews Experimental Forest (HJA) in 1952. Hicks et al. (1991) and Jones & Grant (1996) showed a long-term increase in annual streamflow following clear-cut harvest, but summer streamflows showed an initial increase in flow levels during and immediately following harvest, but quickly decreased to pre-harvest levels and then fell below pre-

harvest streamflow levels. These changes in summer streamflow correspond to changes in the vegetation cover in WS 1. Herbaceous vegetation cover is followed by a period of broadleaf shrub cover, which is followed by a return to conifer dominance.

The objective of this study was to investigate the influence of successional vegetation on summer streamflows following clear-cut harvest in the western Cascades, based on model simulations of streamflow records and vegetation plot data from HJA WS 1& 2. Five sets of aerial photos, vegetation plot data, and a spatially explicit watershed model were used to examine the influences of vegetation on streamflow. Four hydrologically distinct plant functional groups were defined and the vegetation data were aggregated and analyzed based on these functional types. Associations between hydrologic plant functional groups and landscape parameters were determined using repeated measures analysis in order to account for the temporal correlation between measurements. Hypotheses of vegetation-hydrology interactions were experimentally tested using a spatially explicit watershed model. This study indicates that the influence of vegetation on streamflow levels is related to the water use patterns of the species present.

This chapter describes vegetation-hydrology interactions and formulates & evaluates alternative hypotheses of vegetation influences on streamflow in WS 1. The patterns of early successional vegetation in WS 1 are described based on the analysis of aerial photos of the watershed and vegetation plot data. The mechanisms of vegetation influence on streamflow were explored through watershed simulations and the simulation results are presented. The implications of vegetation-hydrology interactions are discussed based on the vegetation analysis and model simulation results.

## **4.2 Background**

### **4.2.1 Influences of Forest Management on Summer Streamflow**

Forest harvest produces reductions in transpiration and interception. This results in increased soil water which may be used by the remaining vegetation or may increase

streamflow levels. The quantity of extra water produced depends on a combination of factors, including the amount and type of vegetation at the site of harvest, the pattern and intensity of land use and the climate of the area. Annual water yield increases associated with land use are generally not distributed uniformly throughout the year (Swank and Johnson, 1994). Forest harvest in areas with shallow soils and significant snow cover produces large increases in flows during spring and summer months in direct response to precipitation patterns and evapotranspiration reductions. Harvest in watersheds with deep soils and rain dominated precipitation regimes produces flow increases in summer and autumn months and may extend into early winter (Swank & Johnson, 1994). If there is little precipitation during the growing season, streamflow increases are produced during the fall recharge period. Reduced evapotranspiration due to harvest means less unused soil water storage capacity during storms because soil moisture levels are already high. This contributes to increased fall peak flows. Generally winter peak flows show the least influence from changes in storage, since soils tend to be fully recharged at that time of year (Swank & Johnson, 1994). When examining the effects of land use on streamflow, it is important to keep in mind that an increase in streamflow is only as permanent as the change that produced the increase. As the vegetation regenerates in clear-cut areas, the annual streamflow levels decrease as interception and transpiration increase (Rothacher, 1970).

In the conifer forests of Russia (Shiklomanov & Krestovsky, 1988), runoff typically rises sharply on newly harvested areas, then declines due to increased water consumption by young forests up to the age of 40-60 years. Water yields level off at decreased levels (below the level of pre-harvest streamflows) for an additional 40-60 years, followed by increases in streamflow after 100 years of growth. Young and middle aged forests transpire 10 - 20% more water than mature forests (120 years old) and 20 - 30% more than old growth forests (200 years old). Young forests are typically more dense and contain more leaf mass per unit area than old forests (Shiklomanov & Krestovsky, 1988).

Analysis of streamflow records in Australia (Borg & Stoneman, 1991) shows a similar pattern in water yields, but in a shorter amount of time. Leaf area in regrowth stands reached that of mature, unlogged stands after 5 - 10 years of regeneration, and continued to increase for another 5 - 10 years, stabilizing above pre-harvest cover

values. This coincided with an increase in streamflow followed by a recession in streamflow to levels below pre-harvest (Borg & Stoneman, 1991).

However, evapotranspiration is not directly proportional to the amount of leaf area, because it is also controlled by availability of soil water and vapor pressure deficit. Nevertheless, when soil water is available it's rate of decline is controlled by the transpiring leaf area. The main influence of a stand with greater leaf area is that the available soil water is used more quickly. (Borg & Stoneman, 1991). This may cause a shift in the seasonality of water use and a decrease in streamflow at the end of the warm, dry season.

#### **4.2.2 Vegetation Water Use Habits**

In addition to soil water and vegetation leaf area influences, species composition also influences evapotranspiration. Differences in plant water use habits, between species, can be described along a gradient of drought tolerance to drought intolerance. The extremes of this gradient have been defined as hydrostable and hydrolabile (Larcher, 1995). Hydrostable plants maintain a stable water balance throughout the day. These plants have sensitive stomatal control, efficient and extensive root systems, and often have mechanisms for root or stem water storage. Hydrolabile plants lose large amounts of water and tolerate the consequent rise in cell sap ion concentration. These plants tolerate strong fluctuations in water potential, as well as temporary wilting. Conifers are considered to be hydrostable, broadleaf deciduous plants moderately hydrostable, and evergreen broadleaf plants hydrolabile (Larcher, 1995).

Conifers are considered to be hydrostable, because they generally maintain a stable leaf water balance throughout the day, due to highly sensitive stomatal control in response to increasing vapor pressure deficits. The maximum stomatal conductance rate is between 2 - 4 mm/s (Waring & Franklin, 1979). Large conifers store enough water in the sapwood to provide more than half the daily water budget (Waring and Franklin, 1979). Conifers develop extensive lateral root systems, and some extend roots into deep soil layers. Conifers have been observed to root into fractured bedrock layers where there are shallow soils (Pabst et al., 1990).

Deciduous broadleaf species are considered moderately hydrostable, because they maintain a fairly stable leaf water balance throughout the day when there is sufficient soil moisture and have a highly sensitive stomatal response to increasing vapor pressure deficits when there is a soil moisture deficit ( $< -1.5\text{mpa}$ ) (Shainsky et al., 1994). Red alder, a key species considered in the vegetation hypotheses about WS 1, has maximum stomatal conductance rates of 8 - 10 mm/s (measured as high as 30 mm/s) (Shainsky et al., 1994). Red alder is considered drought sensitive and begins to close stomata at a plant water potential of  $-1.2\text{mpa}$  and wilting occurs at  $-1.5\text{mpa}$  (Shainsky et al., 1994). Deciduous broadleaf species have a wide range of rooting habits, but some deciduous broadleaf shrubs have been observed to be more shallowly rooted than evergreen broadleaf shrub species (Conard, 1986; Pabst et al., 1990).

Evergreen broadleaf species are considered hydrolabile, because they are tolerant of large water potential deficits. Stomatal response is based on plant water potential rather than vapor pressure deficit. Stomata may begin to close at soil water deficits of  $-2.5\text{Mpa}$ , but wilting point does not occur, for some species, until water potentials of  $-5\text{Mpa}$  (Conard et al., 1985). *Ceanothus sp.*, key evergreen broadleaf species in the vegetation hypotheses about WS 1, have been observed to root to depths of 2.4m and extend roots laterally well past the edge of the canopy (Conard et al., 1985). The maximum stomatal conductance rates for evergreen broadleaf species are between 5 - 7 mm/s (Waring & Franklin, 1979).

Figures 4-1 & 4-2 illustrate stomatal response for these three groups of woody vegetation. These figures show the relative differences in behavior between the three physiological groups used as plant functional groups in this analysis. Maximum stomatal conductance, soil moisture deficit, and vapor pressure deficits were defined based on the representative species found in WS 1 (Conifer - Douglas-fir, Deciduous Broadleaf - Red alder, Evergreen Broadleaf - *Ceanothus sp.*) Figure 4-1 illustrates stomatal response to soil moisture deficit. Figure 4-2 illustrates stomatal response to vapor pressure deficit and is adapted from Waring & Franklin (1979).

As a result of these differences in water use, evergreen species and deciduous broadleaf species have different seasonal water use patterns in the Pacific Northwest. Evergreen species are at an advantage in wet winter, dry summer climates. Due to moderate temperatures, and evergreen foliage these species photosynthesize and

transpire during the winter months. The conical canopies of conifers give them an additional advantage because this canopy shape maximizes the capture of diffuse winter light (Waring & Franklin, 1979). As much as half of conifer assimilation occurs during the winter.

These seasonal differences in water use influence the timing of streamflow. Spring water yields are 20 to 30 % greater from deciduous forests than from conifer forests (Shiklomanov & Krestovsky, 1988). Broadleaf forests may dry out soils and lower the level of the ground-water table more than conifers, due to higher transpiration rates. This decreases summer streamflows in areas that have been converted to broadleaf forest (Shiklomanov & Krestovsky, 1988). Soil moisture depletion has been measured to occur earlier in the summer season under deciduous broadleaf vegetation than under conifers or evergreen broadleaf vegetation (Conard, 1986; Pabst et al., 1990).

Estimates of total annual transpiration from woody vegetation stands in the northern hemisphere range between 300–800 mm/year. Evergreen conifers are estimated to transpire 300–600 mm/year, evergreen broadleaf stands transpire 400–500mm/year, and deciduous broadleaf transpire 500–800 mm/year (Larcher, 1995). While these average values for stand transpiration have been calculated, it is important to note that local estimation of stand transpiration should incorporate the temporal variability in evaporation stress and water availability.

While this study focuses on the differences between hydrologically distinct plant functional groups which are defined based on water use habits, it is worth noting that there are additional influences on water use. The age of the vegetation and landscape position have been observed to influence stomatal control and function.

Tree age may influence the rate of transpiration in two ways. Age related changes in stem resistance have been measured (Mattson-Djos, 1981). Additionally, short, young trees need to overcome less lift, thus less resistance to get water to the leaves. This difference in resistance is due to the distance traveled, thus, for the same amount of vegetation cover, a young tree can remove water from the surface soil more quickly than a mature tree (Borg & Stoneman, 1991). These increases in resistance with age can result in reductions in stomatal conductance, thus reductions in transpiration rates for mature trees (Borg & Stoneman, 1991).

Figure 4-1: Stomatal Response to Soil Moisture Deficit

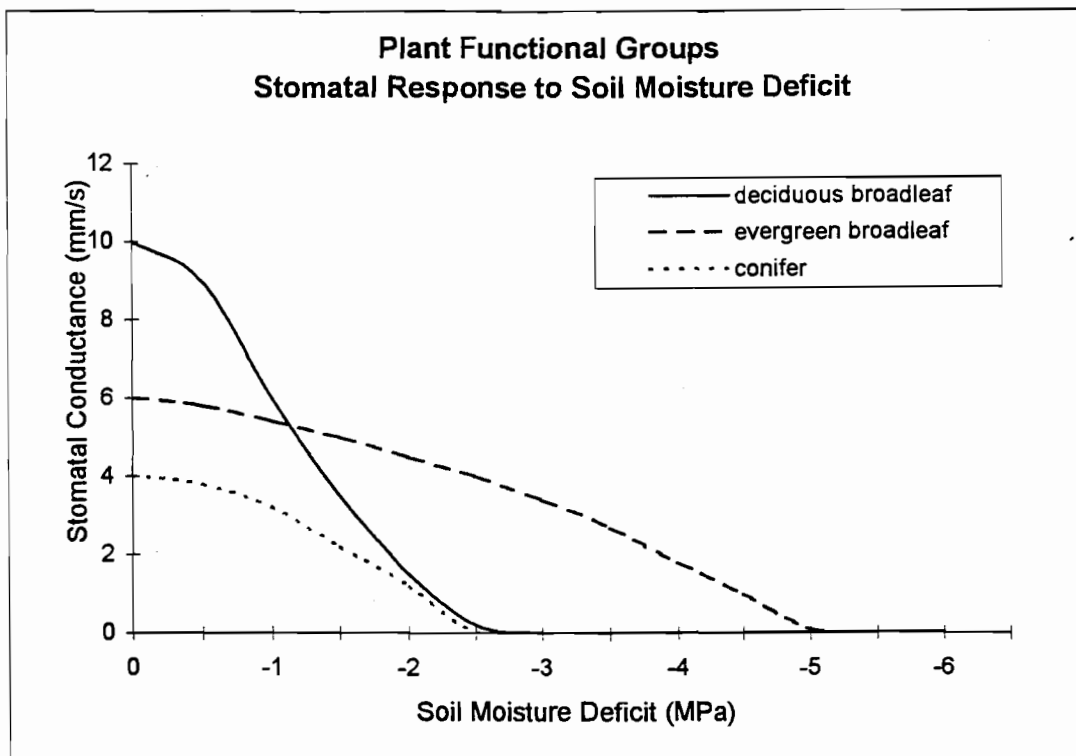
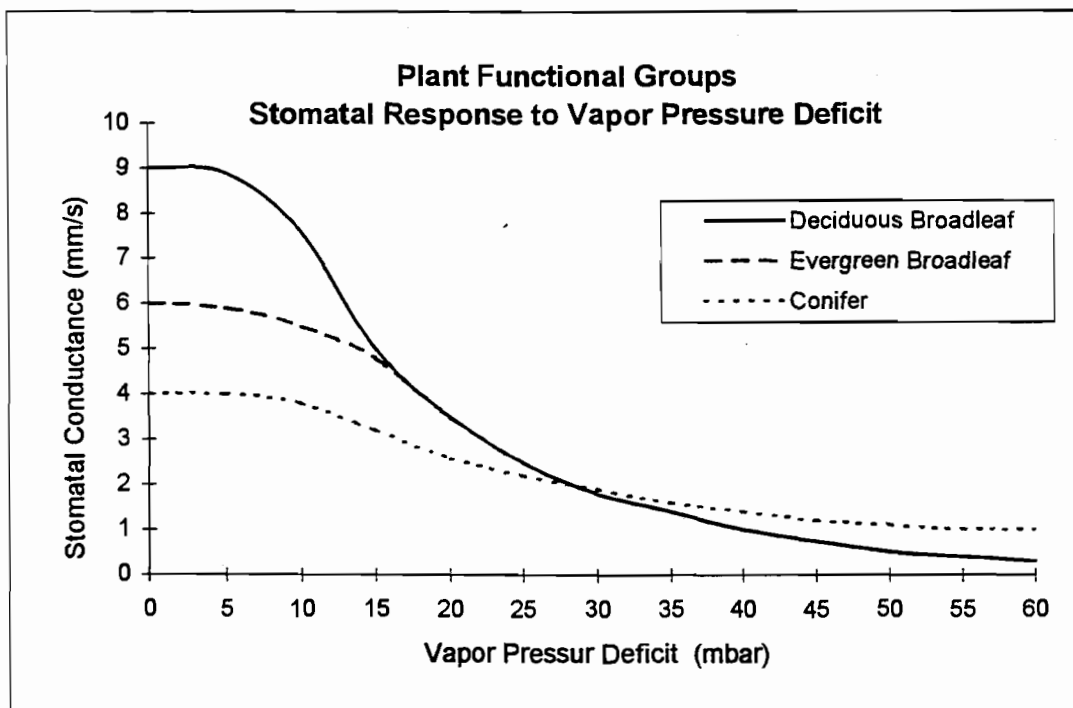


Figure 4-2: Stomatal Response to Vapor Pressure Deficit



(Adapted from Waring &amp; Franklin, 1979)

Plant water use habits have also been observed to vary along a landscape position gradient. Ridge top and valley bottom representatives of the same oak species were found to have different vapor pressure and soil moisture thresholds (Sala & Tenhunen, 1994). Trees on the ridge top exhibited greater control of water loss at high evaporative demand. The trees in the valley bottom showed less control in high evaporative demand conditions (Sala & Tenhunen, 1994). These water use patterns may be influenced by available soil moisture, incident radiation levels, wind speeds and vapor pressure gradients. The valley bottom had greater soil depth for soil water storage, reduced radiation, reduced wind and lower vapor pressure gradients (Sala & Tenhunen, 1994).

#### **4.2.3 Plant - Atmosphere Interactions**

Plants provide a pathway for the movement of water back into the atmosphere from the soil. The vapor pressure gradient (VPG) around the leaf is the driving force for plant water loss. VPG is sometimes represented by the vapor pressure deficit (VPD) which is the difference between the actual and saturated vapor pressure of the air at a particular temperature. When leaf temperature equals air temperature, VPD and VPG are equivalent (Shainsky et al., 1994). Solar radiation and atmospheric saturation deficit are the major environmental variables that influence stomatal conductance. Low levels of solar radiation are sufficient to stimulate stomatal opening in the morning, but during the day increasing atmospheric vapor pressure deficits can lead to a progressive decrease in stomatal conductance (Waring & Schlesinger, 1985).

In a conifer forest, the major constraint on transpiration is the vapor pressure deficit. When the vapor pressure deficit of the air exceeds 3 MPa the trees close their stomata. Wind speed and solar radiation have little effect because the canopy is aerodynamically rough. Rapid, turbulent air movement keeps the canopy temperatures within a few degrees of ambient air temperature (Waring & Schlesinger, 1985). Broadleaf vegetation is sensitive to the total incoming radiation and changes in wind speed. Broadleaf leaf temperatures can climb to 4-8 °C above ambient temperature. This increase in canopy temperature can increase the leaf-air water deficit by 40-60% on

warm days (Monteith & Unsworth, 1990; Waring & Schlesinger, 1985). In order to avoid lethal leaf heating, broadleaf vegetation keeps stomata open during periods of high radiation (Waring & Schlesinger, 1985).

These differences in atmospheric coupling between broadleaf and conifer canopies were illustrated by a comparison made by Baldocchi & Vogel (1996). Evapo-transpiration and local climate measurements were taken at a boreal conifer site and a temperate broadleaf site. While the distance and differences in environment are important to keep in mind, the temperate broadleaf forest evapotranspiration measurements were about three times greater than those for the conifer forest. Solar radiation was the primary explanatory variable for the broadleaf forest, and vapor pressure deficit was the primary explanatory variable for the conifer forest.

The coupling of the overstory canopy with the atmosphere is influenced by the atmospheric roughness created by the rough surface of the forest. As air masses move over the canopy the roughness causes turbulence in the canopy boundary layer and may increase turbulence within the canopy as well (Shiklomanov & Krestovsky, 1988).

The rate of transpiration of individual leaves decreases with increasing stand density because the microclimate within the stand tends to reduce evaporative demand. As stand density increases individual leaves are shielded from radiation and wind. Dense stands also develop high humidity levels within the stand (Larcher, 1995). In Pacific Northwest old growth forests, the understory vegetation is atmospherically buffered by the multi-layered canopy. Humidity, and air and soil temperature fluctuations are relatively small compared to the fluctuations in open areas (Halpern & Spies, 1995).

While calculations of forest transpiration are based primarily on canopy transpiration, it has been found that understory vegetation can make significant contributions to the total forest transpiration, where canopy structure is patchy (Lindroth, 1985). Measurements in a thinned Douglas-fir stand showed that salal, a broadleaf shrub, contributed half of the total stand transpiration on clear days (Black & Kelliher, 1989).

The structure and stature of vegetation can have significant influences on local climate variables. Greater surface and air temperature extremes, humidity extremes and lower rainfall interception were measured at burned sites as compared to unburned sites in Minnesota (Ahlgren, 1981). The range of temperature and humidity extremes

decreased as woody vegetation cover increased. Revegetation began with herbaceous growth, followed by shrub development and the later emergence of mixed forest. Shrub and forest development coincide with a decrease in the temperature extremes and a decrease in soil moisture due to increased interception (Ahlgren, 1981). Measurements before and after forest clearing in Australia showed a rise in mean surface temperature of 4 °C and an increase in the summer diurnal surface temperature range of 12 °C (Silberstein, 1996). Soil surface temperatures in clear-cuts in the western Cascades have been measured to be as high as 65 °C (Conard et al., 1985). It is likely that temperature and humidity extremes increased in HJA WS1 following the harvest and burn treatments.

### **4.3 Materials and Methods**

#### **4.3.1 HJA WS 1 Summer Streamflow Analysis**

Figures 4-3a,b,c illustrate the HJA WS 1 streamflow response to clear-cut harvest and broadcast burn. These figures represent WS 1 streamflow response as corrected for interannual climate variability by comparison with the control watershed, WS 2. Streamflow response was calculated as the difference between WS 1 measured streamflow and WS 1 predicted streamflow. Streamflow was predicted for WS 1, for each water year, based on the measured streamflow in WS 2. These calculations are based on the pre-harvest comparisons between streamflow in WS 1 & 2, in which regression equations were calculated for WS 1 streamflow as a function of WS 2 streamflow. Figure 4-3a illustrates the total annual streamflow response, Figure 4-3b illustrates the summer (July-August) streamflow response, and Figure 4-3c illustrates the late summer streamflow response (August). These figures are adapted from Hicks et al., (1991).

This study focuses on the late summer streamflow patterns. The five periods of interest in the summer streamflow record are marked in Figure 4-3c and are represented in this study by groups of water years that coincide with aerial photos and vegetation data. The periods of interest include: the pre-harvest period (1952-62), a period of increased

summer streamflow (1962-70), the period of rapid summer streamflow recession to pre-harvest levels (1970-76), a period decreased summer streamflow (1977-89) and a second return to pre-harvest streamflow levels (1990-present). These changes in streamflow raise questions about the environmental factors that influence summer streamflow levels. It is hypothesized that these changes in summer streamflow levels are the result of changes in vegetation-hydrology interactions due to post-harvest vegetation succession..

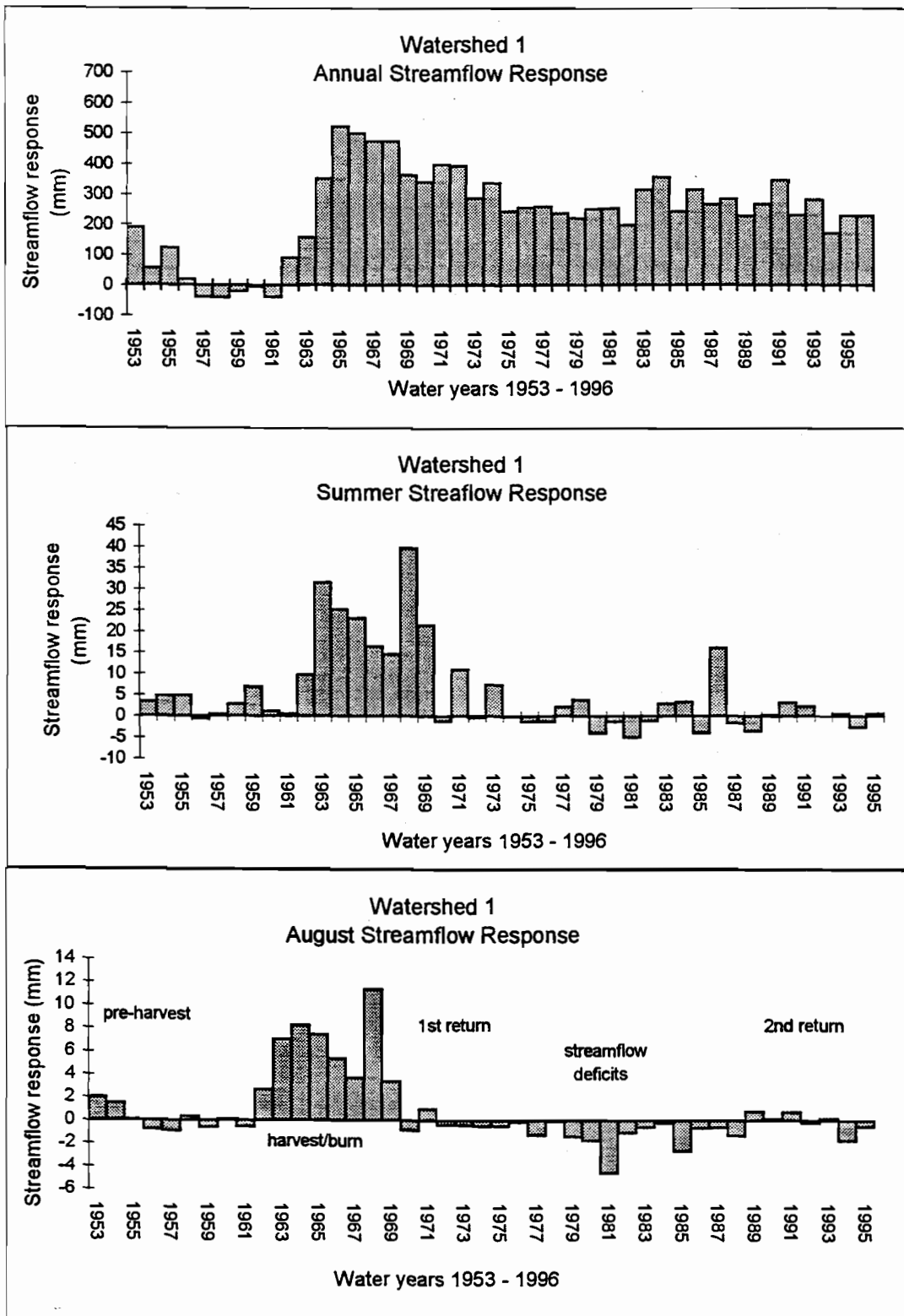
On average, only 2-4% of the annual streamflow occurs during the dry months of July, August and September (Hicks et al., 1991). Stream and riparian organism are particularly sensitive during the summer. While summer flows were 3-5 times greater than the pre-harvest levels during the first few years after logging (Hicks et al., 1991), these initial increases rapidly disappeared. During the period of summer streamflow deficit (1977-1989), streamflow during July and August averaged 14% (1.7mm,  $p=0.039$ ) lower than pre-harvest streamflows and streamflow during August averaged 25% (1.0mm,  $p=0.032$ ) lower (Hicks et al., 1991).

#### **4.3.2 WS1 Vegetation Dynamics**

The pre-harvest forest in WS 1 was dominated by a mixture of old-growth (300-500 yr.) and mature (125 yr. old) Douglas-fir (*Pseudotsuga menziesii* (Mirbel) Franco) with western hemlock (*Tsuga heterophylla* (Raf.) Sarg.) dominating the sub-canopy. Other understory tree species included pacific yew (*Taxus brevifolia* Nutt.), hazel (*Cornus nuttallii* Aud. Ex T. & G.), big-leaf maple (*Acer macrophyllum* Pursh.), chinquapin (*Castanopsis chrysophylla* (Dougl.)A. DC.), sugar pine (*Pinus lambertiana* Dougl.), and western cedar (*Thuja plicata* Donn). The riparian vegetation consisted largely of old-growth conifers and shade-adapted herbaceous species. The overstory canopy cover (> 6m) averaged 59% (Halpern, 1987).

During the four year harvest of WS 1 (1962-66), the pre-cut understory plant communities provided vegetation cover in the watershed. Following the broadcast burn in 1966, colonizing herbaceous species became established providing significant cover

Figures 4-3a,b,c: WS 1 Streamflow Response



Adapted from Hicks et al., 1991

within 2 years (Halpern, 1987). Douglas-fir was aerially seeded during October 1967. Aerial seeding was repeated on a small area of the south facing slope during October 1968. Due to poor Douglas-fir seedling generation, the entire watershed was planted with 2 year old Douglas-fir seedlings in April and May 1969. Open patches on the south facing slope had high seedling mortality and 40 ha of this slope were planted again in April 1971 (Halpern, 1989).

Following harvest in WS1, vegetation succession has followed the general pattern of early succession in the Oregon Cascades. Early grass and herbaceous vegetation was replaced by broadleaf shrubs, which have been replaced by a young Douglas-fir forest. Analysis of long-term vegetation data (Halpern, 1987; Halpern, 1988; Halpern, 1989), provides estimates of vegetation cover in WS 1. Total herb and shrub cover increased rapidly and reached 93% in 1968 (Halpern, 1989). The herbaceous vegetation dominated for 11 years, followed by a period of shrub and herb co-dominance. High shrub densities persisted through the 17th year after harvest then declined abruptly. In 1987, canopy cover of tall shrubs and regenerating tree species had reached 76% and 44% respectively (Halpern, 1989). Conifer dominance began as shrubs declined during the second decade after harvest (Halpern & Franklin, 1990). The riparian corridor is dominated by deciduous broadleaf tree species, particularly red alder, and herbaceous species. This riparian vegetation established within 5 years of the end of harvest. Before harvest, total understory cover of residual and invading species was about 100%. By 1990, total understory cover had increased to approximately 175%. This estimate was based on aggregations of individual species cover measurements (Halpern & Spies, 1995).

The vegetation in WS 1 has not regenerated evenly. The north and south facing slopes show distinct successional trajectories. While a dense stand of Douglas-fir has established on much of the north facing slope, mixed patches of trees, shrubs, herbaceous vegetation and bare ground are scattered over the south facing slope. Vegetation successional trajectories in the HJA Experimental Forest have been classified as slow, average and fast (Nesje, 1996). The north facing slope has followed a fast successional trajectory, skipping from a semi-open, shrub stage directly to a dense young conifer stand in 20-25 years. The east corner of the south-facing slope has followed an average trajectory, with a dense shrub stand that is developing a young

conifer stand. Meanwhile, most of the south facing slope has followed a slow trajectory, with a mixture of shrubs, patches of deciduous broadleaf trees and shrubs and small conifers.

Invading herbaceous species, which were not present prior to harvest, contributed significantly to the vegetation cover during the first five years following harvest. Woodland groundsel (*Senecio sylvaticus* L.), autumn willowweed (*Epilobium paniculatum* Nutt.), and horseweed (*Conyza canadensis* Cronq.) developed dense cover during the first five years after harvest (Halpern, 1989). The major residual herbaceous species include: western starflower (*Trientalis latifolia* Hock.), and white hawkweed (*Hieracium albiflorum* Hook.) (Halpern, 1989).

Invading and residual shrub species ( both deciduous broadleaf and evergreen broadleaf) contributed to the dominant shrub cover during the second decade after harvest. The evergreen broadleaf species were most heavily concentrated in the north-eastern corner of WS 1. Invading shrub species include: snowbrush (*Ceanothus velutinus* Dougl. ex Hook.), buckbrush (*Ceanothus sanguineus* Pursh.), thimbleberry (*Rubus parviflorus* Nutt.), and willow (*Salix scouleriana* Barratt) (Halpern, 1989). Residual shrub species include: vine maple (*Acer circinatum* Pursh.), salal (*Gaultheria shallon* Pursh.), pacific rhododendron (*Rhododendron macrophyllum* G.), Oregon grape (*Berberis nervosa* Pursh.), and California hazel (*Corylus cornuta* Marsh.) (Halpern, 1989). The invading and residual evergreen broadleaf species typically reach maximum height and stand density within 10-15 years and stand senescence begins once the plants are 15-25 years old (Zavitkovski & Newton, 1968; Hughes et al., 1987).

By 1990, Douglas-fir (*Pseudotsuga menziesii* (Mirbel) Franco) was again the dominant conifer tree species, and red alder (*Alnus rubra* Bong.) dominated the riparian corridor. Bigleaf maple (*Acer macrophyllum* Pursh.), pacific dogwood (*Cornus nutallii* Aud. ex T. & G.), pacific madrone (*Arbutus menziesii* Pursh.) and golden chinquapin (*Castanopsis chrysophylla* (Dougl.) A. DC.) were scattered over the hillslopes (Halpern, 1989).

### **4.3.3 WS 1 Hydrologic Hypotheses**

In order to determine how patterns of vegetation succession influence streamflow in WS 1, the patterns of vegetation succession, local climate variability, and streamflow must be linked. Table 4-1 summarizes the observed changes in streamflow, dominant vegetation group, local climate variables, moisture storage mechanisms, and vegetation canopy dynamics. This table serves as a summary of the hypotheses about vegetation-hydrology interactions that are occurring in WS 1. Changes in streamflow are represented as a comparison of the streamflow in WS 1 against the control watershed (WS 2) streamflow, accounting for inter-annual climate differences. Precipitation interception and storage are described on a continuum of low to high. The relative contribution of canopy and epiphyte interception and sapwood storage are represented in Figure 4-4a. Changes in canopy structure and transpiration parameters are represented by values calculated from local vegetation measurements and literature values. Changes in canopy structure variable over time are illustrated in Figure 4-4b. Changes in transpiration parameters over time are illustrated in Figure 4-4c. Changes in local climate variables are represented as relative levels along a continuum of low to high.

The influence of the pre-harvest forest canopy on streamflow in WS 1 is assumed to include high levels of interception and evaporation (Figure 4-4a) due to the mild climate, frequent, low intensity rainstorms during the long rainy season, and dense vegetation canopy (Rothacher, 1970). Potential transpiration is high since summers are dry and warm, and the dense conifer vegetation has a large needle surface area. Actual transpiration is moderately high but constrained in the summer by soil moisture deficits and high vapor pressure deficits (Rothacher et al., 1967). Soil moisture is completely recharged each winter and evaporation from the soil is low under the dense canopy. Clear-cut harvest is assumed to decrease evaporation and transpiration significantly and result in a corresponding increase in streamflow (Rothacher, 1970).

**Table 4-1: Streamflow, Vegetation, and Local Climate Changes Following Harvest in WS 1**

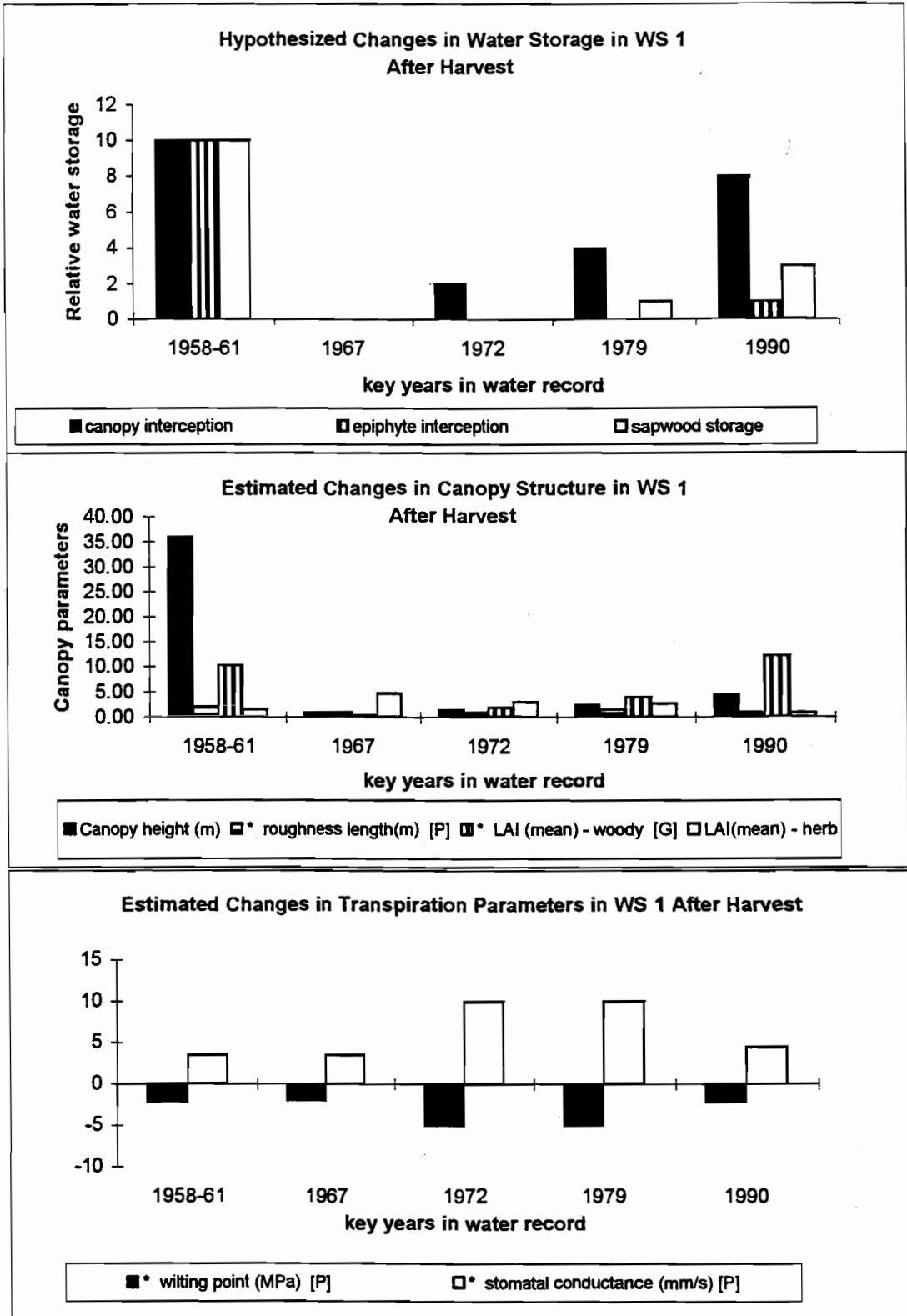
	1958-61	1967	1972	1979	1990
	pre-harvest	1 yr post harvest	6 yr post harvest	13 yr post harvest	24 yr post harvest
<b>streamflow (log(ws1-ws2))</b>	0	60	0	-20	0
seasonality of water use	Sp/S/F	S	S	S	Sp/S/F
1° location of water use	hillslope	hillslope	hillslope	hillslope	hillslope
2° location of water use	riparian	riparian	riparian	riparian	riparian
<b>Vegetation dynamics</b>					
dominant vegetation	C	H	D/H	D/E	C/D
secondary vegetation	E/D	E/D	E	C/H	E/H
<b>Evaporation &amp; Storage</b>					
canopy interception	high	low	moderate	moderate	high
epiphyte interception	high	low	low	low	low
sapwood storage	high	low	low	low	moderate
<b>Canopy structure</b>					
Canopy height (m)	36.00	1.00	1.50	2.50	4.50
* roughness length(m) [P]	2	1	1	1.5	1
* LAI (mean) - woody [G]	10.3	0.4	1.9	4	12.3
LAI(mean) - herb	1.5	4.7	3	2.7	0.9
<b>Maximum Transpiration</b>					
* wilting point (MPa) [P]	-2.2	-2	-5	-5	-2.2
* stomatal conductance (mm/s) [P]	3.5	3.5	10	10	4.5
<b>Local Climate</b>					
Canopy Temperature	ambient	> ambient	> ambient	> ambient	ambient
Canopy Humidity	high	low	low	low	high
Surface Humidity	high	low	moderate	moderate	high
Surface Temperature	low	high	high	moderate	low
Surface Solar Radiation	low	high	high	moderate	low

\*MAPSS-W parameter [P] or gridded [G] input

Sp-spring, S-summer, F-fall

C-conifer, D-deciduous broadleaf, E-evergreen broadleaf, H-herbaceous

Figure 4-4a,b,c: Hypothesized Changes in WS 1 Vegetation Function Following Clear-cut Harvest



#### **4.3.3.1 Increased Summer Streamflow During Harvest**

Since the beginning of the small watershed study in the 1960's a number of hypotheses have been suggested to explain the observed patterns in summer streamflow levels. It is generally accepted that the increases in streamflow during and following harvest are due to the decrease in canopy leaf area and epiphyte surface area (figure 4-4a). This loss of canopy surface area leads to a subsequent decrease in evaporation and transpiration (Rothacher, 1970). Additional increases in streamflow may be due to the loss of water storage in the sapwood of large trees (Waring & Franklin, 1979). The loss of overstory canopy is associated with increased atmospheric interaction with the remaining understory vegetation. Canopy height, roughness length, and woody LAI decrease when the conifer canopy is harvested (Figure 4-4b). The ranges of surface temperature and humidity extremes are likely to increase and there is an increase in incoming solar radiation at the surface.

#### **4.3.3.2 Initial Return to Pre-harvest Streamflow Levels**

The rapid recession in summer streamflow has been hypothesized to be due to the rapid increase in herbaceous vegetation on the hillslopes (Dyrness, 1969). This increase in herbaceous growth is likely due to increased soil moisture and incident solar radiation. This hypothesis is supported by soil moisture measurements taken during the first several years following harvest. During the first year following harvest a 4.5 inch soil moisture surplus was measured, but by the third year after harvest the soil moisture surplus was only .6 inch (Dyrness, 1969). Following harvest and broadcast burn herbaceous vegetation grew rapidly, quickly providing more herbaceous cover than prior to harvest. It is likely that increased air temperatures, decreased relative humidity levels, increased incident solar radiation, and increased soil moisture led to increased herbaceous vegetation growth and water use. Herbaceous vegetation has been observed to consume surface soil water earlier in the season than evergreen broadleaf or conifer species (Pabst et al., 1990). Rapid water use in the early summer might lead to decreased summer streamflows when there is minimal summer precipitation.

Halpern's vegetation analysis (1989) supports this hypothesis. Total herb and shrub cover was 93% in 1968 and the herbaceous vegetation cover dominated for the first 11 years following harvest.

An alternative hypothesis suggests that the decrease in streamflow is due to the rapid establishment of deciduous vegetation in the riparian corridor, in particular the rapid growth of red alder (Rothacher, 1970). Red alder has high maximum stomatal conductance rates (8-10mm/s). Riparian vegetation is rarely water limited and may transpire at maximum rates throughout the summer leading to decreased summer streamflows. The 1972 aerial photo shows that the riparian vegetation is beginning to develop, but it is unlikely that these scattered tree saplings dominated the vegetation influence on streamflow at this time.

#### **4.3.3.3 Summer Streamflow Deficit**

Continued growth of the riparian vegetation, particularly the dominant species red alder, has been hypothesized to be responsible for the summer streamflow deficit that occurred in WS 1 during the second decade following harvest (Hicks et al., 1991; Waring, personal communication). Increased leaf area and continuing optimal conditions for maximum transpiration throughout the summer may lead to streamflow deficits, particularly during the late summer months when the stream is fed by baseflow from the hillslopes. Maximum stomatal conductance rates for red alder are considerably higher than for Douglas-fir (Figure 4-4c).

An alternative hypothesis suggests that evergreen broadleaf vegetation on the hillslopes transpires more water than conifers, due to a higher tolerance of plant water deficit (more negative plant water potential) (Hicks et al., 1991). High transpiration rates may be aided by extensive root systems which may be able to access soil water reserves that are not used by herbaceous, deciduous broadleaf or conifer vegetation (Conard et al., 1985). Evergreen broadleaf species have moderately high stomatal conductance rates and maintain open stomata under conditions of low plant water potential (Figure 4-4c). These alternative hypotheses were tested using MAPSS-W.

The surface and canopy climate conditions would generally encourage high transpiration rates in both the deciduous broadleaf and evergreen broadleaf canopies. High levels of incident radiation on these canopies will increase the canopy temperatures and the plants will generally maintain open stomata to avoid lethal leaf temperatures (Waring & Schlesinger, 1985). While surface roughness is not as high for these canopies as for the old growth canopy (Figure 4-4b), the influence of wind speed may be greater for these canopies (as compared to the understory of an old growth canopy) because they are not protected by overstory vegetation.

#### **4.3.3.4 Second Return to Pre-harvest Streamflow Levels**

Conifer canopy closure is hypothesized to be the dominant mechanism in returning streamflow to pre-harvest levels. This is based on the moderating influence of the conifer canopy on surface and understory canopy temperature and humidity ranges and atmospheric turbulence (Hicks et al., 1991). Additionally, canopy closure shades the understory vegetation. The dominant riparian species, red alder, is shade intolerant (Shainsky et al., 1994) as are many of the evergreen broadleaf species growing on the hillslopes (Zavitkovsky & Newton, 1968; Conard et al., 1985). Shading and changes in canopy climate alter the transpiration rates of these stands.

An alternative hypothesis suggests that the natural senescence of evergreen broadleaf species on the hillslopes leads to decreased summer water use and a return of streamflow levels to pre-harvest levels. These hypotheses were not tested using MAPSS-W, but observations in WS 1 suggest that evergreen broadleaf senescence occurs most quickly in areas where conifer canopy closure is occurring.

#### **4.3.3.5 Future Summer Streamflow Patterns**

Evidence from other forests suggest that there will be another period of summer streamflow deficits (Shiklomanov & Krestovsky, 1988; Borg & Stoneman, 1991). This is based on differences in stand density, transpiring leaf area, height related water

transport resistance and age related water transport resistance between old-growth trees and young trees. This second period of streamflow deficits is likely to occur once conifer canopy closure is complete over the entire watershed area, and before the canopy reaches maximum height.

#### **4.3.4 Definition of Hydrologic Plant Functional Groups**

These hypotheses of vegetation-streamflow interactions led to questions about the patterns of vegetation in WS 1. In order to analyze the aerial photos and long-term species plot data available for WS 1, three hydrologically relevant plant functional groups were defined for the woody vegetation species in WS 1. Plant functional groups are defined according to the manner in which plants and the environment interact to produce identifiable physiological, morphological, or life history vegetation patterns (Smith et al., 1997). In this case the woody plant species were separated on the basis of leaf morphology and the associated differences in water use habits. The differences between conifer, deciduous broadleaf and evergreen broadleaf water use habits include different maximum stomatal conductance rates, wilting points, water acquisition and storage strategies, and canopy-leaf-atmosphere interactions (Larcher, 1995; Waring & Schlesinger, 1985; Baldocchi & Vogel, 1996).

Table 4-2 lists the WS 1 vegetation plot species by functional group designation. The model parameterizations of stomatal conductance and wilting point for each functional group are based on literature values for key species of interest: Douglas-fir (conifers) (Waring & Schlesinger, 1985), red alder (deciduous broadleaf) (Shainsky et al., 1994), and snowbrush (evergreen broadleaf) (Conard et al., 1985).

Table 4-2: Plant Functional Groups - Species List

<b>Conifer</b>	
<i>Pinus lambertiana</i>	sugar pine
<i>Pseudotsuga menziesii</i>	Douglas-Fir
<i>Taxus brevifolia</i>	pacific yew
<i>Thuja plicata</i>	western red cedar
<i>Tsuga heterophylla</i>	western hemlock
<b>Deciduous Broadleaf</b>	
<b>Trees</b>	
<i>Acer macrophyllum</i>	bigleaf maple
<i>Alnus rubra</i>	red alder
<i>Cornus nuttallii</i>	pacific dogwood
<i>Populus trichocarpa</i>	black cottonwood
<i>Prunus emarginata</i>	bitter cherry
<b>Shrubs</b>	
<i>Acer circinatum</i>	vine maple
<i>Acer glabrum</i>	rocky mountain maple
<i>Amelanchieria alnifolia</i>	serviceberry
<i>Ceanothus integerrimus</i>	deerbrush
<i>Ceanothus sanguineus</i>	buckbrush
<i>Corylus cornuta californica</i>	California hazel
<i>Holodiscus discolor</i>	oceanspray
<i>Oemleria cerasiformis</i>	indian plum
<i>Rhamnus purshiana</i>	cascara
<i>Rhus diversiloba</i>	poison oak
<i>Ribes lacustre</i>	prickly current
<i>Ribes sanguineum</i>	winter current
<i>Rosa gymnocarpa</i>	baldhip rose
<i>Rubus parviflorus</i>	thimbleberry
<i>Rubus ursinus</i>	trailing blackberry
<i>Sambucus cerulea</i>	elderberry
<i>Salix scouleriana</i>	willow
<i>Salix sitchensis</i>	willow
<i>Vaccinium membranaceum</i>	blueberry
<i>Vacinium parvifolium</i>	huckleberry
<b>Evergreen Broadleaf</b>	
<b>Trees</b>	
<i>Arbutus menziesii</i>	madrone
<i>Castanopsis chrysophylla</i>	golden chinquapin
<b>Shrubs</b>	
<i>Arctostaphylos columbiana</i>	manzanita
<i>Berberis nervosa</i>	dwarf Oregon grape
<i>Ceanothus velutinus</i>	snowbrush
<i>Gaultheria shallon</i>	salal
<i>Rhododendron macrophyllum</i>	Pacific rhododendron

### **4.3.5 Vegetation Pattern Analysis**

#### **4.3.5.1 Aerial Photo Interpretation**

Five sets of aerial photos were used to describe temporal and spatial changes in vegetation cover in WS 1. These sets of photos coincide with periods of interest in the streamflow record (1959, 1967, 1972, 1979, & 1990). The photo interpretations were based on plant functional groups and resulted in cover maps for each of the plant functional groups. The cover maps were then used to create vegetation input layers for MAPSS-W simulations. The photos taken in 1959 and 1967 are black and white and the photos taken in 1972, 1979, and 1990 are color. Table 4-2 summarizes the photo dates, resolutions, and photo numbers. Black and white copies of the photos used to create the vegetation cover maps are included in Appendix A.

**Table 4-3: HJA Aerial Photos Used for WS 1 & 2 Vegetation Analysis**

<b>Date</b>	<b>Resolution</b>	<b>Flight line</b>	<b>Photo #</b>
7-8-59	1:12000	18	31-99, 31-100
6-15-67	1:16000	17	5-19, 5-20
7-18-72	1:16000	17	6-114, 6-115
7-24-79	1:12000	22	278-86, 278-85
8-1-90	1:12000	25	1190-38, 1190-39

To determine the spatial patterns and cover density of each vegetation functional group, aerial photos were examined as stereopairs. Photos were examined for the three woody vegetation groups (conifers, deciduous broadleaf and evergreen broadleaf) and for herbaceous vegetation. The conifer and evergreen broadleaf vegetation were identified based on canopy shape; shrubs and herbaceous vegetation were distinguished based on vegetation density and color. Vegetation cover estimates were determined within 25% cover categories (0-25%, 25-50%, 50-75%, and 75-100%) and, in areas of scattered deciduous broadleaf canopies, a 10% cover category was added. Cover maps were drawn for the functional plant groups for the 1972, 1979, and 1990

aerial photo sets. In some cases the functional plant groups were aggregated because the young age and small size of the vegetation made it difficult to distinguish conifers from evergreen broadleaf plants. Conifer overstory cover estimates were made from the 1959 (pre-harvest) photos. Cover maps were not made for the 1967 photos, the year after the harvest and burn were completed in WS 1, because these photos did not show significant vegetation cover in WS 1. Canopy cover maps developed from the 1959, 1972, 1979, and 1990 aerial photos are presented in Appendix A.

The pre-harvest photos (1959) were used to create an overstory canopy map for WS 1. Conifer canopy age and density determinations were based on a comparison of the WS 1 & 2 aerial photos against overstory vegetation maps for WS 2 (Hawk & Dyrness, unpublished).

The 1972 photos (6 years post-harvest) represent vegetation during the first return of streamflows to pre-harvest levels. At this point conifer seedlings were too young to be distinguished from evergreen broadleaf shrubs, so these functional groups were combined for aerial photo interpretation. Cover maps were developed for herbaceous vegetation, deciduous broadleaf vegetation, and the combined conifer-evergreen broadleaf categories.

The 1979 photos (12 years post-harvest) represent vegetation during the period of summer streamflow deficit. Conifer canopies were still not tall enough to be distinct against the surrounding evergreen broadleaf canopies, so these categories were combined for aerial photo interpretation. Cover maps were developed for herbaceous vegetation, deciduous broadleaf vegetation, and the combined conifer-evergreen broadleaf categories.

The 1990 photos (24 years post-harvest) represent vegetation during the second return of streamflows to pre-harvest levels. Conical conifer canopies were tall enough to be distinguished against the rounded deciduous broadleaf canopies and the dense, dark green areas of evergreen broadleaf canopy and the lighter green areas of herbaceous cover.

#### 4.3.5.2 Vegetation Plot Data

Long-term vegetation plot measurements were begun in WS 1 in 1962. These measurements included understory plant community designations and measurements of topographic variables (% slope and aspect). Post-harvest measurements were taken annually between 1966 and 1973, in alternating years through 1980, and are now taken every four years. A total of 131 plots are located along 6 transects that cross the watershed, perpendicular to the stream channel. The transects are unevenly spaced, and the initial plot on each transect was randomly located along the north or south ridge. The rest of the plots on each transect are separated by 30.5m. These 2 x 2 m plots were designed to assess the abundance of understory vascular plant species during post-harvest early succession (Dyrness, 1973; Halpern, 1987; Halpern, 1988; Halpern, 1989). These plots provide substantial representation of the hillslope vegetation, but very limited representation of the riparian corridor and ridge tops. Only two of the plots fall in the riparian corridor.

The percent cover measurements used in this study were taken as visual estimates of projected canopy cover for all understory species (< 6m tall) (Halpern, 1987). Cover values from 0-10% were estimated to the nearest integer, while cover > 10% was estimated to the nearest 5% class. Vascular plant taxonomy and nomenclature follow Hitchcock and Cronquist (1973) (Halpern, 1987).

Five sets of plot data were chosen to coincide with the aerial photos and periods of interest in the streamflow record. Four of the plot data and aerial photo pairs were taken during the same season and year. The pre-harvest plots were measured in 1962 and the pre-harvest photo was taken in 1959. Species data were aggregated into the hydrologic plant functional groups (conifer, deciduous broadleaf, and evergreen broadleaf) as listed in Table 4-2.

To create maps of the plot data, the coordinates of the transect end plots were measured using a Trimble Pathfinder global positioning system (GPS). Figure 4-5 illustrates the basic transect map that was created in ArcInfo7.0.4 (ESRI, 1996). Maps were created for each vegetation functional group, for each year of interest. This allowed visual analysis of the aggregated categories, and comparisons between the plot

measurement of percent cover and the aerial photo estimate of percent cover. The plot maps are presented in Appendix A.

#### 4.3.5.2.1 Spatial Analysis

Qualitative examination of the plot data maps suggested that the measurements of percent cover were spatially autocorrelated along transects. Spatial autocorrelation is common in data that are collected along regularly space transects, and violates the assumption of independence in statistical analysis. In order to establish whether or not it would be appropriate to perform statistical analysis on the plot data, Moran's I (Legendre & Fortin, 1989; Sokal & Oden, 1978) was calculated for the three longest transects (4, 5, & 6). Moran's I was computed using vgram (Marks, unpublished).

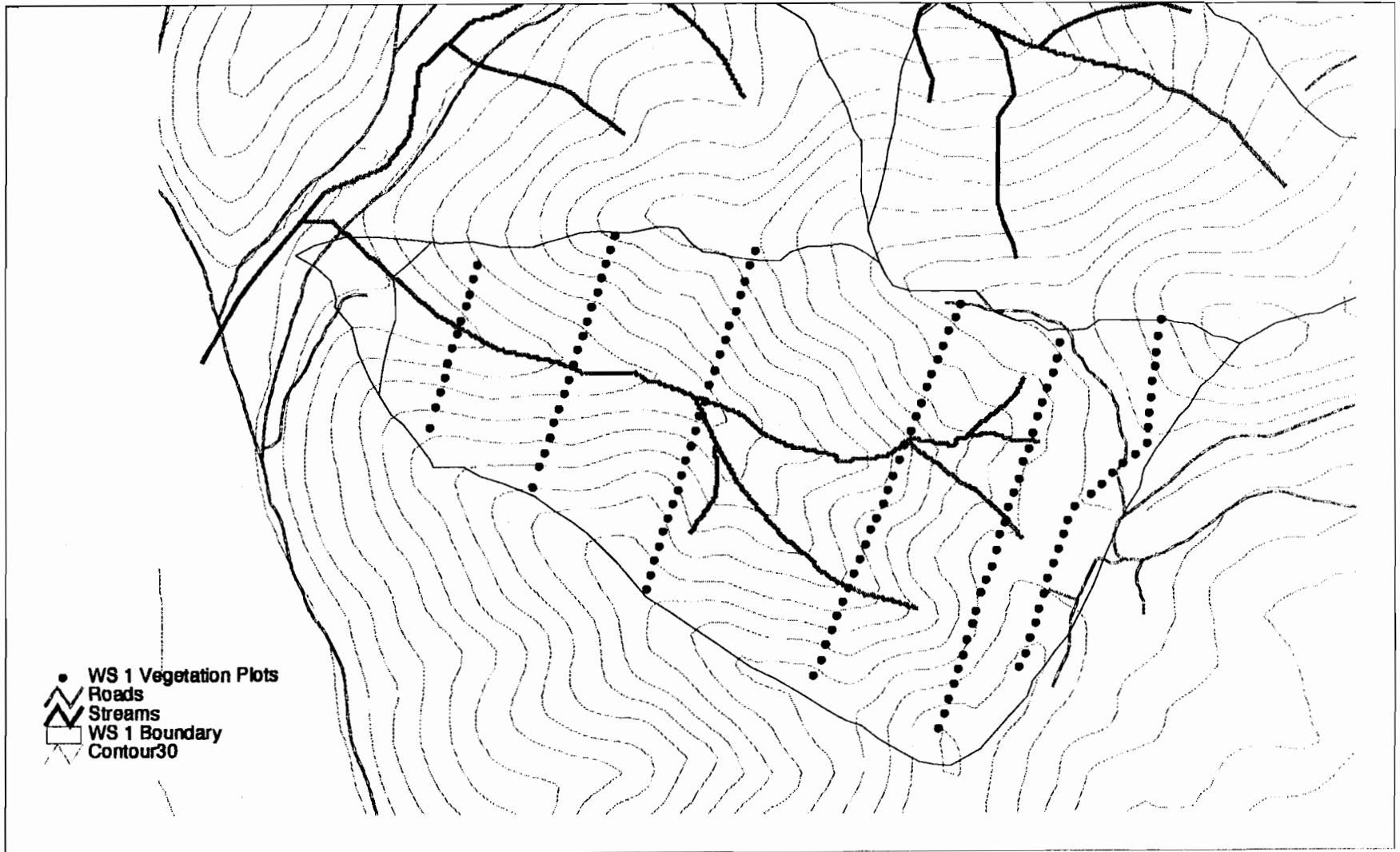
#### 4.3.5.2.2 Repeated Measures Analysis

Plot data were examined for evidence of relationships between vegetation cover and landscape features. Aspect, elevation and slope are often used to represent the influence of temperature and solar radiation in spatial analysis (Nesje, 1996). These three explanatory variables were measured for each vegetation plot and were used to estimate the influence of temperature and solar radiation on vegetation cover.

Repeated measures analysis accounts for the temporal correlation inherent in measurements that are taken on the same subject over time (von Ende, 1993). Repeated measures analysis is a form of analysis of variance (ANOVA) that calculates the correlation between repeated measurements and explanatory variable and adjusts for temporal correlations. Repeated measures analysis can also calculate trends over time or make comparisons to reference measurements.

Repeated measures analysis was run for each hydrologic functional group. The percent cover data was transformed using a logit transformation to improve the normality of the data distribution. This transformation decreased the residual patterns, but it should be noted that the data were not normally distributed. Many of the plots had cover values

Figure 4-5: Location of Vegetation Transects in WS 1



near the extremes (0% or 100%). This analysis was performed using continuous explanatory variables rather than categorical explanatory variables, because the plots are not adequately distributed along the topographic gradients of slope percentage, aspect or elevation. Slope percentage and elevation were measured as continuous variables. Aspect was designated as one of the eight cardinal directions. Two continuous aspect variables were created, from these measurements, to represent the influence of north vs. south facing slopes and the influence of east vs. west facing slopes.

The repeated measure analysis was performed in SAS 6.12 (SAS Institute, 1996). Univariate analyses of the correlation between vegetation group percent cover and the environmental variables were performed. Additionally each post-harvest time period was contrasted with the preceding time period to examine the data for temporal trends related to aspect, slope percentage or elevation.

Comparisons were performed between the aerial photo maps and the understory vegetation plot maps for 1972, 1979, and 1990 to assess the accuracy of the aerial photo interpretation. These comparisons were made by overlaying the plot maps on the aerial photo maps and determining the intersection between the plot designations and the aerial photo map unit designations. These years were chosen for comparison because the aerial photo interpretations best represent the hydrologically distinct plant functional groups.

#### **4.3.6 MAPSS-W Simulations**

##### **4.3.6.1 MAPSS-W Vegetation Layers**

MAPSS-W requires spatially distributed vegetation input layers. These data layers are provided in units of functional leaf area index (LAI) for the three lifeforms (trees, shrubs, and herbs) represented by the model. Functional LAI represents a measure of the transpiring leaf area per unit of ground. For this application of MAPSS-W, LAI values are based on single sided LAI values. The calibration and evaluation of MAPSS-W for

WS 1 & 2 was performed using uniform vegetation grids, in which every grid cell had the same LAI values.

In order to test hypotheses about the influence of vegetation on streamflow, it was necessary to create realistically distributed vegetation. The vegetation layers for WS 1 were created from the aerial photo cover maps. The vegetation layers used for WS 2 were created from overstory and understory vegetation maps (Hawk & Dyrness, unpublished). These percent cover maps were multiplied by maximum LAI values for each vegetation functional group. The maximum LAI values for each time period are different because the stature of the trees and shrubs increased throughout the post-harvest period, increasing the area of the canopies. Table 4-4 lists the maximum LAI values used to create the vegetation input layers for each period of interest. The percent cover maps were converted to 30m grids in ArcGrid 7.0.4 (ESRI, 1996) and multiplied against the appropriate maximum LAI value. These grids were then transferred to IPW format (Frew, 1990) for use in MAPSS-W.

It was necessary to combine some of the aerial photo cover maps to create vegetation layers that would correspond to the MAPSS-W lifeforms. For the pre-harvest vegetation layers, trees were represented by the conifer overstory, shrubs were represented by the understory trees and shrubs, and the herbaceous layer was a uniform grid. The 1967 dataset was created as uniform grids for trees (.2), shrubs (.2), and herbs (6) because the aerial photo does not show significant vegetation cover and the plot measurements suggest that herbaceous cover expanded rapidly during the first several years after harvest. For the 1972 and 1979 vegetation layers, trees were represented by the deciduous broadleaf layer, shrubs were represented by the combined conifer and evergreen broadleaf layer, herbs by the herbaceous layer. For the 1990 vegetation layers, trees were represented by a combination of the conifer and deciduous broadleaf maps, shrubs were represented by the evergreen broadleaf layer and herbs were represented by the herbaceous layer.

**Table 4-4: Maximum Leaf Area Index Values**

	1959	1967	1972	1979	1990
<b>conifer</b>	15	*.2	**4	**6	12
<b>evergreen broadleaf</b>		*.2			4
<b>deciduous broadleaf</b>	***4	*.2	3	6	8
<b>herbs</b>	1	6	6	5	4

\*Slightly greater than zero to represent residual sprouting woody vegetation.

\*\*Evergreen broadleaf and conifer included in one cover map and used to represent the shrub layer.

\*\*\*Evergreen broadleaf and deciduous broadleaf included in one cover map and used to represent the shrub layer.

#### 4.3.6.2 Vegetation-Hydrology Hypothesis Testing

Vegetation-hydrology hypothesis testing was performed using MAPSS-W. The model parameterizations for each period of interest are based on observed changes in vegetation functional groups and assumed changes in canopy climate and atmospheric interactions. These changes in vegetation and climate are summarized in table 2. Climate data was developed, as described in Chapter 2, for sets of water years that correspond with the plot data, aerial photos and key streamflow periods. Three model parameters were chosen to represent the changes in vegetation function. These parameters are maximum stomatal conductance, maximum wilting point, and roughness length. Maximum stomatal conductance and wilting point determine the maximum transpiration potential. Roughness length represents the atmospheric coupling of the vegetation.

The initial goal of the experimental simulations was to test whether crude changes in vegetation function groups could explain the observed changes in streamflow for the five periods of interest. An additional goal was to test specific alternative vegetation-hydrology interaction hypotheses to determine the dominant influence on streamflow during particular periods. Table 4-5 summarizes the parameter settings used for these experimental simulations. The vegetation parameterizations are based on the dominant vegetation for each time period, as determined by the aerial photo and plot data analysis. These changes in parameterization were applied to the simulations run for WS 1. All WS

2 simulations were run using the pre-harvest parameterization values and the pre-harvest vegetation layers.

For WS 1, the pre-harvest years (1958-61) were parameterized for old growth/mature conifer vegetation. Roughness length ( $z_0$ ) was based on calculations of canopy roughness from canopy height measurements. The wilting point ( $wp$ ) and maximum stomatal conductance ( $cond\_max$ ) values were based on literature values for Douglas-fir. The years of excess summer streamflow (1967, 68) were parameterized for herbaceous vegetation. Herbaceous vegetation growth was constrained to a maximum LAI of 6. The first period of streamflow return to pre-harvest levels (1972, 73) was parameterized for deciduous vegetation. Two parameterizations were used to test the alternative hypotheses of deciduous or evergreen broadleaf dominance for the years of

**Table 4-5: Key Transpiration Parameters in MAPSS-W**

	1958-61	1967,68	1972,73	1979.80	1990.91
	old growth conifer	herb	DB	EB / DB	young conifer
<b>cond_max (G)</b>	3.50	3.50	3.50	3.5/3.5	3.50
<b>cond_max (T)</b>	3.5	3.50	10.00	7.0/10.0	4.50
<b>cond_max (S)</b>	5.00	5.00	10.00	7.0/10.0	5.00
<b>wp (G)</b>	-2.00	-2.00	-2.00	-2/-2	-2.00
<b>wp (T)</b>	-2.20	-2.00	-5.00	-5/-2.5	-2.20
<b>wp (S)</b>	-5.00	-2.00	-5.00	-5.0/-2.5	-5.00
<b>z0(G)</b>	0.005	0.005	0.005	0.005	0.005
<b>z0(T)</b>	0.200	0.100	0.100	0.15	0.10
<b>z0(S)</b>	0.010	0.010	0.010	0.010	0.010

cond\_max - maximum stomatal conductance

G-herbs;  
T-trees;  
S-shrubs

EB - evergreen broadleaf  
DB - deciduous broadleaf

wp - maximum wilting point

z0 - roughness length

summer streamflow deficit (1979, 80). The second period of streamflow return to pre-harvest levels was parameterized for young conifer. Due to the short stature of the trees and shrubs during these simulation periods, these vegetation layers were given the same parameter values.

### **4.3.6.3 Evaluation of MAPSS-W Simulations**

Experimental simulations were evaluated on the basis of summer streamflow comparisons with measured summer streamflows in WS 1 & 2. Direct comparisons of the total summer streamflow for each watershed were made, as well as comparisons between the watersheds.

## **4.4 Results**

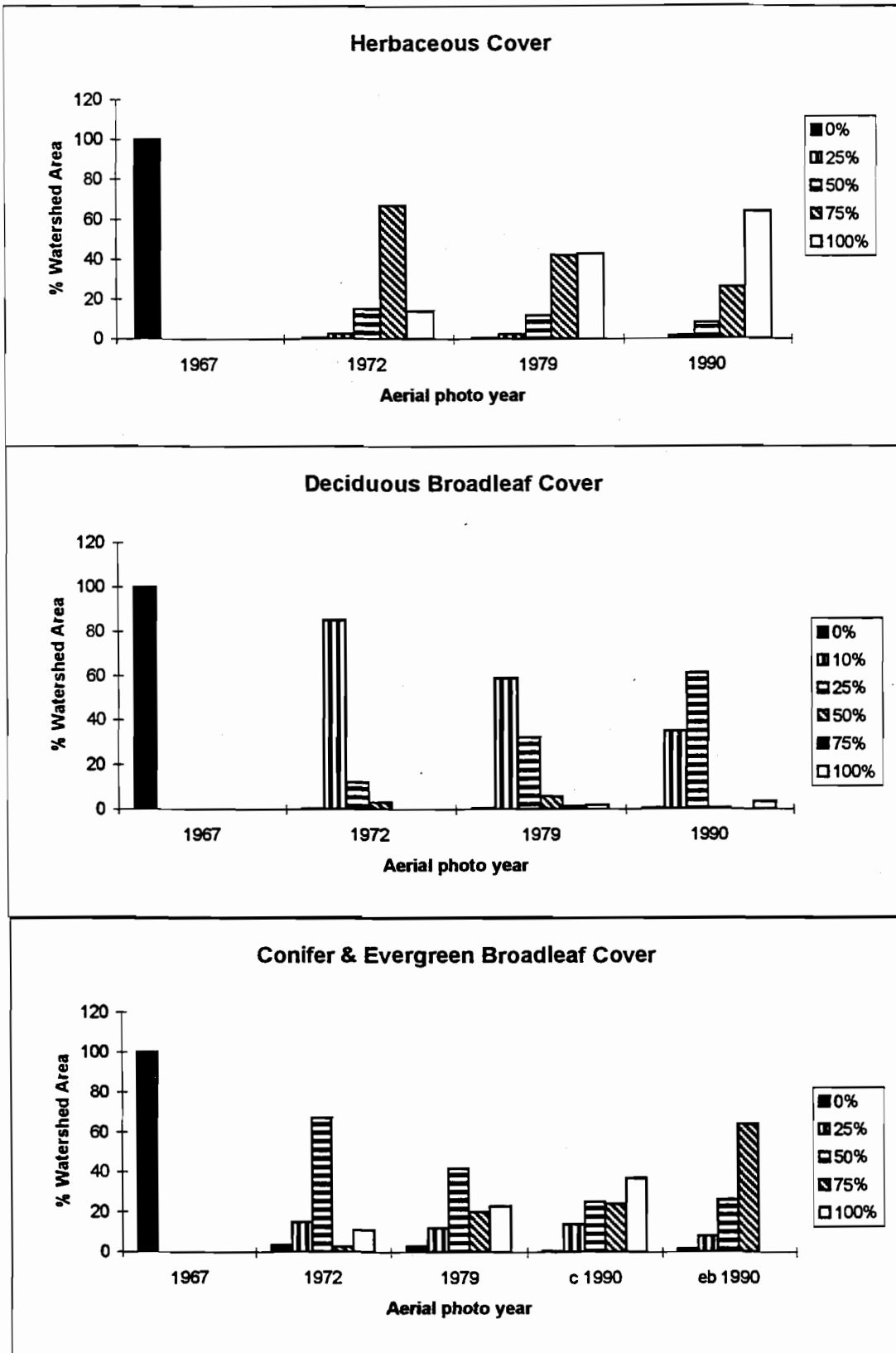
### **4.4.1 Vegetation Analysis**

#### **4.4.1.1 Aerial Photo Cover Maps**

In the pre-harvest photo (1959) there are two distinct Douglas-fir age classes, old-growth and mature canopy. The mature stands have tighter, more dense canopies. Old growth forest covered approximately 69% of WS 1 & 2; mixed canopies covered approximately 20% of WS 1 & 2; mature forest covered approximately 10% of WS 1 & 2; and, overstory canopy gaps covered approximately 1% of WS 1 & 2. The overstory and understory cover maps for WS 1 & 2 (Appendix A) highlight the difference in spatial information available from vegetation survey maps and aerial photo interpretation. The cover map for WS 1, based on aerial photo interpretation, is less detailed than the cover map for WS 2, which is based on canopy maps created from field observations.

The accuracy of the aerial photo interpretation was assessed through comparison of the percent cover maps against the plot cover measurements. Some differences were expected between the mapped cover percentages and the plot measurements, because of the difference in the resolution of the mapped areas and the 2x2m plot size. The mapped areas were drawn with an expectation that there was significant heterogeneity in the vegetation cover within each map unit. These results are presented in Appendix B.

**Figure 4-6a,b,c:**  
**Aerial Photo Interpretations by Functional Group as % of Watershed Area**



The 1972 herbaceous cover map agreed with the plot data for 45 plots, and in general overestimated herbaceous cover. The 1972 conifer and evergreen broadleaf cover map agreed with the plot data for 31 plots, and in general overestimated conifer and evergreen broadleaf cover. The 1972 deciduous broadleaf cover map agreed with the plot data for 58 plots, and in general underestimated deciduous cover. The 1979 conifer and evergreen broadleaf cover map agreed with the plot data for 35 plots, and in general overestimated conifer and evergreen broadleaf cover. The 1979 deciduous broadleaf cover map agreed with the plot data for 44 plots, and in general underestimated deciduous cover. The 1990 herbaceous cover map agreed with the plot data for 27 plots, and in general overestimated herbaceous cover. The 1990 evergreen broadleaf cover map agreed with the plot data for 18 plots, and in general overestimated evergreen broadleaf cover. The 1990 conifer cover map agreed with the plot data for 28 plots, and in general overestimated conifer cover. The 1990 deciduous broadleaf cover map agreed with the plot data for 35 plots. These map assessments were not used to adjust the cover maps for two reasons. The resolution of the map units was quite a bit larger than the plot size, and there was no discernible spatial pattern in the plot data that could have been used to adjust the cover maps.

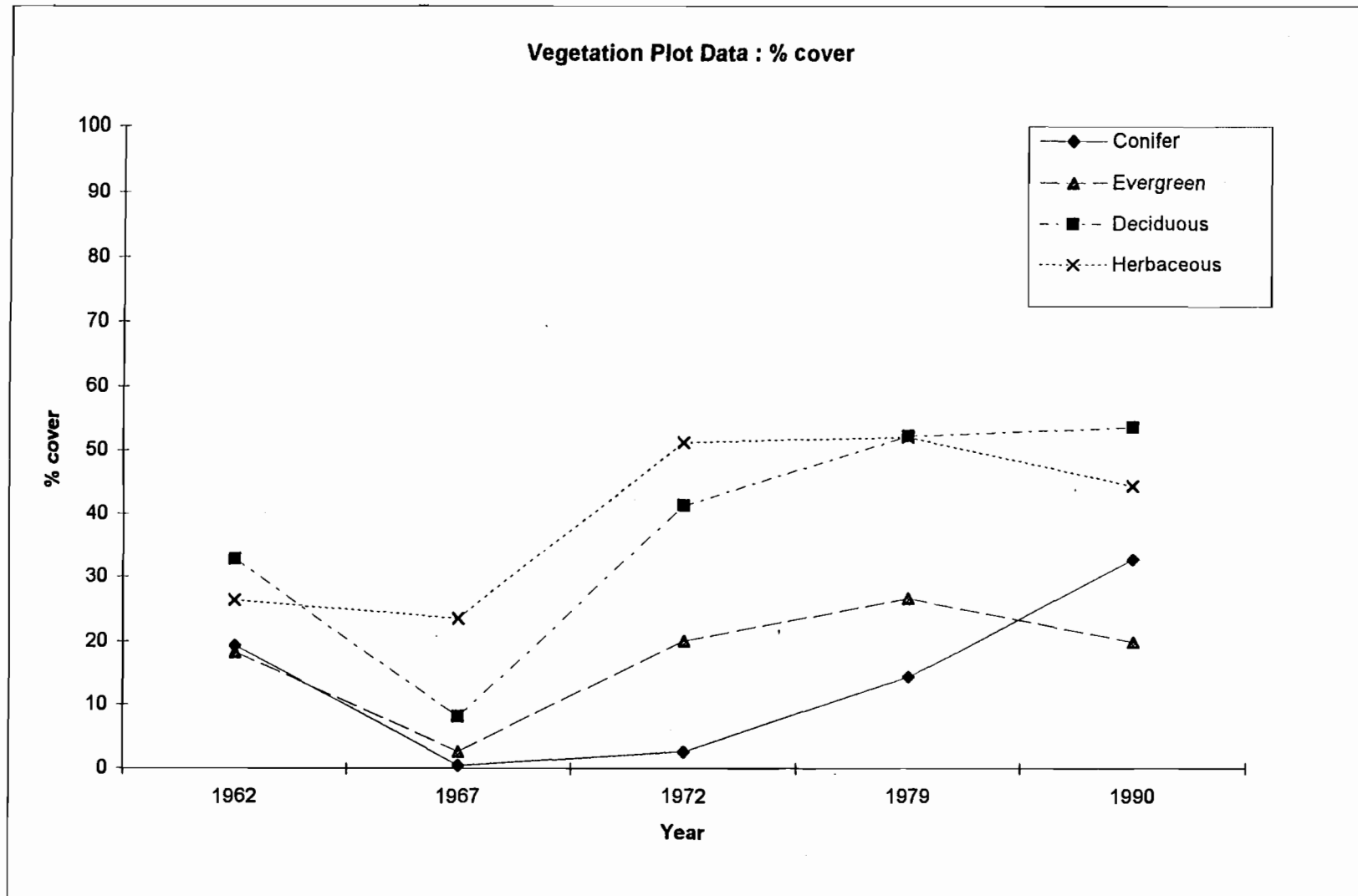
The cover maps developed from the aerial photos are presented in Appendix A. The change in cover as a percentage of the total area in WS 1 is illustrated in Figures 4-6 a, b, & c. for each functional group. Herbaceous vegetation cover increased rapidly following harvest, providing 75-100% cover over most of the watershed in 1979 and 1990. The deciduous broadleaf vegetation cover was patchy, generally providing less than 50% cover, except in the riparian corridor. Deciduous broadleaf vegetation reaching 75-100% cover in the riparian corridor in 1979 and 1990. The conifer and evergreen broadleaf vegetation were difficult to distinguish in the 1972 and 1979 photos due to the small stature of the conifer seedlings. The groups established dense patches along the north edge of the watershed. It was possible to distinguish between conifer crowns and evergreen broadleaf canopies in the 1990 photo. By 1990 the planted Douglas-fir had developed dense canopy in more than 50% of WS 1. Much of this dense conifer cover is on the north-facing slope.

#### 4.4.1.2 Vegetation Plot Data

Qualitative examination of the vegetation plot maps provides insight about the location of vegetation functional groups. The pre-harvest (1962) vegetation plot maps (Appendix A) show a greater concentration of herbaceous cover on the north facing slopes, and a slight concentration of evergreen broadleaf cover along the north edge of the watershed. The 1967 vegetation plot maps (Appendix A) show rapid growth of herbaceous vegetation on the north-facing slopes, and limited cover for the other vegetation groups. The 1972 vegetation plot maps (Appendix A) show patches of deciduous broadleaf cover and herbaceous cover throughout the watershed, and a dense concentration of evergreen broadleaf cover along the north edge of the watershed. The 1979 vegetation plot maps (Appendix A) show scattered conifer cover, dense deciduous broadleaf vegetation throughout the watershed and an increase in evergreen broadleaf density along the north edge of the watershed. The 1990 vegetation plot maps (Appendix A) show a significant increase in conifer cover scattered throughout the watershed, a decrease in the density of evergreen broadleaf cover along the north edge of the watershed, a decrease in herbaceous cover throughout the watershed, and continued dominance of deciduous broadleaf cover in the understory. Plots with high deciduous or evergreen broadleaf cover generally had less herbaceous cover. Plots with high evergreen broadleaf cover generally had low deciduous broadleaf cover values.

Figure 4-7 shows the average cover trajectories for the four vegetation functional groups based on the vegetation plot data. All of the understory vegetation groups have higher cover percentages in 1990 than they did in 1962. Deciduous broadleaf cover increased rapidly following harvest and leveled off at 50% or greater cover throughout the watershed. Evergreen broadleaf cover increased rapidly and peaked in 1979. The highest evergreen broadleaf densities were primarily concentrated on flat ground along the eastern edge of the watershed. Conifer cover increased minimally during the first five years after harvest, but increased more rapidly between 1972 and 1990. Of all the vegetation groups, herbaceous cover decreased the least between 1962 and 1967, maintaining an average of 25% cover throughout the watershed. Herbaceous vegetation increased rapidly between 1967 and 1972 and decreased between 1972 and 1990.

Figure 4-7: Vegetation Plot Data - Trajectories by Functional Group



#### 4.4.1.2.1 Spatial Analysis

Based on the qualitative examination of the vegetation plot maps, spatial autocorrelation was expected between adjacent plots. Moran's I was calculated for each vegetation group for transects 4, 5, & 6, but moderate correlation was found in only three instances for adjacent evergreen broadleaf plots. The Moran's I for evergreen broadleaf cover in 1972 along transects 4 and 5 was 0.36 and 0.9 respectively at a lag of one (adjacent plots). The Moran's I for evergreen broadleaf cover in 1979 along transect 5 was 0.33 at lag one. These results indicated that some autocorrelation exists between adjacent plots. Spatial correlation was not found for deciduous broadleaf, conifer or herbaceous plots. This analysis suggested that plots were spatially independent, thus the assumption of data independence in repeated measures analysis was not violated.

#### 4.4.1.2.2 Repeated Measures Analysis

The repeated measures contrasts between time periods did not result in consistent vegetation trajectories and will not be presented. The significant results of the univariate analyses based on all data for each vegetation group are presented. These results were calculated after accounting for the temporal correlation of the measurements. It turns out that each vegetation group was correlated with a single environmental variable. Aspect is the key influential environmental variable correlated to vegetation cover. Slopes facing north and south had different amounts of herbaceous (p-value = .004), deciduous broadleaf (p-value = .0001), and conifer (p-value = .0001) cover. Overall, plots on north facing slopes have higher herbaceous and conifer cover and lower deciduous broadleaf cover than plots on south facing slopes. Evergreen broadleaf cover was correlated with slope percentage (p-value = .0086). Overall, plots on slopes of < 50% incline had higher percent cover than plots on slopes of > 50%. Figures 4-8a,b,c,d show the growth trends for each functional group as influenced by the significant environmental factor. Percent cover was not statistically significant at each time period. This is illustrated by the standard deviations for each time period in Table 4-6.

**Figure 4-8a,b,c,d: Repeated Measures ANOVA  
Environmental Influences on Vegetation Cover**

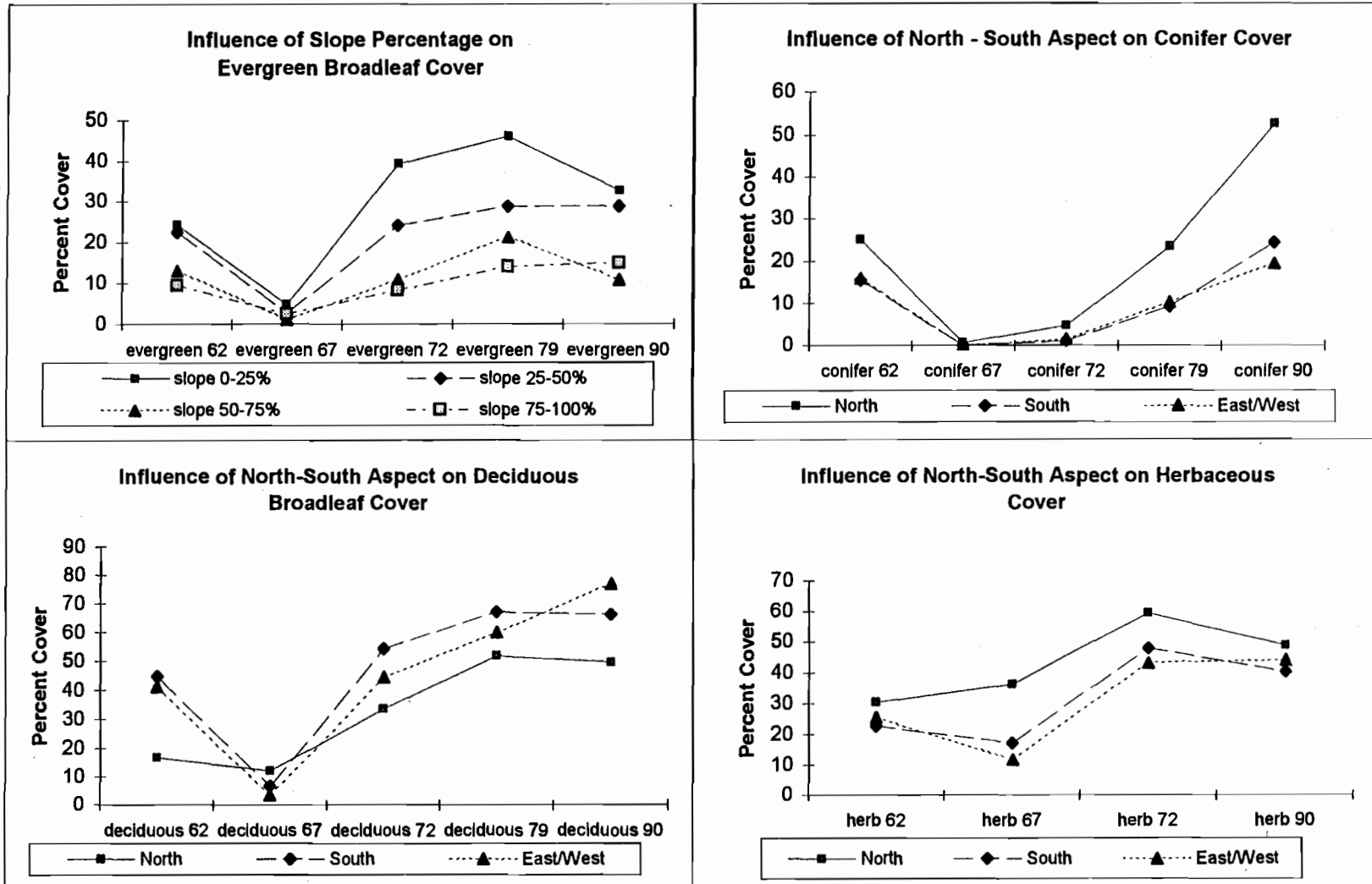


**Table 4-6: Repeated Measures ANOVA  
Environmental Influences on Vegetation Cover**

**Slope**

<b>Percent Cover - Evergreen Broadleaf</b>					
	<b>1962</b>	<b>1967</b>	<b>1972</b>	<b>1979</b>	<b>1990</b>
<b>0-25% slope</b>	24.23 (32.45)	4.71 (12.73)	39.38 (40.64)	46.09 (40.91)	32.71 (47.19)
<b>25-50% slope</b>	22.44 (30.58)	2.69 (6.17)	24 (36.29)	28.84 (40.43)	28.75 (43.72)
<b>50-75% slope</b>	12.96 (25.14)	1.09 (4.14)	10.84 (20.52)	21.39 (36.47)	10.86 (19.88)
<b>75-100% slope</b>	9.49 (12.2)	2.48 (5.71)	8.22 (11.03)	14.1 (26.21)	15.05 (18.94)

**Aspect**

<b>Percent Cover - Conifer</b>					
	<b>1962</b>	<b>1967</b>	<b>1972</b>	<b>1979</b>	<b>1990</b>
<b>North</b>	25 (33.65)	0.69 (2.9)	4.67 (13.83)	23.38 (31.24)	52.6 (46.64)
<b>South</b>	15.55 (23.73)	0.02 (0.14)	1.04 (2.1)	9.25 (19.11)	24.27 (39.12)
<b>East/West</b>	15.85 (25.11)	0 (0)	1.41 (2.19)	10.26 (15.79)	19.49 (31.22)

<b>Percent Cover - Deciduous Broadleaf</b>					
	<b>1962</b>	<b>1967</b>	<b>1972</b>	<b>1979</b>	<b>1990</b>
<b>North</b>	16.72 (26.15)	11.98 (20.4)	33.61 (33.89)	51.85 (41.65)	49.8 (48.24)
<b>South</b>	44.83 (36.43)	6.49 (10.96)	54.21 (40.09)	67.18 (50.16)	66.55 (51.57)
<b>East/West</b>	41.3 (35.76)	3.44 (3.92)	44.54 (38.1)	59.85 (55.51)	77.23 (53.61)

<b>Percent Cover - Herbaceous</b>				
	<b>1962</b>	<b>1967</b>	<b>1972</b>	<b>1990</b>
<b>North</b>	30.4 (28.81)	36.25 (27.74)	59.51 (21.53)	48.79 (28.34)
<b>South</b>	22.69 (22.7)	17.24 (21.58)	47.82 (25.55)	40.2 (28.3)
<b>East/West</b>	25.54 (26.48)	11.73 (14.65)	43.21 (26.73)	43.93 (27.23)

#### **4.4.1.3 Vegetation Data Comparison**

As illustrated in the tables in Appendix B, the aerial photo interpretations of herbaceous, conifer and evergreen broadleaf cover is higher than the plot measurements for 1972, 1979, and 1990. Conversely the aerial photo interpretation of deciduous broadleaf cover was lower than the plot measurements in 1972 and 1979. Deciduous broadleaf cover was overestimated in the aerial photo cover map for 1990.

While the cover maps and the plot data do not correspond very well, these comparisons were not used to adjust the cover maps. The differences in resolution between the map units (coarse resolution ( $> 30\text{m}^2$ )) and the vegetation plot area (fine resolution ( $2\times 2\text{m}$ )) did not provide a strong basis for adjustments. The coarse map units include heterogeneous areas of vegetation cover.

#### **4.4.2 MAPSS-W Simulations**

##### **4.4.2.1 Summer Streamflow Results**

The summer streamflow results for simulations based on the assumptions summarized in table 2 are presented in Figures 4-9a,b,c. Figure 4-9a illustrates the results for WS 1 simulations. Figure 4-9b illustrates the results for WS 2 simulations. Figure 4-9c illustrates the results as the log difference between the two watersheds in order to filter out the effects of inter-annual climate differences.

Direct comparison of simulated streamflow and measured streamflow for WS 1 indicate that MAPSS-W comes close to predicting summer streamflow levels. In all but one of the pre-harvest years MAPSS-W underestimated summer streamflow, and in all but one of the post-harvest years MAPSS-W overestimated summer streamflow.

Direct comparison of simulated streamflow and measured streamflow for WS 2 show reasonable, but inconsistent summer streamflow predictions. The vegetation input layers and vegetation parameters were not varied for the WS 2 simulations, so the variation in simulation results may be related to changes in vegetation that are not represented by

the input data layers or to variations in climate not represented by the climate data layers.

Figure 4-9c shows the comparisons of the measured and simulated summer streamflow that have been corrected for inter-annual climate change. The MAPSS-W simulations reproduce the pattern of the key time periods in the water record. Simulated summer streamflow increases directly after harvest (1967, 68), returns to pre-harvest levels (1972, 73), decreases below pre-harvest levels (1979, 80) and returns to pre-harvest levels a second time (1990, 91).

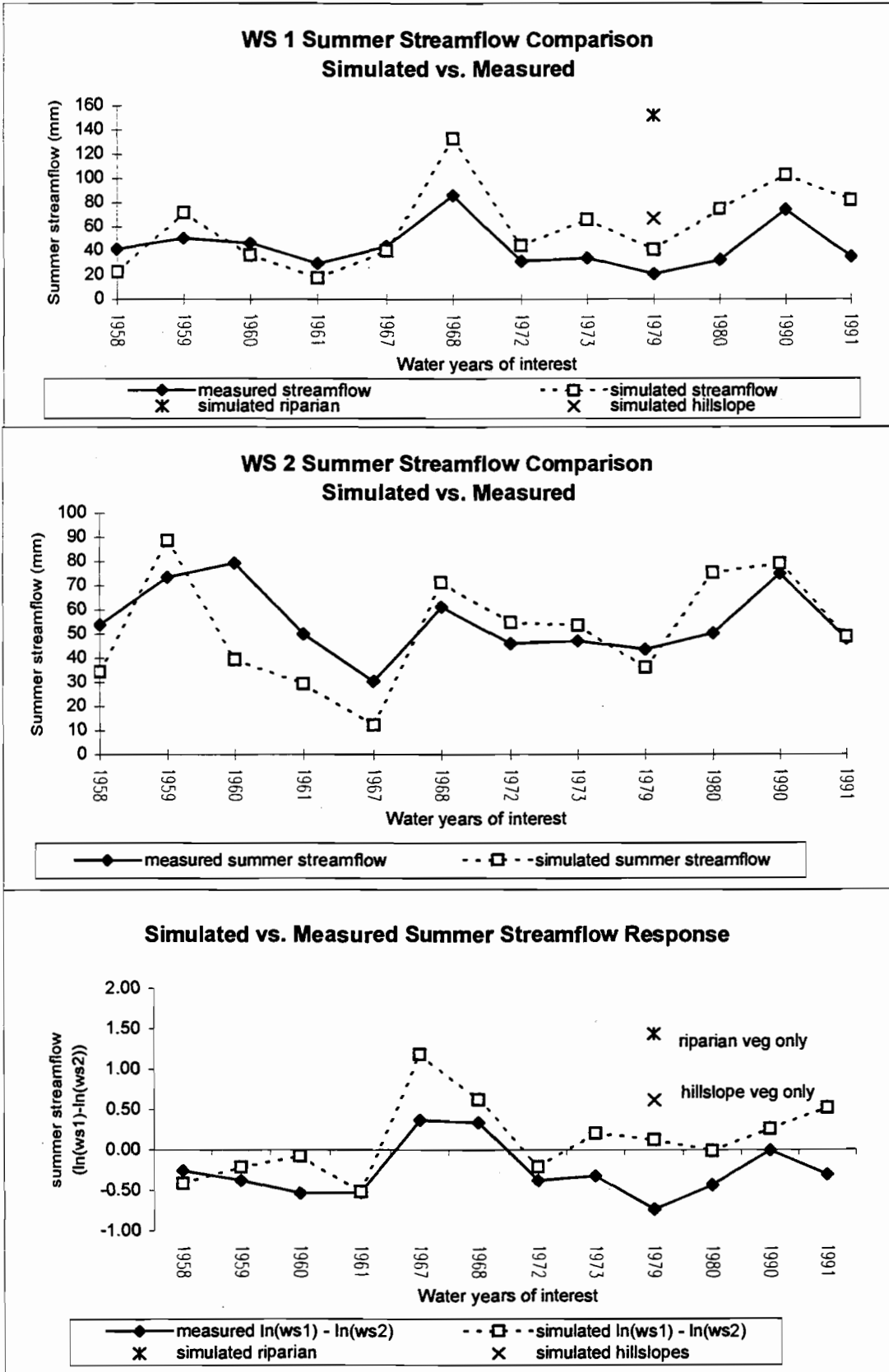
#### **4.4.2.2 Hillslope vs. Riparian Comparison**

The riparian corridor in WS 1 represents 10% of the watershed area using a 30m digital elevation model and contributed 20% of the simulated summer transpiration for WS 1 in 1979. It is estimated that the riparian corridor really occupies 1% of the watershed area (Jones, personal communication), and thus would contribute approximately 2% of the simulated summer transpiration for WS 1 in 1979. The hillslope vegetation represents the other 90% of the watershed area and contributed 80% of the simulated summer transpiration for WS 1 in 1979. In order to produce summer streamflow levels similar to the measured level, both the riparian and hillslope vegetation needed to be active. The results of these comparisons are illustrated in Figures 4-9a & c.

#### **4.4.2.3 Deciduous vs. Evergreen Broadleaf Comparison**

Comparative MAPSS-W simulations were run for water year 1979 to explore the relative influence of deciduous and evergreen broadleaf vegetation on streamflow. One simulation was parameterized for deciduous broadleaf vegetation and the other for evergreen broadleaf. This difference in parameterization made no difference to the annual or summer streamflow results. These simulations resulted in an annual streamflow difference of 10mm and a summer streamflow difference of 1mm. These results are due to the difference in maximum stomatal conductance and wilting point for

Figure 4-9a,b,c: Summer Streamflow Simulation Results



these two vegetation groups. The deciduous broadleaf maximum stomatal conductance parameter was set at 10mm/s and the wilting point parameter was set to -2.5. The evergreen broadleaf maximum stomatal conductance parameter was set at 7mm/s and the wilting point parameter was set to -5.0. These parameter settings allowed the vegetation to transpire the same amount of water through different processes. The evergreen broadleaf vegetation maintained transpiration during lower soil water potential than the deciduous broadleaf vegetation, but a lower rate.

## **4.5 Discussion**

### **4.5.1 Repeated Measures Analysis - Influence of Environmental Factors on Percent Cover**

The correlations, between environmental factors and percent cover for each vegetation group determined through repeated measures analysis indicate that the distribution and growth of vegetation is related to aspect and slope position. The topographic variables used in this analysis are indirect explanatory variables of environmental influence. Aspect served as a surrogate for the influence of solar radiation and temperature, as a function of solar radiation. Temperature exerts an indirect effect on vegetation growth through influences on potential evapotranspiration and soil moisture availability. Temperature directly influences plant growth and decomposition processes through control of enzymatic mechanisms (Lauenroth et al., 1993). In the Pacific Northwest, radiation loads and temperatures are higher on south aspects than on north aspects (Cleary, 1978). Slope served as a surrogate for the influences of soil moisture related to soil depth (Zheng et al., 1995).

These results indicate that herbaceous, deciduous broadleaf and conifer species location and growth may be influenced by solar radiation and temperature. The amount of incident solar radiation may influence surface and soil temperatures and local relative humidity. While herbs and conifers developed the highest cover values on the north-facing slope, deciduous broadleaf vegetation developed the highest cover values on the

south-facing slopes. Evergreen broadleaf species were concentrated in the northeastern corner of WS 1, an area of thin rocky soils.

Analysis using categorical explanatory variables would have provided more quantitative information about the relationships between topographic variables and vegetation cover; however, this dataset did not provide sufficient representation for each categorical division.

## **4.5.2 Implications of Vegetation-Hydrology Interactions**

### **4.5.2.1 Role of Herbaceous Vegetation**

The results of the vegetation analysis suggest that herbaceous vegetation expanded quickly following clear-cut harvest and broadcast burn. Herbaceous cover dominated the watershed within the first two years following harvest. This increase in herbaceous vegetation cover, to above pre-harvest levels, combined with increased surface temperatures, increased levels of solar radiation, and decreased relative humidity levels produces conditions which likely lead to rapid water use by the herbaceous vegetation during the summer. This dominant influence of herbaceous vegetation is likely limited to the first few years of clear-cut regrowth because the deciduous and evergreen broadleaf growth quickly shades the herbaceous vegetation. This shading changes the surface climate conditions, decreasing surface temperatures and solar radiation levels, and increasing relative humidity levels.

### **4.5.2.2 Role of Deciduous Broadleaf Shrubs and Trees**

#### **4.5.2.2.1 Riparian**

Deciduous broadleaf vegetation, particularly red alder, started to be apparent along the stream channel in the 1972 aerial photo. The alder tree canopies were widely spaced

and appeared to provide 25% or less of the vegetation cover in the riparian area at that time. The overall influence of deciduous riparian vegetation was probably small during 1972. By 1979, the deciduous broadleaf riparian vegetation cover had increased significantly, providing 50% or more cover. While the riparian vegetation is approximately 10% of the watershed area, MAPSS-W simulations indicate that the deciduous broadleaf riparian vegetation may contribute as much as 20% of the summer transpiration budget. The actual riparian corridor has been estimated to be only 1% of the watershed area (Jones, personal communication), which means that the riparian vegetation may only contribute 2% of the summer transpiration budget. By 1990, the deciduous broadleaf canopies had expanded to provided 75-100% cover over the riparian corridor. This increase in deciduous leaf area in the riparian corridor would be expected to transpire more than the riparian vegetation in 1979, unless the riparian canopy climate conditions had been modified by the increased height of the surrounding conifer vegetation. It is likely that local riparian climate conditions were moderated by the conifer canopies on the steep, surrounding hillslopes, increasing relative humidity, decreasing temperature extremes, and decreasing solar radiation levels. These changes in atmospheric conditions, which were not incorporated into the model runs because data was not available at this scale, would moderate the riparian transpiration rates. If so, the total water use by riparian alder may have declined between 1979 and 1990 despite the increase in leaf area.

#### 4.5.2.2.2 Hillslope

The vegetation plot data analysis highlights the importance of broadleaf vegetation on the hillslopes as well as in the riparian corridor. Deciduous broadleaf shrub and tree species are distributed throughout the watershed. Overall, the cover values for deciduous broadleaf species are higher than cover values for conifer, evergreen broadleaf or herbaceous vegetation groups. Transpiration by deciduous broadleaf vegetation may be constrained on the hillslopes by soil moisture deficits during the dry periods, but under conditions of maximum stomatal conductance it may contribute significantly to total transpiration from the site. It is likely that both riparian and hillslope

deciduous broadleaf vegetation played a major hydrologic role in WS 1 during the period of streamflow deficits in 1979. By 1990, the influence of hillslope deciduous broadleaf vegetation was likely moderated by canopy closure in the same way as described above for the riparian vegetation.

#### **4.5.2.3 Role of Evergreen Broadleaf Shrubs and Trees**

As illustrated in the vegetation plot figures, the dense evergreen broadleaf vegetation cover is restricted to a small portion of the watershed (Appendix A). It is unlikely that this stand of evergreen broadleaf vegetation had a significant influence on summer streamflow levels, due to the location and size of the stand. Model simulations indicate that evergreen broadleaf vegetation would likely contribute significantly to the total summer transpiration, if evergreen broadleaf vegetation dominated more of the watershed area. This is based on the comparison of MAPSS-W results for runs in which the entire watershed was parameterized for deciduous broadleaf vegetation versus runs in which the entire watershed was parameterized for evergreen broadleaf vegetation. These simulations indicate that evergreen and deciduous broadleaf vegetation use equivalent amounts of water, but through different processes.

#### **4.5.2.4 Role of Conifers**

Conifer cover does not appear to play a significant role in the watershed until the second return to pre-harvest streamflow levels 20 to 25 years after harvest, 24 years after the last planting. Conifers develop much more slowly than the herbs, deciduous broadleaf and evergreen broadleaf vegetation. Conifer canopy closure influences streamflow in two ways, indirectly through influences on the other vegetation groups and directly due to conifer stomatal conductance rates and seasonality of water use. In the areas of WS 1 which had reached canopy closure by 1990, the herbaceous, and deciduous and evergreen broadleaf vegetation is likely suppressed the dense overstory canopy. The understory climate is moderated, shade intolerant species decrease, and

the influence of solar radiation and turbulence are decreased. Conifers have lower stomatal conductance rates than deciduous and evergreen broadleaf species. Additionally conifer dominance may increase streamflow in the summer, but decrease streamflow levels in the spring and fall. It appears that conifers are just beginning to have a significant influence on streamflow, and complete canopy closure may have further effects on WS 1 hydrology.

#### **4.5.3 Additional Influences on Summer Streamflow**

Changes in vegetation water storage may also influence summer streamflows. Old-growth conifers may store as much as 250m<sup>3</sup>/ha of water in their sapwood (Waring & Franklin, 1979). This may contribute as much as half of the daily transpiration budget, and is at least partially recharged at night while stomata are closed. Full sapwood hydration occurs during the wet, winter months and likely contributes to early summer transpiration. When this storage mechanism is removed due to timber harvest, the water that might be stored contributes to elevated fall, winter and spring streamflows and is not available for use later in the year.

#### **4.6 Conclusions**

The vegetation patterns in WS 1 and the MAPSS-W simulation results support the hypotheses that changes in vegetation cover and species composition play significant roles in altering summer streamflow levels. During the first three decades of vegetation regeneration following clear-cut logging, the changes in summer streamflow level in WS 1 appear to be the result of shifts in vegetation functional group dominance. These hydrological functional groups have different characteristics along a gradient of hydrostable to hydrolabile water use. Conifers are hydrostable and maintain fairly stable plant water potentials. Deciduous broadleaf and herbaceous plants are moderately hydrostable, maintaining fairly stable plant water potential when there is sufficient soil

water available, but wilting when there are dry soil conditions. Evergreen broadleaf plants are hydrolabile and tolerate fairly large changes in plant water potential.

The initial increase in summer streamflow corresponds to removal of old-growth canopy and understory vegetation due to harvest techniques and broadcast burn. The rapid return of summer streamflow to pre-harvest levels corresponded with a rapid increase in herbaceous vegetation cover. Herbaceous vegetation expanded in response to decreased competition for available soil moisture and incident solar radiation. The herbaceous vegetation likely maintained high levels of transpiration due to the influence of increased incident solar radiation on canopy temperatures and humidity levels, which increased transpiration. Deciduous and evergreen broadleaf vegetation establishment was concurrent with the expansion of herbaceous cover, but took 5 to 10 years to become the dominant vegetation group.

The period of summer streamflow deficits corresponds to deciduous broadleaf expansion throughout the watershed and in the riparian corridor, and the development of an evergreen broadleaf stand along the north edge of the watershed. During this period the deciduous vegetation maintained high transpiration rates due to high levels of incident solar radiation and the influence of solar radiation on canopy temperatures and humidity levels. The deciduous broadleaf vegetation in the riparian corridor had unlimited access to water and maintained high transpiration rates during the summer. The transpiration rates of the deciduous broadleaf vegetation on the hillslopes likely decreases as soil moisture reserves decrease throughout the summer, dry period. The hillslope species may have established more extensive root systems than the plants growing in the riparian corridor, due to differences in soil moisture accessibility. The evergreen broadleaf vegetation likely maintained high transpiration rates throughout the summer in response to high evaporative demand, via the ability to withstand low plant water potentials and the tendency to establish extensive, deep root systems. The vegetation influence on streamflow during this period, in WS 1, appeared to be dominated by a combination of the riparian and hillslope deciduous broadleaf vegetation.

The second return to pre-harvest summer streamflow levels corresponded to the beginning of conifer canopy closure, and the senescence of much of the evergreen broadleaf vegetation. Evergreen broadleaf senescence may have been influenced by conifer canopy closure, but senescence also occurs naturally after about 20 years for

several of the key evergreen species (Conard et al., 1985; Hughes et al., 1987; Zavitkovski & Newton, 1968). Conifer canopy closure likely influences the transpiration rate of deciduous broadleaf vegetation on the hillslopes and in the riparian corridor by moderating temperatures and humidity levels, thus decreasing evaporative demand. Conifer maximum transpiration rates are generally lower than the maximum transpiration rates of deciduous broadleaf vegetation, so the demand for summer soil moisture may decrease somewhat. Conifer dominance may also extend the period of plant water use into the mild spring and fall months, influencing streamflow throughout the year.

Conifer canopy closure is patchy in WS 1, with the greatest conifer density on the north-facing slopes. The dense, young conifers stands appear to have higher leaf area than the pre-harvest old-growth stands. These stands may also have higher transpiration rates than the pre-harvest old-growth stands, due to height and age influences on internal hydraulic resistance (Borg & Stoneman, 1991; Shiklomanov & Krestovsky, 1988). However, these dense, young stands have lower roughness lengths than the mature forest and this may influence transpirational demand. If the net effect of these influences on transpiration is higher transpiration in the young conifer stands, then it is possible that there will be a second period of summer streamflow deficits once the young conifer canopy becomes dominant throughout the watershed.

## **5. Chapter 5: Conclusions**

### **5.1 Accomplishments**

In the process of investigating the influence of vegetation on summer streamflow levels, MAPSS-W (Daly, 1994) data sets were prepared, model calibration and evaluation analyses were carried out, and experimental simulations were performed. In addition, vegetation data was analyzed to determine temporal and spatial patterns of successional vegetation in watershed 1 at the H.J. Andrews Experimental Forest.

The dataset development included distribution of four climate variables (precipitation, temperature, vapor pressure, and wind speed), digitizing the small watershed soil survey and creation of vegetation datasets from aerial photos. Calibration and evaluation of MAPSS-W included single parameter sensitivity analysis, data set comparisons, and evaluation of the inter-annual variability in simulated streamflow results. The experimental simulations explored hypotheses of vegetation-streamflow interactions in an attempt to explain the changes in streamflow levels observed in WS 1 during 30 years of revegetation following clear-cut harvest.

Aerial photo and plot data analyses were based on three hydrological vegetation functional groups. These vegetation functional groups were defined based on physiological differences between conifers, deciduous broadleaf vegetation, and evergreen broadleaf vegetation. Aerial photo analysis provided the basis for the MAPSS-W vegetation layers. Plot data analysis allowed the identification of areas of vegetation concentrations. Correlations between vegetation functional groups and environmental factors were developed through repeated measure ANOVA.

### **5.2 Lessons**

While it would be useful to be able to predict streamflow results for unmonitored basins, it is difficult to do this using a spatially distributed watershed model because of the model's extensive input data requirements. MAPSS-W was useful in exploring the

hypotheses of vegetation-hydrology interactions, but has limited use in direct management applications. MAPSS-W requires knowledge of snow dynamics, soil hydraulics, and vegetation function in the watershed(s) of interest, as well as, distributed climate, soils, and vegetation datasets.

This study highlighted the importance of climate data measurements and spatial distribution techniques, appropriate environmental parameter values and dataset resolution in spatially explicit model applications. While the H.J. Andrews Experimental Forest has an extensive meteorological measurement program, only three of the four climate variables required for MAPSS-W were available for the water years of interest. Snow dynamics and soil hydrology parameters were critical for accurate simulation of monthly streamflow patterns. The resolution of a spatially explicit dataset must be fine enough to capture distinct areas of the watershed. In this case, the distinction between hillslopes and stream channel.

The vegetation analyses highlighted the hydrologic importance of herbaceous vegetation in the first few years following clear-cut harvest. Deciduous broadleaf vegetation appeared to dominate vegetation-hydrology interactions during the second decade following clear-cut. This has been followed by a return to conifer dominance, with associated changes in canopy-atmosphere interactions.

## Bibliography

- Abbott, M.B., J.C. Bathurst, J.A. Cunge, and others. 1986. An introduction to the European Hydrological System - System Hydrologique Eyropean "SHE", 1: history and philosophy of a physically-based, distributed modeling system. *Journal of Hydrology* 87:45-59.
- Ahlgren, C.E. 1981. Seventeen-year changes in climatic elements following prescribed burning. *Forest Science* 27:1, 33-39.
- Baldocchi, D.D. & C. A. Vogel. 1996. Energy and CO<sub>2</sub> flux densities above and below a temperate broad-leaved forest and a boreal pine forest. *Tree Physiology* 16:5-16.
- Beven, K.J. & M.J. Kirkby. 1979. A physically based, variable contributing area model of basin hydrology. *Hydrological Sciences-Bulletin* 24: 43-69.
- Black & Kelliher 1989. *Phil Trans Royal Soc Bulletin* 324:625-631.
- Borg, H. & G.L. Stoneman. 1991. Long-term implications for streamflow of changes in vegetation cover and stand height in regenerating karri stands in south-west Western Australia. *Forest Ecology & Management* 40:65-73.
- Cleary, B., R. Greaves, & R. Hermann (ed.). 1978. *Regenerating Oregon's Forests: A Guide for the Regeneration Forester*. Oregon State University Extension Service: Corvallis, OR.
- Conard, S.G. 1986. Comparative water relations of three shrub species- preliminary results. *FIR Report* 7: 4-5.
- Conard, S.G. & S.R. Radosevich. 1981. Photosynthesis, xylem pressure potential, and leaf conductance of three montane chaparral species in California. *Forest Science* 27:627-639.
- Conard, S.G., A.E. Jaramillo, K.Cromack, Jr., & S. Rose. 1985. The role of the genus *Ceanothus* in western forest ecosystems. USDA, Pacific Northwest Forest and Range Experiment Station, Portland, OR.
- Daly, C. 1994. Modeling climate, vegetation, and water balance at landscape to regional scales. Ph.D. Dissertation, General Sciences Department, Oregon State University.
- Daly, C., R.P. Neilson, and D.L. Phillips. A statistical-topographic model for mapping climatological precipitation over mountainous terrain. *Journal of Applied Meteorology* 33:140-158.
- Duan, J. 1996. A coupled hydrologic-geomorphic model for evaluating effects of vegetation change on watersheds. Ph.D. Dissertation, Department of Forest Engineering, Oregon State University.

Dyrness, C.T. 1969. Hydrologic properties of soils on three small watersheds in the western Cascades of Oregon. Pacific Northwest Research Note. Forest and Range Experiment Station, USDA, Portland, OR.

Dyrness, C.T. 1973. Early stages of plant succession following logging and burning in the western cascades of Oregon. *Ecology* 54: 57-69.

Environmental Research Systems, Incorporated (ESRI). 1996. ArcDoc Version 7.0.4: on-line documentation. Redlands, CA.

Forest Science Data Bank (FSDB). a partnership between the Department of Forest Science, Oregon State University, and the U.S. Forest Service Pacific Northwest Research Station, Corvallis, Oregon.

Franklin, J. & C.T. Dyrness. 1988. *Natural Vegetation of Oregon and Washington*. Oregon State University Press: Corvallis.

Franks, S.W., K.J. Beven, P.F. Quinn, & I.R. Wright. 1997. On the sensitivity of soil-vegetation-atmosphere transfer (SVAT) schemes: equifinality and the problem of robust calibration. *Agricultural and Forest Meteorology* 86: 67-75.

Fredriksen, R.L. & R.D. Harr. 1979. Soil, vegetation and watershed management of the Douglas-fir region. In: Heilman, P.E., H.W. Anderson, & D.M. Baumgartner. *Forest soils of the Douglas-fir region*. Washington State Cooperative Extension, Pullman, WA.

Frew, J.E. 1990. *The Image Processing Workbench*. Ph.D. dissertation, University of California at Santa Barbara.

Gholz, H.L., F.K. Fitz, & R.H. Waring. 1976. Leaf area differences associated with old-growth forest communities in the western Oregon Cascades. *Canadian Journal of Forest Research* 6:49-57.

Grayson, R.B., I.D. Moore, & T.A. McMahon. 1992. Physically based hydrological modeling 1. A terrain-based model for investigative purposes. *Water Resources Research* 28(10):2639-2658.

Halpern, C.B. 1987. *Twenty-one years of secondary succession in Pseudotsuga forests of the western Cascade Range, Oregon*. Dissertation, Forest Science Department, Oregon State University.

Halpern, C.B. 1988. Early successional pathways and the resistance and resilience of forest communities. *Ecology* 69: 1703-1715.

Halpern, C.B. 1989. Early successional patterns of forest species: interactions of life history traits and disturbance. *Ecology* 70: 704-720.

Halpern, C.B. and J.F. Franklin. 1989. Understory development in *Pseudotsuga* forests: multiple paths of succession. *Symposium on Land Classifications Based on Vegetation: Applications for Resource Management*.

- Halpern, C.B. and T.A. Spies. 1995. Plant species diversity in natural and managed forests of the Pacific Northwest. *Ecological Applications* 5: 913-934.
- Harr, R.D. 1977. Water flux in soil and subsoil on a steep forested slope. *Journal of Hydrology* 33: 37-58.
- Hawk, G.M., J.F. Franklin, W.A. McKee, & R.B. Brown. 1978. H.J. Andrews Experimental Forest reference stand system: establishment and use history. Bulletin No. 12, Coniferous forest Biome ecosystem analysis studies, IBP.
- Hawk, G. & C.T. Dyrness. unpublished (19??). Vegetation and soils of watershed 2 and 3, H.J. Andrews Experimental Forest. Internal Report 49. USDA Forest Service.
- Hicks, B.J., R.L. Beschta, and R.D. Harr. 1991. Long-term changes in streamflow following logging in western Oregon and associated fisheries implications. *Water Resources Bulletin*. 27: 217-226.
- Hillerdal-Hagstromer, K., E. Mattson-Djos, & J. Hellkvist. 1982. Field studies of water relations and photosynthesis in Scots pine. *Physiologia plantarum* 54(3):295-301.
- Hughes, T.F., C.R. Latt, J.C. Tappeiner II, M. Newton. 1987. Biomass and leaf-area estimates for varnishleaf *Ceanothus*, deerbrush, and whiteleaf manzanita. *Western Journal of Applied Forestry*. 2: 124-127.
- Jarvis, P.G., G.B. James & J.J. Landsberg. 1976. Coniferous forest. In J.L. Monteith (ed.). 1976. *Vegetation and the atmosphere*, vol. II. Case studies. London: Academic Press.
- Johnson, J.D., & W.K. Ferrell. 1983. Stomatal response to vapor pressure deficit and the effect of plant water stress. *Plant, Cell & Environment* 6: 451-456.
- Larcher, W. 1995. *Physiological Plant Ecology*, 3rd ed. Springer Press.
- Lauenroth, W.K., D.L. Urban, D.P. Coffin, W.J. Parton, H.H. Shugart, T.B. Kirchner, and T.M. Smith. 1993. Modeling vegetation structure-ecosystem process interactions across sites and ecosystems. *Ecological Modeling* 67: 49-80.
- Leavesley, G.H., R.W. Lichty, B.M. Troutman, and L.G. Saindon. 1983. Precipitation-runoff modeling system: user's manual. USGS Water Resources Investigation 83-4238:207.
- Legendre, P. & M-J. Fortin. 1989. Spatial pattern and ecological analysis. *Vegetatio* 80:107-138.
- Lindroth, A. 1985. Canopy Conductance of coniferous forests related to climate. *Water Resources Research* 21:297-304.

- Marks, D. 1990. The sensitivity of potential evapotranspiration to climate change over the continental United States. Pages IV-1 to IV-31 in H. Gucinski, D. Marks, and D.P. Turner, editors. Biospheric feedbacks to climate change: the sensitivity of regional trace gas emissions, evapotranspiration, and energy balance to vegetation redistribution. EPA/600/3-90/078. U.S. Environmental Protection Agency, Corvallis, Oregon, USA.
- McKee, A. & F. Biermaier. 1987. H.J. Andrews Experimental Forest, Oregon. In: Greenland, D. ed. The climates of the Long-Term Ecological Research sites. Occas. Pap 44. Boulder, CO: Institute of Arctic and Alpine Research, University of Colorado: 11-17.
- Monteith, J.L. & M.H. Unsworth. 1990. Principles of Environmental Physics 2nd ed. Edward Arnold division of Hodder & Stoughton, London
- Neilson, R.P. 1995. A model for predicting continental-scale vegetation distribution and water balance. Ecological Applications 5: 362-385.
- Nesje, A.M. 1996. Spatial patterns of early forest succession in Lookout Creek Basin. Masters of Science Research Paper, Department of Geosciences, Oregon State University.
- Oke, T.R. 1978. Boundary Layer Climates. Methuen, London.
- Pabst, R.J., J.C. Tappeiner II & M. Newton. 1990. Varying densities of Pacific madrone in a young stand in Oregon alter soil water-potential, plant moisture stress, and growth of Douglas fir. Forest Ecology and Management 37: 267-283.
- Pezeshki, S. R. & T.M. Hinkley. 1982. The stomatal response of red alder and black cotton wood to changing water status. Canadian Journal of Forest Research. 12:761-771.
- Ritchie, J.T. & E. Burnett. 1971. Dryland evaporative flux in a subhumid climate. II. Plant influences. Agronomy Journal. 63(1):56-62.
- Rosentrater, L.D. 1997. The thermal climate of the H.J. Andrews experimental forest, Oregon. Masters of Science Thesis, Department of Geography, University of Oregon.
- Rothacher, J. 1963. Net precipitation under a Douglas-fir forest. Forest Science 9:423-429.
- Rothacher, J., C.T. Dyrness, and R.L. Fredriksen. 1967. Hydrologic and related characteristics of three small watersheds in the Oregon Cascades. Pacific Northwest Forest and Range Experiment Station. FS USDA
- Rothacher, J. 1970. Increases in water yield following clear-cut logging in the Pacific Northwest. Water Resources Research 6: 653-658.
- Running, S.W., D.L. Peterson, M.A. Spanner, & K.B. Teuber. 1986. Remote sensing of coniferous forest leaf area. Ecology 67:273-276.

- Sala, A. & J.D. Tenhunen. 1994. Site-specific water relations and stomatal response of *Quercus ilex* in a Mediterranean watershed. *Tree Physiology* 14:601-617.
- SAS Institute. 1996. SAS/STAT User's Guide. Version 6, 4th Ed. Vol. 1 & 2. Cary, NC.
- Schulze, E.D. 1982. Plant Life Forms and Their Carbon, Water and Nutrient Relations. In: O.L. Lauge, et al. 1987. *Physiological Plant Ecology II*, Vol. 128 of the *Encyclopedia of Plant Physiology*. pp. 615-676.
- Shainsky, L.J., B.J. Yoder, T.B. Harrington, & S.S.N. Chan. 1994. Physiological characteristics of red alder: water relations and photosynthesis. In: Hibbs, D.E., D.S. DeBell, & R.F. Tarrant. eds. *The Biology & management of Red Alder*. OSU Press, Corvallis, OR.
- Shiklomanov, I.A. & O.I. Krestovsky. 1988. Hydrologic Process Models. in: E.R.C. Reynolds & F.B. Thompson eds. *Forests, Climate, and Hydrology: Regional Impacts*. The United Nations University.
- Silberstein, R.P. 1996. An investigation into water and energy balances at small catchment scales: Modeling and validation. PhD Thesis University of Western Australia, CWR Reference ED 1215 RS.
- Smith, N.J. & D.R. Clark. 1990. Estimating salal leaf area index and leaf biomass from diffuse light attenuation. *Canadian Journal of Forest Research* 20: 1265-1269.
- Smith, T.M., H.H. Shugart, & F.I. Woodward. 1997. *Plant Functional Types*. Cambridge University Press.
- Sokal, R.R. & N.L. Oden. 1978. Spatial autocorrelation in biology. 1. Methodology. *Biology Journal Linnean Society*. 10:199-228.
- Swank, W.T. and C.E. Johnson. 1994. Small catchment research in the evaluation and development of forest management practices. In: Moldan, B. and J. Cerny. (eds.). *Biogeochemistry of small catchments: a tool for environmental research*. John Wiley; Chichester, England.
- Teklehaimanot, Z. and P.G. Jarvis. 1991. Direct Measurement of Evaporation of Intercepted Water from Forest Canopies. *Journal of Applied Ecology* 28: 603-618.
- USA-CERL. 1993. GRASS 4.1 User's Manual. U.S. Army Corps of Engineers, Champaign, IL.
- U.S. Department of Agriculture, Forest Service. 1964. Soil survey report of the H.J. Andrews Experimental Forest, Willamette National Forest. Portland, OR: U.S. Department of Agriculture, Forest Service, Pacific Northwest Region, Division of Watershed Management.

von Ende, C.N. 1993. Repeated-measures analysis: growth and other time-dependent measures. Scheiner, S.M. & J.Gurevitch, eds. Design and Analysis of Ecological Experiments. Chapman & Hall.

Waring, R.H. & J.F. Franklin. 1979. Evergreen coniferous forests of the Pacific Northwest. Science 204: 1380-1386.

Waring, R.H. & Schlesinger, W.H. 1985. Forest ecosystems: Concepts and management. Academic Press, Inc. Harcourt Brace Jovanovich, Pub,  
Whitehead, D. & M. Kelliher. 1991. Modeling the water balance of a small *Pinus radiata* catchment. Tree Physiology 9:17-33.

Wigmosta, M. S., L.W. Vail, & D. P. Lettenmaier. 1994. A distributed hydrology-vegetation model for complex terrain. Water Resources Research 30: 1665-1679.

Woodward, F.I. 1987. Climate and plant distribution. Cambridge University Press, London, England.

Zavitkovski, J. & M. Newton. 1968. Ecological importance of snowbrush (*Ceanothus velutinus*) in the Oregon Cascades. Ecology 49:1134-1145.

Zheng, D., E.R. Hunt, & S.W. Running. 1995. Comparison of available soil water capacity estimated from topography and soil series information. Landscape Ecology

**Appendices**

## Appendix A: Vegetation Data Summary

### Vegetation Plot Data

1962  
1967  
1972  
1979  
1990

### Aerial Photos

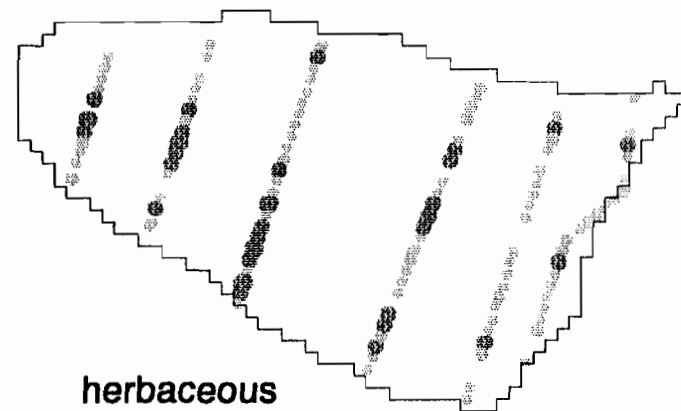
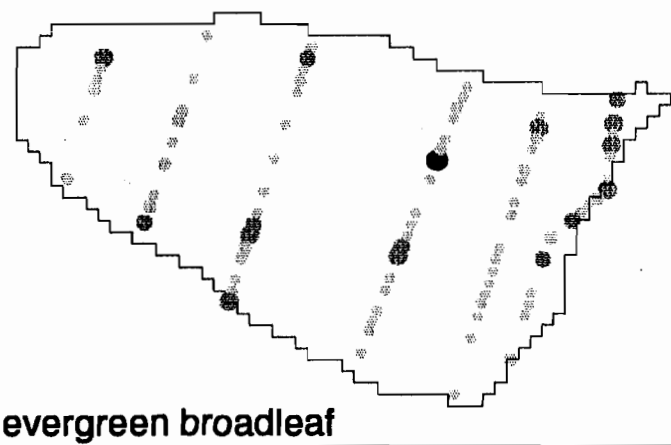
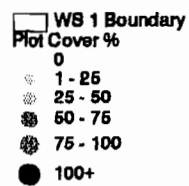
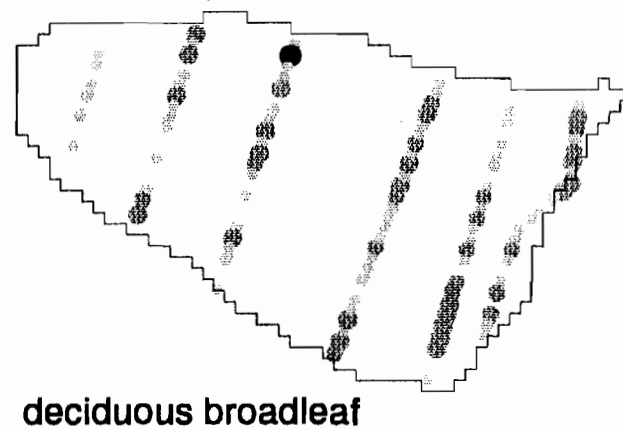
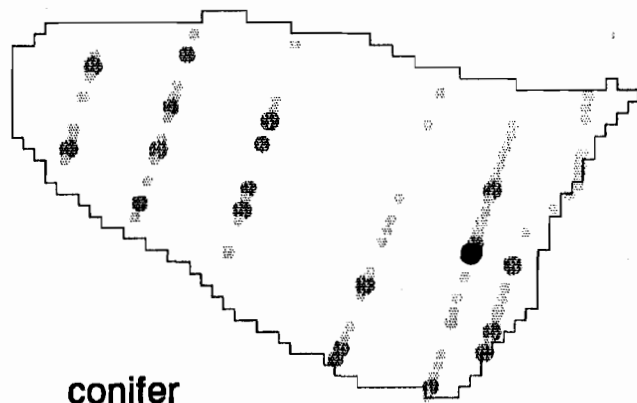
1959  
1967  
1972  
1979  
1990

### Aerial Photo Cover Maps

1959  
1972  
1979  
1990

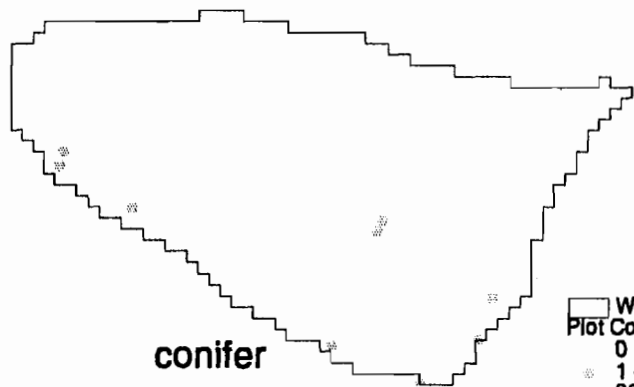
# WS 1 Understory Vegetation Plots Hydrological Functional Types

1962

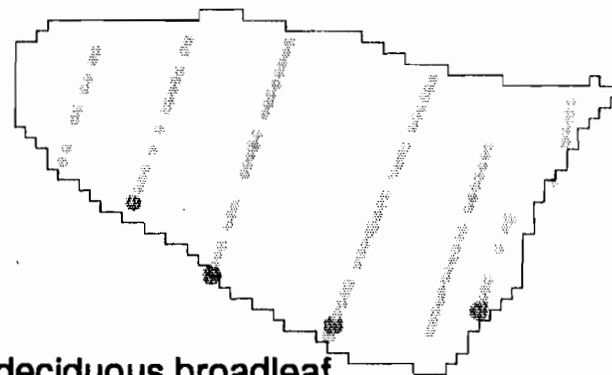


**WS1 Understory Vegetation Plots  
Hydrological Functional Types**

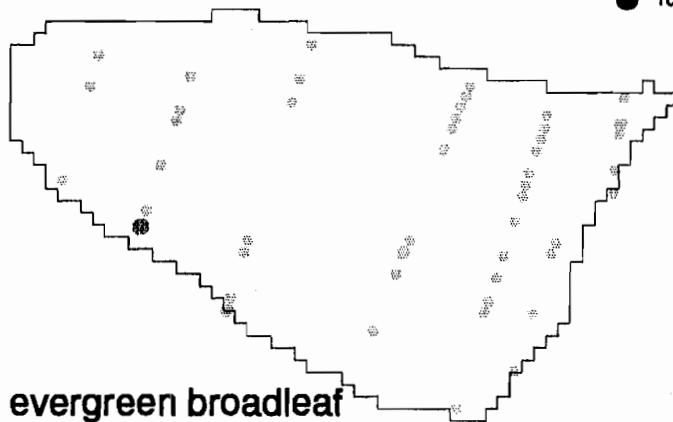
**1967**



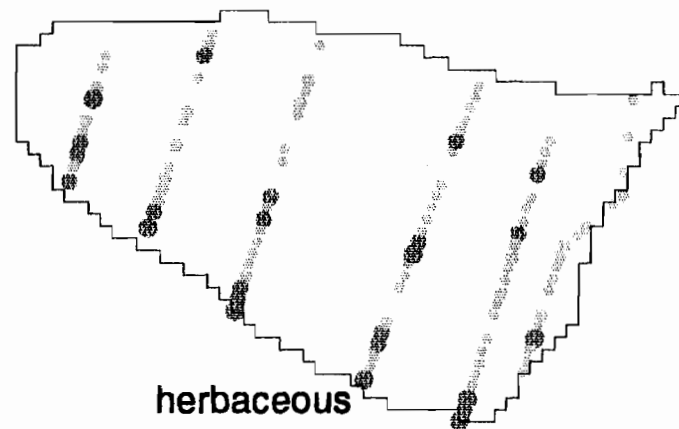
**conifer**



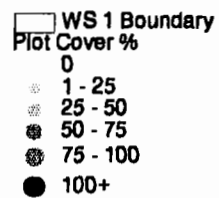
**deciduous broadleaf**



**evergreen broadleaf**



**herbaceous**

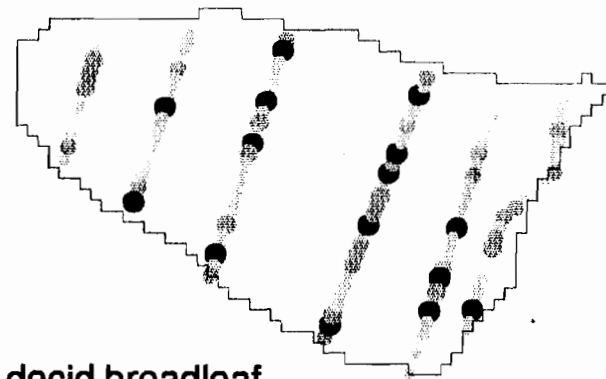


**WS 1 Understory Vegetation Plots**  
**Hydrological Functional Types**

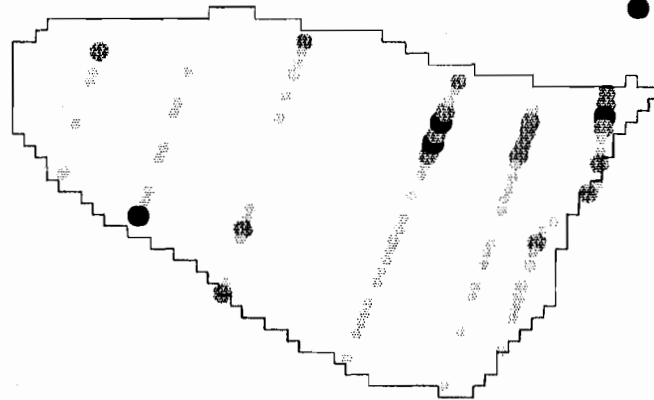
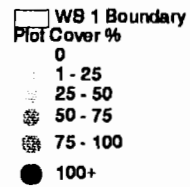
1972



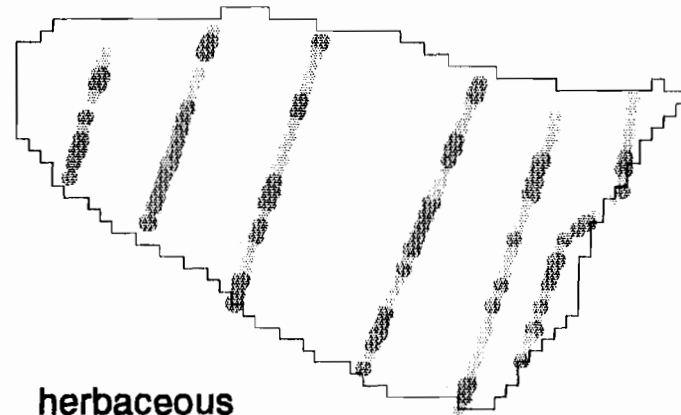
conifer



decid broadleaf



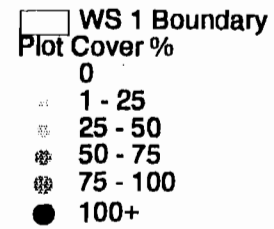
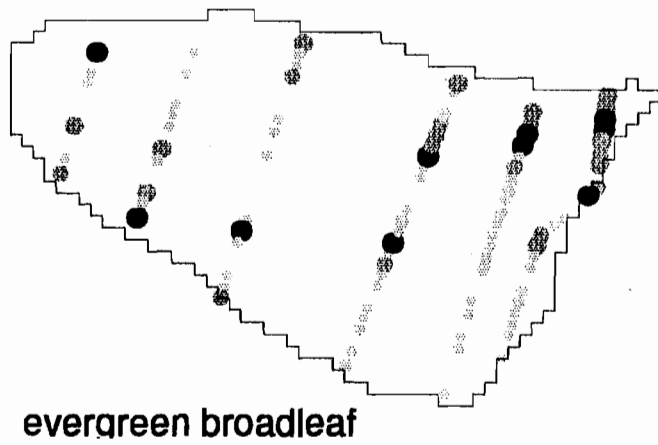
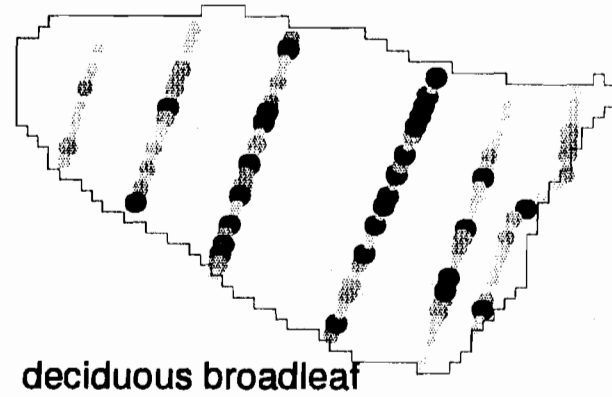
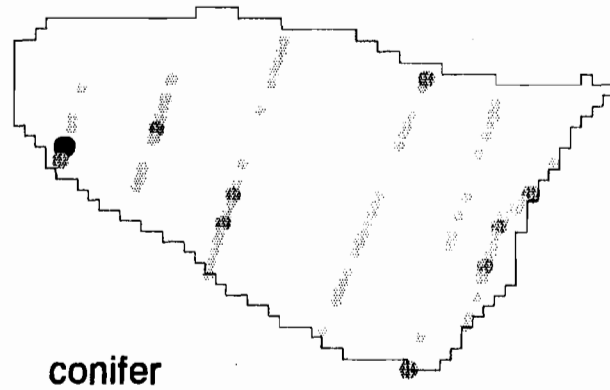
evergreen broadleaf



herbaceous

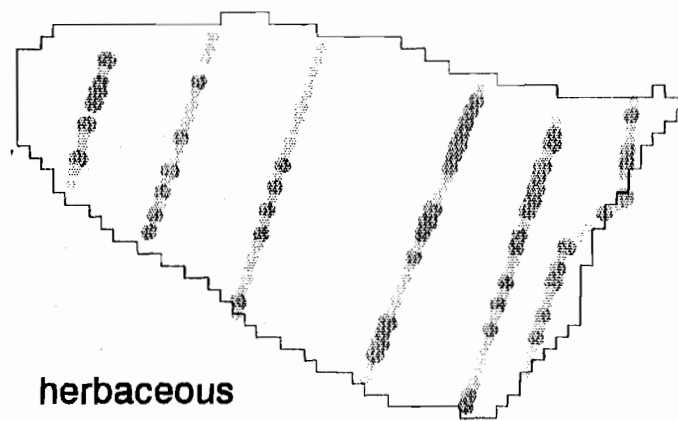
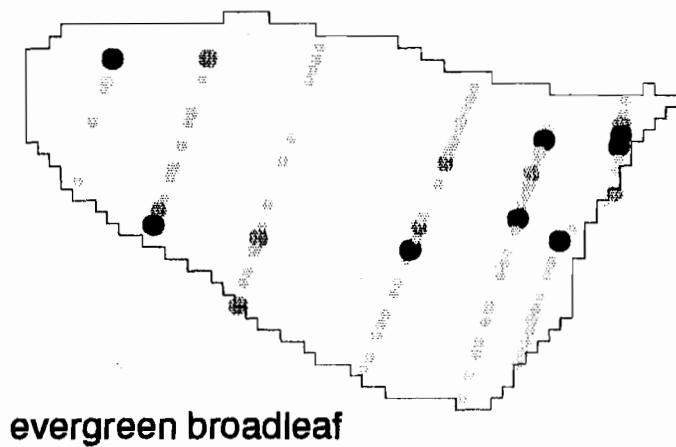
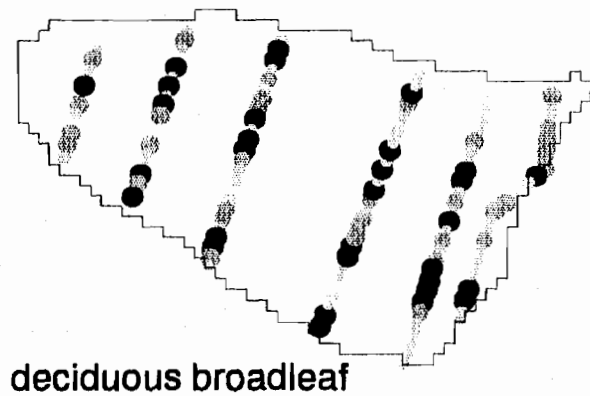
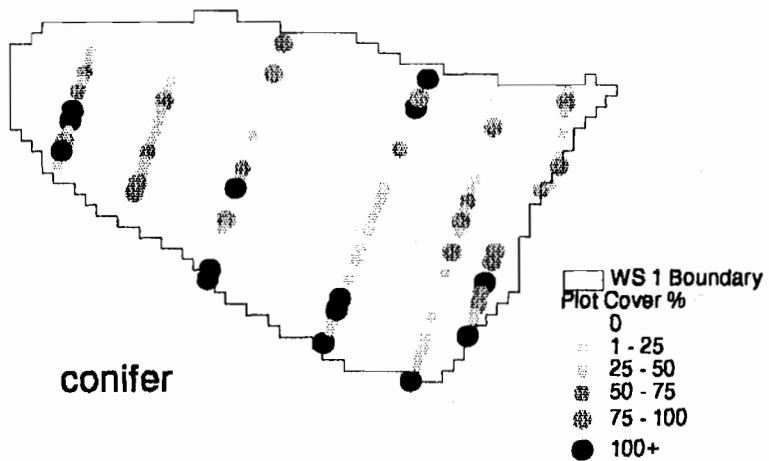
**WS 1 Understory Vegetation Plots  
Hydrological Functional Types**

**1979**



# WS 1 Understory Vegetation Plots Hydrological Functional Types

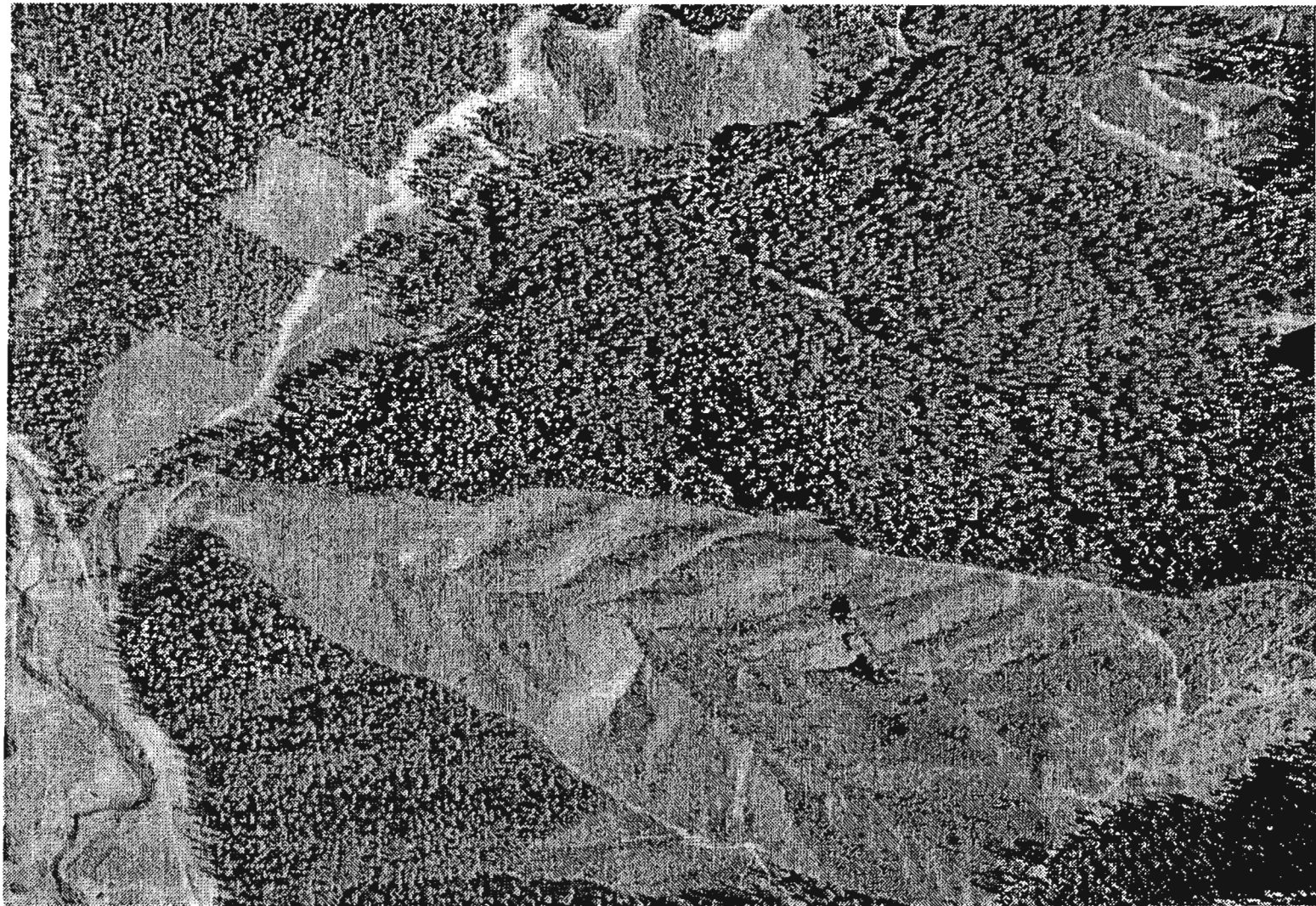
1990



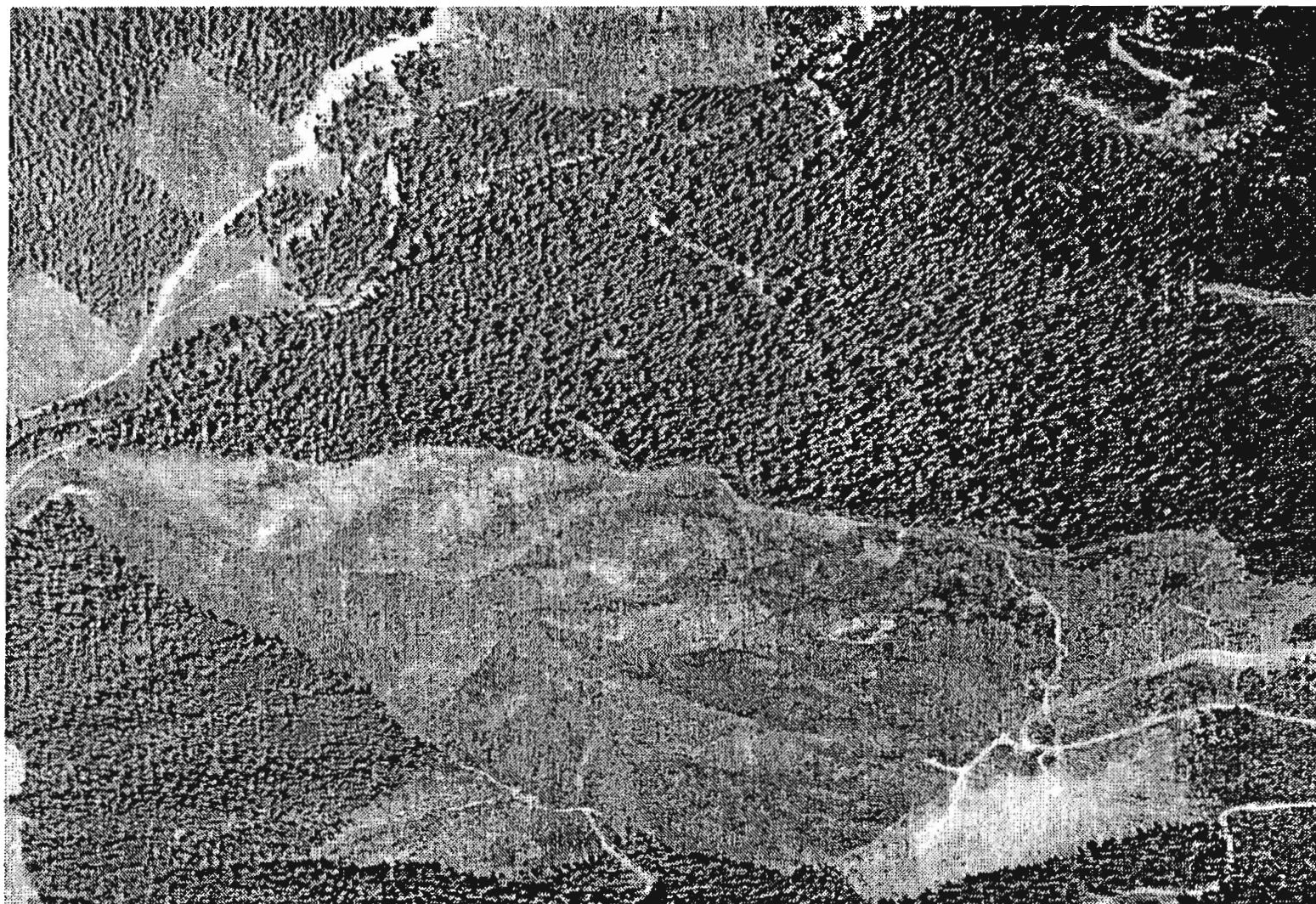
1959 Aerial Photo



1967 Aerial Photo



1972 Aerial Photo



1979 Aerial Photo

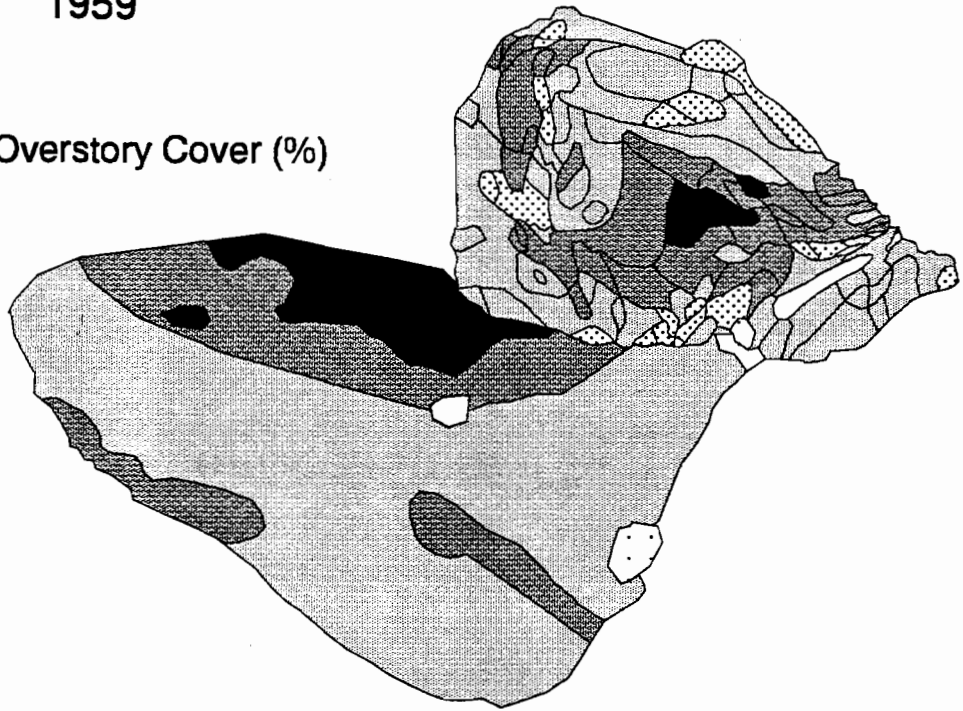


1990 Aerial Photo

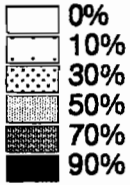


1959

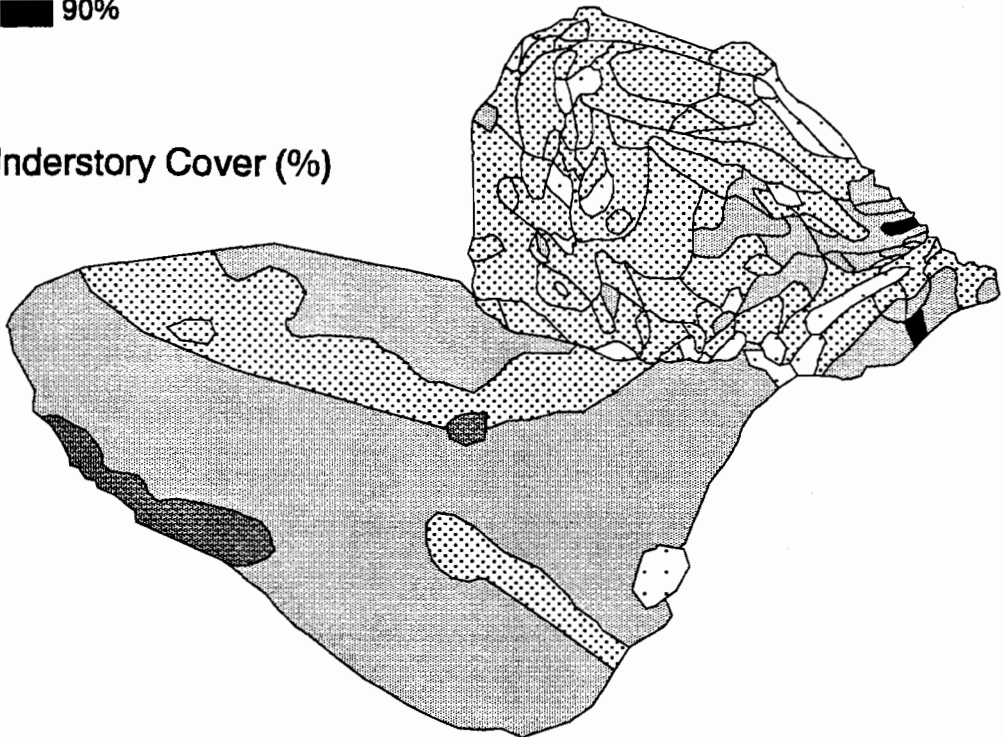
Overstory Cover (%)



Percent Cover

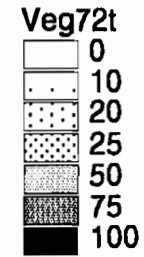
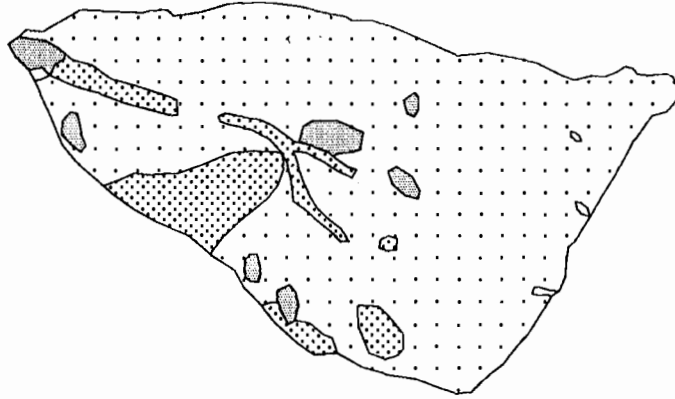


Understory Cover (%)



1972 -- Aerial Photo Percent Cover

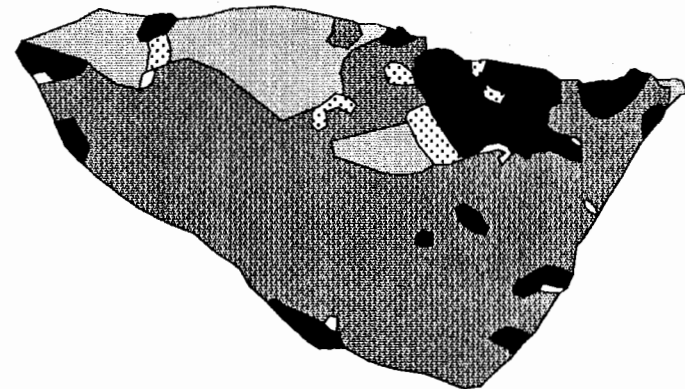
Deciduous Cover %



Conifer & Evergreen Broadleaf Cover %

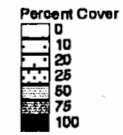
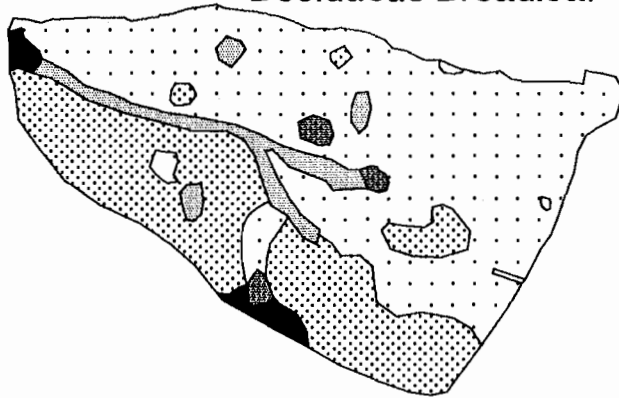


Herbaceous Cover %



1979 -- Aerial Photo Percent Cover

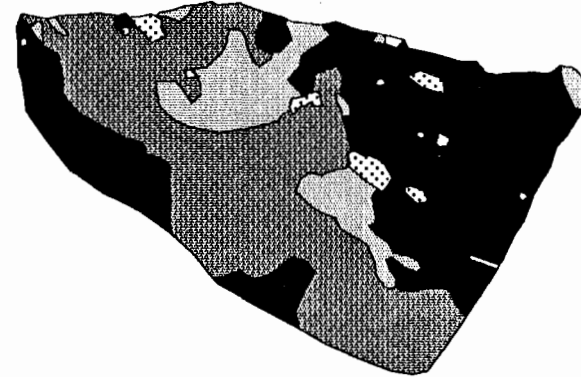
Deciduous Broadleaf



Conifer & Evergreen Broadleaf



Herbaceous

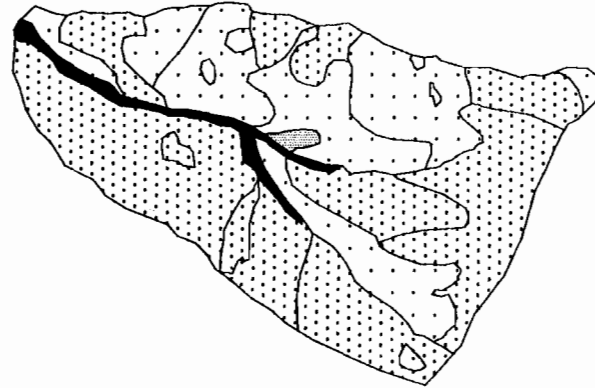


1990 -- Aerial Photo Percent Cover

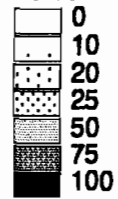
1990 Conifer



1990



Percent Cover



1990 Evergreen Broadleaf



1990



## Appendix B

### Cover Map Assessment Results - 1972 Aerial Photo Interpretation - Herbaceous Vegetation

map	plots			
	0-25%	25-50%	50-75%	75-100%
0-25%	1	1	2	0
25-50%	2	6	2	4
50-75%	15	27	35	18
75-100%	4	7	4	3

### Cover Map Assessment Results - 1972 Aerial Photo Interpretation - Conifer & Evergreen Broadleaf Vegetation

map	plots			
	0-25%	25-50%	50-75%	75-100%
0-25%	15	1	1	2
25-50%	84	4	4	8
50-75%	0	0	0	0
75-100%	5	2	2	9

### Cover Map Assessment Results - 1972 Aerial Photo Interpretation - Deciduous Broadleaf Vegetation

map	plots			
	0-25%	25-50%	50-75%	75-100%
0-25%	58	29	21	26
25-50%	0	0	0	0
50-75%	0	0	0	0
75-100%	0	0	0	0

### Cover Map Assessment Results - 1979 Aerial Photo Interpretation - Conifer & Evergreen Broadleaf Vegetation

map	plots			
	0-25%	25-50%	50-75%	75-100%
0-25%	11	5	2	3
25-50%	33	6	3	8
50-75%	15	5	2	8
75-100%	7	7	3	16

**Cover Map Assessment Results - 1972 Aerial Photo Interpretation - Deciduous Broadleaf Vegetation**

map	plots			
	0-25%	25-50%	50-75%	75-100%
0-25%	43	25	20	41
25-50%	1	1	1	2
50-75%	0	0	0	0
75-100%	0	0	0	0

**Cover Map Assessment Results - 1990 Aerial Photo Interpretation - Herbaceous Vegetation**

map	plots			
	0-25%	25-50%	50-75%	75-100%
0-25%	1	1	0	0
25-50%	7	1	2	1
50-75%	16	6	8	2
75-100%	22	24	26	17

**Cover Map Assessment Results - 1990 Aerial Photo Interpretation - Evergreen Broadleaf Vegetation**

map	plots			
	0-25%	25-50%	50-75%	75-100%
0-25%	10	1	0	1
25-50%	26	4	1	1
50-75%	64	10	4	10
75-100%	0	0	0	0

**Cover Map Assessment Results - 1990 Aerial Photo Interpretation - Conifer Vegetation**

map	plots			
	0-25%	25-50%	50-75%	75-100%
0-25%	7	0	0	1
25-50%	22	4	2	5
50-75%	16	5	0	6
75-100%	34	6	7	17

**Cover Map Assessment Results - 1990 Aerial Photo Interpretation - Deciduous Broadleaf Vegetation**

map	plots			
	0-25%	25-50%	50-75%	75-100%
0-25%	2	2	1	3
25-50%	11	6	1	15
50-75%	12	4	2	9
75-100%	21	9	8	25